Nonlinear Control of Unmanned Aerial Vehicles with Cable Suspended Payloads

by

AMEYA R. GODBOLE

Presented to the Faculty of the Graduate School of

The University of Texas at Arlington in Partial Fulfillment

of the Requirements

for the Degree of

DOCTOR OF PHILOSOPHY

THE UNIVERSITY OF TEXAS AT ARLINGTON

August 2019

Copyright © by Ameya R. Godbole 2019

All Rights Reserved

To my Mother Dr. Sangeeta Godbole, my Father Dr. Rajendra Godbole, my Baby Sister Dr. Anuja Godbole, my Cousin Sonali Kulkarni and my Cousin-in-Law Atul Aranke.

ACKNOWLEDGEMENTS

I take this opportunity to thank my mentor and dissertation supervisor Dr. Kamesh Subbarao. I would like to thank him for believing in me and guiding me through some tough times. I would also like to thank Dr. Animesh Chakravarthy, Dr. Alan Bowling, Dr. Brian Huff, Dr. Gaik Ambartsoumian and Dr. Ashfaq Adnan for taking time out to be on my supervising committee. My deep gratitude to all my teachers in the University of Texas at Arlington and back home in India. Without them I would have been a lesser individual.

Special thanks to Dr. Nicholas Gans, Cody Lundberg, Edward Dwayne Cotton and Jared Beaty for providing training and access to the Vicon Motion Capturing System at the University of Texas at Arlington Research Institute (UTARI), which enabled me to perform my experiments. I would like to express my gratitude to Dr. Atilla Dogan, Dr. Kamesh Subbarao, Dr. Brian Huff, Dr. Manfred Huber and Dr. Yan Wan and acknowledge the financial support provided by the National Science Foundation under the project "S&AS:FND: Safe Task-Aware Autonomous Resilient Systems (STAARS)" and award number 1724248. Thank you for giving me an opportunity to work on this challenging and interesting project. I would also like to thank the Office of Graduate Studies at The University of Texas at Arlington and College of Engineering for the financial support I was provided through the Summer Dissertation Fellowship. I am grateful to Dr. Erian Armanios for recommending me for the Summer Dissertation Fellowship.

I would like to thank my colleagues at the Aerospace Systems Laboratory, Gus, Alok, Pengkai, Pavan, Laura, Paul, Shashank, Tracie, Roopak, Murali, Denish, Rajnish, Diganta, Karan, Mitchell, Kati, Prabhjeet, Abel, Baris and Cem for their constant support and encouragement. Moreover, I would like to thank the past and present administrative staff

members in the Mechanical and Aerospace Engineering Department, especially, Debi Barton, Lanie Gordon, Janet Gober, Ayesha Fatima, and Wendy Lee Ryan.

I would like to express gratitude to my uncle, Sharad Kulkarni, my Aunt, Nutan Kulkarni, my Cousin, Sonali Kulkarni and my Cousin-in-law, Atul Aranke for taking care of me during my emergency Appendectomy. I would like to thank Dr. Monish Tandale who recommended me to apply to the University of Texas at Arlington for my graduate studies. It was a life-changing decision. I am grateful for the support and advice during crucial stages of my student life from my uncles, Col. Shashishekhar Kulkarni and Upendra Kulkarni, and my cousins, Dr. Sameer Kulkarni and Dr. Anagha Kulkarni. I would like to thank my cousin Swarada Kulkarni for the support, care and for ensuring that I had proper meals when things got busy at school.

I am lucky to have friends like Suhrud, Rushi, Gautam, Ameya Purandare, Vikas, Anand, Varun, Ateen, Pritish, Dhruva, Sohan, Yasir, Prashant, Zankar, Sandeep, Minal, Ravi, Michael and Selene who supported me during tough times and cherished my achievements as one of theirs. I would like to thank Prof. Avinash Prabhudesai and Team KJSCE Robocon for giving me the platform and allowing me to take my first baby-steps as a robotics engineer.

I owe all the good things in my life to my parents, my sister and my family. I thank them for all the sacrifices they have made for my success and happiness.

August 12, 2019

ABSTRACT

Nonlinear Control of Unmanned Aerial Vehicles with Cable Suspended Payloads

Ameya R. Godbole, Ph.D.

The University of Texas at Arlington, 2019

Supervising Professor: Kamesh Subbarao

The research focuses on the mathematical modeling and control of an unmanned aerial vehicle with cable suspended payload. A comprehensive mathematical model is derived for a quadcopter with a cable suspended payload using the Newton-Euler method and the Euler-Lagrange formulation. These methods assume that the cable is massless and always taut and cannot be used to simulate the cases when the cable is flexible. Hence, an alternative approach to model the flexibility of the cable is presented using Lagrangian mechanics by approximating the cable to be a chain of serially connected links.

The motion of the payload induces disturbances on the aerial platform and must be mitigated for stable operation. The solution to this control problem is presented through the implementation of a passivity based controller, and an extended state observer based active disturbance rejection controller. The implementation of the passivity based controller requires the knowledge of time derivatives of the payload oscillations. Assuming only the swing angles of the payload with respect to the unmanned aerial vehicle are measured, these states (primarily the angular velocity) are estimated using a continuous-discrete Kalman Filter. Alternately, since the payload cable swing angles are difficult to measure or requires additional on-board sensors, an active disturbance rejection controller is designed and im-

plemented wherein the disturbances induced in the system due to the motion of the payload are estimated using the extended state observer. A comparison between the passivity based controller and the extended state observer based active disturbance rejection controller is performed using a high fidelity numerical simulation. The simulation results are verified experimentally using a quadcopter platform in the Aerospace Systems Laboratory at The University of Texas at Arlington.

Furthermore, the mathematical modeling of a multi-agent system consisting of multiple quadcopters connected to a rigid body payload via cables is presented. A distributed extended state observer based active disturbance rejection controller is implemented on this system to achieve the cooperative control task of safely transporting the payload while attenuating the swing of the payload.

TABLE OF CONTENTS

LIST OF ILLUSTRATIONS

LIST OF TABLES

Executive Summary

Multicopters offer various advantages over fixed wing aircraft like hovering at a certain location and vertical take-off and landing. This allows us to deploy them for the payload delivery operations when the drop-off point is of prime importance. This problem is similar to the overhead cranes manipulating a payload. The mathematical modeling and control design of multicopters with cable suspended payloads has received a great deal of attention in recent years. Various control algorithms have been discussed in the literature which deal with the control of the the multirotor vehicles and stabilization of the cable suspended payload. The motion of the payload during operation induces disturbances on the aerial platform and needs to be mitigated for stable operation. The goal of this research is to develop a high fidelity simulation model of a multirotor unmanned vehicle system with cable suspended payload and design nonlinear control algorithms for the stable operation of the vehicle, and to attenuate the oscillations of the payload.

In this dissertation, all of the above concepts are applied to a quadcopter with a cable suspended payload. The first research objective discussed in this proposal is comprehensive mathematical modeling of a quadcopter with cable suspended payload, along with its propulsion system and an electric power consumption model. The simulation environment also considers the aerodynamic profile drag acting on the quadcopter and the payload. The mathematical model of the quadcopter is derived in two different ways using the Newton-Euler method and the Euler-Lagrange formulation. Since these methods assume that the payload cable is massless and always taut, the applicability of these modeling techniques is limited for the cases when the cable is flexible and deformed. Hence, an alternate modeling technique is presented which assumes the payload cable to be composed of several serially-

connected links. The mathematical model is formulated using Lagrangian mechanics.

The next objective is to design control algorithms to control the quadcopter with cable suspended payload and stabilize the swing of the payload. The solution to this control problem is presented in two ways. The first solution to this problem is presented through the design of an extended state observer based active disturbance rejection controller. The disturbance induced in the system due to the motion of the payload is estimated using the extended state observer with position of the quadcopter as the input to the observer. Using these disturbance estimates, an active disturbance rejection controller to achieve a favorable performance of the quadcopter is designed.

The second solution to the control problem is presented using an energy based approach called passivity based controller that asymptotically stabilizes the swing of the payload during transportation. The implementation of the passivity based controller requires the knowledge of higher time derivatives of the payload oscillations. Assuming only the swing angles of the payload with respect to an Unamnned Aerial Vehicle (UAV) are measured, these states (primarily the angular velocity) are estimated using a continuous-discrete Kalman filter.

The simulation environment is used to demonstrate the performance of the two control algorithms. The extended state observer based active disturbance rejection controller is further implemented on an experimental quadcopter platform to validate controller. Finally, a mathematical model for a multi-agent system of quadcopters carrying a cable suspended rigid body payload is presented. A distributed cooperative control policy is used to address this control problem and verified in a high-fidelity numerical simulation, paving the way for future research extensions of this control framework.

CHAPTER 1

Introduction and Motivation

The advancements in sensor technology and increase in on-board computation power has led to the availability of inexpensive aerial robots capable of performing aggressive maneuvers and dynamic trajectory generation and tracking. This has opened up a possibility of deploying aerial vehicles for surveillance, search and rescue operations, and to supply aid in disaster situations like floods and earthquakes. Given the advantages like hovering at a certain location, agile mobility, and vertical take-off and landing capability, the multirotor vehicles have proven to be useful for payload delivery when the drop-off location of the payload is critical.

The payload transportation using multicopter unmanned aerial vehicles can be useful in variety of applications like construction, and repair of structures at high altitudes or operating in difficult-to-access, remote, or hazardous locations for sample delivery or retrieval problem. Additionally, a multi-agent system consisting of multiple vehicles can be deployed for transporting heavier payloads.

The payload transportation problem using multicopters can be addressed using robotic manipulators attached to the aerial vehicle [1, 2] or through the use of cable to carry the payload[3]. Although the use of multicopters with manipulators provide the advantage of payload being rigidly connected to the body of the vehicle, it also increases the overall inertia of the system thus limiting the maximum weight of the payload it can lift. The use of cable suspended payload is an alternative solution to this problem.

The multirotor helicopter with cable suspended payload is a coupled underactuated dynamical system. The multicopter is controlled using the thrust generated due to the pro-

pellers but there is no direct control available to control the motion of the payload. The motion of the multicopter would thus induce disturbances and the cable suspended payload would oscillate. The motion of the payload in return, would induce a disturbance acceleration on the multicopter. This would lead to catastrophic effects if the amplitude of the oscillations grows unbounded, which is a risk to the operational environment and/or the payload itself. Thus, it is necessary to design a controller to attenuate the oscillations of the payload while trying to maintain the desired trajectory (position, velocity and acceleration) of the multicopter for the overall safe operation. Additionally, the control framework should be capable of rejecting external disturbances like drag force due to the wind induced on the system.

The focus of this research is to develop a mathematical model of a multicopter with cable suspended payload and design a nonlinear control framework. The nonlinear control framework is verified in the simulation and implemented on a quadcopter platform with cable suspended payload to provide the experimental validation. Additionally, a mathematical model of a multi-agent system of multicopters transporting a cable suspended payload is formulated and the control problem is addressed through a distributed cooperative control policy in the simulation.

1.1 Background

1.1.1 Mathematical Modeling of Quadcopter with Cable Suspended Payload

The problem involving unmanned aerial vehicles for transporting cable suspended payloads has been studied extensively in recent years. A detailed modeling effort to account for the propulsion system namely the battery power consumption, accounting for the profile drag on the quadcopter subject to steady prevailing wind was done in [4, 5]. The Newton-Euler method to model the quadcopter with cable suspended payload is one of the

approaches presented in this dissertation. The quadcopter model presented in [4, 5] has the capability to augment the disturbance forces acting on the quadcopter due to the prevailing wind as well as due to the oscillations of the payload. The dynamics of the payload is dependent on the quadcopter states. Using these quadcopter states, the dynamics of the cable slung payload was derived in [6–8]. The disturbance forces acting on the quadcopter due to the motion of the payload were computed using the dynamics of the payload and these forces were augmented in the mathematical model of the quadcopter derived using the Newton-Euler method [4, 5].

Alternately, the Euler-Lagrange formulation based on the kinetic and potential energy of the system has been used to derive the equations of motion of the quadcopter with cable suspended payload [9]. The translational dynamics of the quadcopter and the payload are assumed decoupled from the attitude dynamics of the quadcopter. Hence, assuming that the attitude of the quadcopter is controlled perfectly, the control problem of the quadcopter-slung load system becomes similar to the control of an overhead crane or an inverted spherical pendulum [10].

In [3] and [6–12], it is assumed that the cable is massless and rigid. Hence, these models cannot be used to simulate cases when the cable is deformed and the applicability is restricted. Reference [13] addressed the problem of simulating the system of flexible cables and pulleys. The work focused on obtaining feasible animation instead of accurate simulation. The hair strands, similar to the flexible cable were modeled as a continuum object using the cantilever beam equations in [14]. The common approach to model the flexible structures like the cables or hair strands is to approximate them as discrete systems by means of a chain of links [15, 16]. A coordinate-free form of the equations of motion for chain pendulum connected to a cart moving on the horizontal plane was presented in [17]. This approach was extended and implemented to model a quadcopter attached to payload using a flexible cable in [18]. An alternate approach to model the quadcopter attached to

a payload using a flexible cable has been presented in this dissertation similar to the approaches presented in [17, 18].

Using these modeling techniques, a comprehensive simulation environment is created to simulate the dynamics of the quadcopter with cable suspended payload. This simulation environment is used to test the control techniques designed to control the quadcopter and stabilize the payload motion. Additionally, this simulation environment can be used to simulate and study the effect of different propellers and how the payload carrying capacity can change. Also, the effect of wind on the range and endurance of the quadcopter with cable suspended payload subject to steady wind can be studied in a deterministic sense using this simulation model. These range estimates can be used by the path-planning algorithms to determine if a feasible path can be obtained within the reachable domain of the quadcopter under given environmental conditions and given available power for a specific quadcopter model.

1.1.2 Nonlinear Control of Quadcopter with Cable Suspended Payload

The quadcopter with cable suspended payload is an interconnected underactuated dynamical system. There have been implementations of different nonlinear control designs on multicopter platforms. Some of the applications of nonlinear control have only been verified through simulation while others have been validated by hardware experiments.

If we assume that the attitude of the quadcopter is controlled perfectly, then the problem becomes similar to the payload stabilization problem for the overhead cranes. In the past there has been focus on feedback control for wire-suspended mechanism transporting payloads [19,20]. The feedback for the payload cable angle in the experimental setup was measured through rotary encoders. References [21,22] focused on trajectory generation for underactuated control of a cable suspended payload and agile motion of the base vehicle. The problem of trajectory generation for the minimum swing of the payload attached to

a differential drive robot using a winch system was addressed in [12]. The dynamic programming approach was used to address the problem of trajectory generation for swing-free maneuvers for quadcopters with cable suspended payloads in [6] and towards a system consisting of two robotic manipulators carrying a cable suspended payload in [11]. The problem of stabilizing the swinging payload attached to an underactuated system has been solved using feedback linearization in [23]. In the recent work [18, 24], it was established that the quadcopter with cable suspended payload is a differentially flat system and a geometric control was implemented to determine the trajectory of the quadcopter to track the given trajectory of the payload.

The concept of interconnection and damping assignment passivity based control (IDA-PBC) was introduced in [25] and was used in [26] for the quadcopters with cable suspended payloads. An interaction and damping assignment passivity-based controller to change the dynamical parameters of the quadcopter was proposed in [27]. The design procedure for the IDA-PBC for the stabilization of under actuated systems was introduced in [28]. The passivity based control technique has been used to design robust control algorithms for systems described by the Euler-Lagrange formulation. In this technique, the mechanical systems are stabilized by shaping the potential energy of the system and providing a closed-loop energy function which is a difference between the energy of the system and the energy supplied by the controller. The IDA-PBC requires solving partial derivatives which is computationally very costly.

In [29,30], a downward-facing camera was employed to estimate the state of the payload relative to the vehicle using an onboard computer and a closed-loop payload control in the full three-dimensional workspace was demonstrated. In [29] the position, velocity, and the yaw angle of the quadcopter are obtained from a VICON system and fused with the payload attitude, and IMU. Additionally, while the paper solves the full problem, it is under the assumption that the cable always remains taut. The motion planning of the load is hence

carried out so as to guarantee this condition by synthesizing a load trajectory (differentiable upto 6th order) by solving a quadratic programming problem. The purpose of [29] is to develop a controller that will utilize payload swings and the anticipation of their swings with the rationale that, doing so is more energy optimal (this and the full implication of the payload swings on optimality has not been shown though). In [29, 30], since the intent is to utilize the payload swing for a purpose, it is necessary to estimate the payload motion, and synthesize a load trajectory that will accomplish the stated objectives. A load cell and an inertial measurement unit was utilized in [31] to estimate the swing angle. References [3, 32] also study the control of the quadcopter and 3-D payload motion, but it is assumed that the payload trajectory is synthesized using a VICON system and subsequently utilized in the control law.

A passivity based control framework motiviated by [33] and [34] was employed for the quadcopter with cable suspended payload in [35, 36]. Since the controller design depends upon the knowledge of the payload swing angle and its derivatives, a state estimation filter was utilized in [35, 36] to estimate the angular velocity of the payload assuming that the payload swing angle is measured. References [33–36] used a simplified mathematical model of the quadcopter with cable suspended payload with longitudinal plane restriction to demonstrate the efficacy of the controllers designed. The control strategy used in [35,36] along with the continuous-discrete Kalman filter implementation is described in this dissertation and is extended to the comprehensive mathematical model containing all six degrees of freedom (DOF) of the quadcopter and 2DOF of the cable suspended payload.

Since the swing angle of the payload cable is difficult to measure or requires additional sensors to estimate the state of the payload relative to the quadcopter [29–31] and the knowledge of the higher derivatives of the paylad cable angle is required by the passivity based controller [33–36], an active disturbance rejection control strategy, motivated by [37] is designed here to provide an alternate solution to control the quadcopter with cable

suspended payload and attenuate the oscillations of the payload. The payload motion is treated as a disturbance, and an extended state observer [38] is used to estimate the disturbances introduced in the system due to the motion of the payload. Using these disturbance estimates, a disturbance rejection controller is designed. While [36, 37] uses a simplified mathematical model of the quadcopter with cable suspended payload restricted to the longitudinal plane, the following research builds on this work and the extended state observer based active disturbance rejection controller is implemented for the comprehensive quadcopter model with cable suspended payload. The extended state observer based active disturbance rejection control strategy relies only on the quadcopter state measurements. Hence, additional sensors are not required to estimate the state of the payload. A desired control thrust for position tracking is derived first which leads to the synthesis of a desired attitude. A nonlinear control law is designed to track the desired attitude to complete the control design.

1.1.3 Distributed Cooperative Control of Multiple Quadcopters with a Cable Suspended Payload

To enhance the payload carrying capacity or the range and operation time, a cooperative control strategy involving multiple quadcopters carrying a rigid body cable suspended payload is proposed [39–43]. A geometric control approach was proposed for multiple quadcopters transporting a cable suspended payload was proposed in [40, 41, 43]. While the geometric control strategy was proposed for multiple quadcopters with point load connected via rigid and massless cables in [40], the work was extended to incorporate rigid bodies in [43]. The work was further extended to include the flexible cables in [41]. The strategy involved computing the desired forces along the orthogonal plane of the cable and along the plane normal to the cable to control the position and orientation of the payload and the direction of payload cable angle respectively.

In [44], an element of underactuation was added to the system of multiple quadcopters carrying a cable suspended flat plate in the form of a freely moving ball on the plate. The solution to this problem is synthesized by decoupling the quadcopters from the ball-plate system and computing the desired forces in the cable. These forces are then generated by the respective quadcopters to control the system using the backstepping strategy presented in [45].

A continuum deformation agent coordination approach to transport and manipulate objects using multiple quadcopters with collision avoidance guarantees was proposed in [42]. The system uses tensegrity muscles to carry a suspended payload instead of cables. A passivity based control approach was used for formation control of multiple unmanned aerial vehicles carrying a cable suspended payload in [39]. A kinematic formation controller based on null-space theory [46] was proposed in [47] to transport a cable suspended payload with two unmanned aerial vehicles.

An active disturbance rejection control approach for decentralized tracking in interconnected systems was proposed in [48] and implemented on a set of gantry cranes, subject to uncertainty and interaction while trying to independently track a prescribed position reference trajectory in a decentralized manner. A similar approach is adopted in this dissertation to address the cooperative control problem of multiple quadcopters transporting a rigid body cable suspended payload. The idea behind adopting this distributed control policy is that, all the uncertainties in the system are treated as total disturbance. These uncertainties arise due to unknown state dependent nonlinearities of the system, the environmental exogenous effects like the aerodynamic drag and the coupled dynamic interaction between the quadcopter-payload system. This total disturbance is estimated for each quadcopter in the system using an extended state observer and a disturbance rejection controller is designed to track a prescribed position in a decentralized manner.

1.2 Summary of Contributions

1. Developed a comprehensive mathematical model for a quadcopter with cable suspended payload along with its propulsion system, electric power consumption and aerodynamic drag model subject to steady wind conditions.

2. Designed an Extended State Observer Based Active Disturbance Rejection Controller to track the trajectory of the quadcopter while attenuating the oscillations of the cable suspended payload.

3. Designed a Passivity Based Controller to control the trajectory of the quadcopter while attenuating the oscillations of the cable suspended payload.

4. Compared the efficacy of the nonlinear controllers using the simulation environment.

5. Implemented the extended state observer based active disturbance rejection controller on an experimental quadcopter platform with cable suspended payload.

6. Developed a mathematical model of multiple quadcopters carrying a rigid body payload using rigid cables.

7. Implemented the distributed extended state observer based active disturbance rejection controller for the cooperative control task of transporting the cable suspended payload using multiple quadcopters.

List of Published Works

Journal Publications:

(a) Objective 1,2,3,4:

A. R. Godbole and K. Subbarao, "Nonlinear Control of Unmanned Aerial Vehicles with Cable Suspended Payloads," in Journal of Aerospace Science, and Technology (Elsevier),vol.93, p.105299, 2019, doi: https://doi.org/10.1016/j.ast.2019.07.032. (Reference [36])

(b) Objective 2,5:

A. R. Godbole and K. Subbarao, "Extended State Observer Based Active Disturbance Rejection Controller for a Multirotor Unmanned Aerial Vehicle with Cable Suspended Payload," in IEEE Transactions on Control Systems Technology (*Pending*)

Additional Publications:

(a) Objective 1:

A. R. Godbole, K. Subbarao, A. Dogan, and B. Huff, "Range and endurance characterization of a quadcopter subject to steady wind," in 2018 International Conference on Unmanned Aircraft Systems (ICUAS). IEEE, 2018, pp. 1279–1287. (Reference [4])

(b) Objective 1:

A. Godbole, K. Subbarao, A. Dogan, and B. Huff, "Semi-analytical range and endurance computation of battery-powered multi-copter unmanned aerial systems under steady wind conditions," in Proceedings of the Institution of Mechanical Engineers, Part G: Journal of Aerospace Engineering, April, 2019. [Online]. Available: https://doi.org/10.1177/0954410019842714 (Reference [5])

(c) Objective 3:

A. R. Godbole and K. Subbarao, "Mathematical modeling and control of an unmanned aerial system with a cable suspended payload," in 2018 IEEE 14th International Conference on Control and Automation (ICCA). IEEE, 2018, pp. 570–575. (Reference [35])

(d) Objective 5: (Point to point minimum-jerk trajectoy design used in Experiment 2)

A. Godbole, V. Murali, P. Quillen and K. Subbarao, "Optimal Trajectory Design and Control of a Planetary Exploration Rover," in Advances in the Astronautical Sciences Space flight Mechanics, vol. 160, 2017. (Reference [49])

1.3 Dissertation Outline

This dissertation is organized as follows: In Chapter 2, some mathematical concepts like the 2-Norm of a vector, positive definite matrix, stability of the dynamical systems, and the convergence rates for linear system are introduced. Chapter 3 presents a detailed mathematical model of the quadcopter with cable suspended payload along with its propulsion system, an electric power consumption model and aerodnamic profile drag model. The mathematical model of the quadcopter is derived using two different ways using the Newton-Euler approach and the Euler-Lagrange formulation. These two methods assume that the cable is massless and always taut. Hence, an alternate technique is presented to model the dynamics of the quadcopter with a payload that is connected via a flexible cable, which is modeled as a system of serially-connected links using the Lagrangian mechanics. An extended state observer based active disturbance rejection controller is designed in Chapter 4. The proof for the convergence of estimation errors of the extended state observer is also provided. Chapter 5 describes the design procedure for the passivity based

controller. The performance of the extended state observer based active disturbance rejection controller and the passivity based controller is compared in Chapter 6. Chapter 7 describes the experimental platform which will be used to implement the extended state observer based active disturbance rejection controller. The chapter gives the details about the software and communication network setup and flow of information between various components in the network. The extended state observer based active disturbance rejection controller is implemented on the quadcopter platform and the experimental results are presented in Chapter 8. A mathematical model is formulated for multiple quadcopters carrying a cable suspended rigid body payload in Chapter 9. A distributed extended state observer based active disturbance rejection controller is implemented on this multi-agent system to achieve the control objective of damping the oscillations of the payload while transporting it. Finally, in Chapter 10, the concluding remarks are stated along with the end goal of this research.

CHAPTER 2

Mathematical Preliminaries

2.1 Norm of a vector

The 2-Norm of a vector $\mathbf{x} \in \Re^n$ is defined by

$$\|\mathbf{x}\| = \sqrt{\mathbf{x}^T \mathbf{x}}$$

2.2 Hat Map and Vee Map

The hat map $\hat{\cdot} : \Re^3 \to SO(3)$ is defined by the condition that $\hat{\boldsymbol{x}}\boldsymbol{y} = \boldsymbol{x} \times \boldsymbol{y}$ for any $\boldsymbol{x}, \boldsymbol{y} \in \Re^3$, and it transforms a vector in $\Re^3$ to a 3×3 skew-symmetric matrix. More explicitly, it is given by

$$\hat{\boldsymbol{x}} = \begin{bmatrix} 0 & -x_3 & x_2 \\ x_3 & 0 & -x_1 \\ -x_2 & x_1 & 0 \end{bmatrix} \tag{2.1}$$

for $\boldsymbol{x} = \begin{bmatrix} x_1, & x_2, & x_3 \end{bmatrix}^T \in \Re^3$. The inverse of the hat map is the *vee* map $\vee : SO(3) \to \Re^3$.

2.3 Positive Definite Matrix

A square $n \times n$ matrix $\mathbf{Q}$ is positive definite $(p.d)$ if a vector $\mathbf{x} \in \Re^n$ and $\mathbf{x} \neq \mathbf{0}$ then,

$$\mathbf{x}^T \mathbf{Q} \mathbf{x} > 0$$

Furthermore, the following holds true for a p.d matrix $\mathbf{Q}$

$$\lambda_{min}(\mathbf{Q}) \|\mathbf{x}\|^2 \leq \mathbf{x}^T \mathbf{Q} \mathbf{x} \leq \lambda_{max}(\mathbf{Q}) \|\mathbf{x}\|^2$$

where, $\lambda_{min}(\mathbf{Q})$ is the smallest eigenvalue of $\mathbf{Q}$ and $\lambda_{max}(\mathbf{Q})$ is the largest eigenvalue of $\mathbf{Q}$.

2.4 Stability of Dynamical Systems

The Lyapunov stability theory is presented here which will be used to study the convergence rates for the linear systems. These concepts are used to prove the convergence of the extended state observer which will be designed in the later section. The complete analysis of Lyapunov stability theory can be found in [50, 51].

An equilibrium point is stable if all solutions starting at nearby points stay nearby; otherwise it is unstable. It is asymptotically stable if all solutions starting at nearby points not only stay nearby, but also tend to the equilibrium point as time approaches infinity. The concept of spherical region or ball denoted by $\mathbf{B}_R$ is introduced here which is defined as $\|\mathbf{x}\| < R$ in the state-space of the system and $\mathbf{S}_R$ the sphere itself, defined by $\|\mathbf{x}\| = R$.

Consider an autonomous system

$$\dot{\mathbf{x}} = f(\mathbf{x}) \tag{2.2}$$

where the function $f : D \to \Re^n$ is a locally Lipschitz mapping from a subset $D \subset \Re^n$ into $\Re^n$. The state $\mathbf{x} = \mathbf{0}$ is an equilibrium point if $f(\mathbf{0}) = \mathbf{0}$.

The equilibrium state $\mathbf{x} = \mathbf{0}$ is stable if given some r, where $0 < r < R$, the equilibrium point is stable in the sense of Lyapunov if

$$\|\mathbf{x}(0)\| < r \Longrightarrow \|\mathbf{x}(t)\| < R, \forall t \geq 0$$

Further, an equilibrium point $\mathbf{x} = \mathbf{0}$ is asymptotically stable if given some $r > 0$, then

$$\|\mathbf{x}(0)\| < r \Longrightarrow \mathbf{x}(t) \to \mathbf{0}, \text{as } t \to \infty$$

The objective of the stability proofs is to show that the system's energy is continuously dissipated as the system settles at an equilibrium point. The concept of stability for the system given in eq. (2.2) is presented using Lyapunov's direct method in [51]. In this method, a scalar energy function, $V : \Re^n \to \Re$ is defined which is the representation of the

total energy of the system. Now, the objective is to show that the function $V(\mathbf{x})$ is a valid Lyapunov function, which will establish the asymptotic stability of the system.

Let $V(\mathbf{x})$ be a non-negative function and $\dot{V}(\mathbf{x})$ be its time derivative along the state trajectories of the system. The following properties must be satisfied in order for the function to be considered as a valid Lyapunov function and the system to be considered asymptotically stable

- $V(\mathbf{x}) = 0$, only at $\mathbf{x} = \mathbf{0}$.
- $V(\mathbf{x}) > 0$.
- $\dot{V}(\mathbf{x}) < 0$

2.5 Convergence Rates For Linear Systems

Consider a candidate Lyapunov function for the autonomous system $\dot{\mathbf{x}} = \mathbf{A}\mathbf{x}$ given in eq. (2.2) as

$$V = \mathbf{x}^T \mathbf{P} \mathbf{x}$$

where, $\mathbf{P}$ is a symmetric positive definite matrix. Differentiating the positive definite function V

$$\dot{V} = \dot{\mathbf{x}}^T \mathbf{P} \mathbf{x} + \mathbf{x}^T \mathbf{P} \dot{\mathbf{x}} = -\mathbf{x}^T \mathbf{Q} \mathbf{x}$$

where, $\mathbf{A}^T \mathbf{P} + \mathbf{P}\mathbf{A} = \mathbf{Q}$. Now, if $\mathbf{Q}$ is positive definite, then V satisfies the conditions of the Lyapunov function and the origin is globally asymptotically stable.

Let $\lambda_{max}(\mathbf{P})$ be the largest eigenvalue of the matrix $\mathbf{P}$ and $\lambda_{min}(\mathbf{Q})$ be the smallest eigenvalue of the matrix $\mathbf{Q}$ and their ratio $\frac{\lambda_{min}(\mathbf{Q})}{\lambda_{max}(\mathbf{P})}$ be denoted by γ. Therefore,

$$\begin{aligned} \mathbf{P} &\leq \lambda_{max}(\mathbf{P})\mathbf{I} \\ \mathbf{Q} &\geq \lambda_{min}(\mathbf{Q})\mathbf{I} \end{aligned}$$

Hence,

$$\mathbf{x}^T \mathbf{Q}\mathbf{x} \geq \frac{\lambda_{min}(\mathbf{Q})}{\lambda_{max}(\mathbf{P})} \mathbf{x}^T \left(\lambda_{max}(\mathbf{P})\mathbf{I}\right)\mathbf{x} \geq \gamma V \tag{2.3}$$

This implies that

$$\dot{V} \leq -\gamma V$$

This implies that $\|\mathbf{x}\| \to 0$ as $t \to \infty$. Therefore, $\mathbf{x}$ converges to $\mathbf{0}$.

CHAPTER 3

Mathematical Model of Quadcopter with Cable Suspended Payload

A quadcopter is an underactuated helicopter with four rotors. It consists of two pairs of rotors in a cross configuration. One pair spins in clockwise direction and other in counter clockwise direction. These rotors which are capable of spinning at different angular velocities produce the desired thrust and torque in order to achieve the desired translational and rotational motion.

This chapter presents a comprehensive mathematical model of the quadcopter with cable suspended payload. First, the governing equations of motion of the quadcopter are derived using Newton-Euler approach, Euler-Lagrange formulation. These methods assume that the cable connecting the quadcopter to the payload is massless and rigid. Hence, a third method which approximates the payload cable as a system of serially-connected links is presented using the Lagrangian mechanics. The chapter also discusses the aerodynamic drag model and finally, the propulsion system of the quadcopter consisting of the motor, fixed pitch propeller, and the battery is modeled.

3.1 Quadcopter Dynamics using Newton-Euler Approach

Figure 3.1 shows the coordinate frames associated with the quadcopter with cable suspended payload. Consider an inertial coordinate frame $\{\mathbf{I}\}$ fixed to the ground and a body fixed frame attached to the center of mass of the quadcopter $\{\mathbf{B}\}$. Let $\mathbf{X}_Q = \left[x_Q,\, y_Q,\, z_Q\right]^T$ denote the position vector of the quadcopter in the inertial frame; $\mathbf{V}_B = [u,\, v,\, w]^T$ represents the linear velocity of the quadcopter expressed in the body frame components; $\mathbf{\Theta} = [\phi,\, \theta,\, \psi]^T$ denote the Euler angles (roll, pitch, and yaw), i.e., the orien-

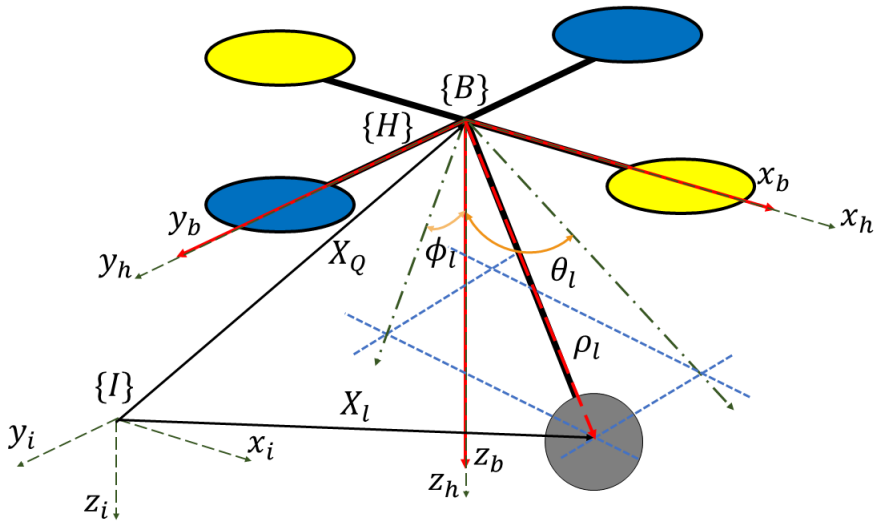

Figure 3.1: Description of coordinate frames associated with the quadcopter with cable suspended payload

tation of the quadcopter with respect to the Inertial frame; The body frame angular velocity of the quadcopter is represented by $\mathbf{\Omega} = [p,\ q,\ r]^T$; $\mathbf{R_{BI}} \in SO(3)$ is the direction cosine matrix representing the inertial frame to body frame transformation; m_Q be the mass of the quadcopter; $\mathbf{I}_Q \in \mathbb{R}^{3\times 3}$ represents the moment of inertia of the quadcopter.

Using the Newton-Euler approach [5,52], the quadcopter dynamics are expressed as,

$$\begin{aligned}
\dot{\mathbf{X}}_Q &= \mathbf{R}_{BI}^T \mathbf{V}_B \\
\dot{\mathbf{V}}_B &= -\mathbf{\Omega} \times \mathbf{V}_B + \frac{1}{m_Q}\mathbf{T} + \mathbf{R_{BI}} \begin{bmatrix} 0 \\ 0 \\ g \end{bmatrix} + \frac{\mathbf{D}}{m_Q} + \frac{\mathbf{F}_l}{m_Q} \\
\dot{\mathbf{\Theta}} &= \mathbf{W}(\phi, \theta, \psi)\,\mathbf{\Omega} \\
\mathbf{I}_Q \dot{\mathbf{\Omega}} &= -\mathbf{\Omega} \times \mathbf{I}_Q \mathbf{\Omega} + \boldsymbol{\tau}
\end{aligned} \tag{3.1}$$

where, g is the acceleration due to gravity.

$$\mathbf{R_{BI}} = \begin{bmatrix} c(\theta)c(\psi) & c(\theta)s(\psi) & -s(\theta) \\ s(\theta)s(\phi)c(\psi) - c(\phi)s(\psi) & s(\theta)s(\phi)s(\psi) + c(\psi)c(\phi) & c(\theta)s(\phi) \\ s(\theta)c(\phi)c(\psi) + s(\phi)s(\psi) & s(\theta)c(\phi)s(\psi) - c(\psi)s(\phi) & c(\theta)c(\phi) \end{bmatrix} \tag{3.2}$$

$$\mathbf{W}(\phi, \theta, \psi) = \begin{bmatrix} 1 & \sin(\phi)\tan(\theta) & \cos(\phi)\tan(\theta) \\ 0 & \cos(\phi) & -\sin(\phi) \\ 0 & \sin(\phi)\sec(\theta) & \cos(\phi)\sec(\theta) \end{bmatrix}$$

and $c(\cdot) = \cos(\cdot)$ and $s(\cdot) = \sin(\cdot)$. $\mathbf{T} \in \mathbb{R}^3$ denotes the total thrust acting on the quadcopter in the body frame and $\boldsymbol{\tau} \in \mathbb{R}^3$ represents the total torque acting on the quadcopter due to propeller thrust. $\mathbf{D} \in \mathbb{R}^3$ represents the aerodynamic profile drag acting on the quadcopter. $\mathbf{F}_l \in \mathbb{R}^3$ represents the force exerted on the quadcopter due to the motion of the cable suspended payload. The computation of the aerodynamic profile drag, $\mathbf{D}$, and the force exerted on the quadcopter due to the motion of the cable suspended payload, $\mathbf{F}_l$, will be discussed in sections 3.2 and 3.3 respectively.

If T_i is the individual thrust generated by each propeller in the body frame, the total thrust acting on the quadcopter expressed in the body frame is given by

$$\mathbf{T} = \begin{bmatrix} 0 \\ 0 \\ -\sum_{i=1}^{i=4} T_i \end{bmatrix} \tag{3.3}$$

The torque acting on the quadcopter can be expressed as a combination of the moments due to each propeller and the gyroscopic effects of the propellers as shown below.

$$\boldsymbol{\tau} = \boldsymbol{\tau_G} + \boldsymbol{\tau}_{prop} \tag{3.4}$$

The gyroscopic effect due to propeller's moment of inertia, J_m, the angular speed ω_i and the body attitude rate, $\mathbf{\Omega}$, assuming idential moment of inertia for all the rotors, is expressed as

$$\boldsymbol{\tau_G} = \sum_{i=1}^{i=4} \left(J_m \left(\mathbf{\Omega} \times \begin{bmatrix} 0 \\ 0 \\ 1 \end{bmatrix} \right) \omega_i \right)$$

Thus,

$$\boldsymbol{\tau_G} = J_m \left(\mathbf{\Omega} \times \begin{bmatrix} 0 \\ 0 \\ 1 \end{bmatrix} \right) \omega_{prop} \tag{3.5}$$

where, $\omega_{prop} = \sum_{i=1}^{i=4} \omega_i$ is the sum of angular speeds of all four rotors.

The roll, pitch and yaw moment due to propeller thrusts can be expressed as,

$$\boldsymbol{\tau_{prop}} = \begin{bmatrix} \tau_x \\ \tau_y \\ \tau_z \end{bmatrix} = \begin{bmatrix} d\,(T_2 - T_4) \\ d\,(T_1 - T_3) \\ (-\tau_{m1} + \tau_{m2} - \tau_{m3} + \tau_{m4}) \end{bmatrix} \tag{3.6}$$

where, d is the arm length of the quadcopter; τ_{m1}, τ_{m2}, τ_{m3} and τ_{m4} are the torques required to turn the propellers.

3.2 Aerodynamic Drag Model

The expression to compute the aerodynamic profile drag acting on the quadcopter is derived in this section. Figure 3.2 represents the wind vector in the inertial frame. Let V_w be the wind speed, ν_w represents the polar angle measured from the inertial z axis to the $x-y$ plane and the azimuthal angle χ_w is measured from inertial x axis to y axis. The wind velocity vector can be represented in the inertial frame as,

$$\mathbf{V}_w = \begin{bmatrix} V_w \sin(\nu_w) \cos(\chi_w) \\ V_w \sin(\nu_w) \sin(\chi_w) \\ V_w \cos(\nu_w) \end{bmatrix} \tag{3.7}$$

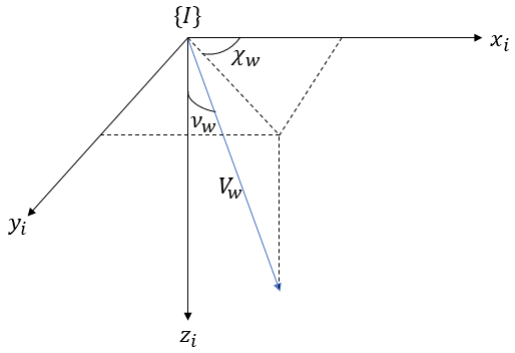

Figure 3.2: Steady State Wind Vector in Inertial Frame

The wind velocity vector $\mathbf{V}_w$ is transformed into body frame and the relative wind velocity in the body frame is expressed as,

$$\mathbf{V}_{rel} = \mathbf{V}_B - \mathbf{R}_{BI}\mathbf{V}_w$$

Using the relative velocity, the atmospheric drag is computed as,

$$\mathbf{D} = \frac{1}{2} C_D \rho_{air} \left| (\mathbf{S} \cdot \mathbf{V}_{rel}) \right| (-\mathbf{V}_{rel}) \tag{3.8}$$

where, ρ_{air} is the air density, C_D is the drag coefficient and $\mathbf{S}$ is the reference area vector. Assuming the quadcopter is a disk of radius r and height h, the reference area vector is given by $\mathbf{S} = \begin{bmatrix} 2rh & 2rh & \pi r^2 \end{bmatrix}^T$ and $C_D \approx 1.20$ (see [53]). Note, even when there is no wind, the magnitude of the drag force $\mathbf{D} \neq 0$ as it should be in reality.

3.3 Mathematical Modeling of the Cable Suspended Payload

This section presents the mathematical modeling of the cable suspended payload as a point mass spherical pendulum suspended from a single point and the computation of the forces exerted on the quadcopter due to the motion of the payload. These forces are included in the dynamics of the quadcopter derived earlier in section 3.1 using the Newton-Euler approach. The following assumptions are made for the dynamic analysis of the quadcopter with a cable suspended payload

- The payload is assumed to be a point mass.
- Suspension point is same as the center of mass of the quadcopter.

- Suspension is frictionless.
- The cable is massless and has no slack.

As shown in figure 3.1, let $\{\mathbf{H}\}$ be the hook coordinate frame attached to the suspension point which is always coincident and parallel to the body fixed frame $\{\mathbf{B}\}$. The position of the payload with respect to the suspension point can be expressed using the angles ϕ_l and θ_l measured from the z_H axis about x_H and y_H axes of the hook coordinate frame respectively. Let l be the length of the cable. Using the angles ϕ_l and θ_l, the position of the payload from the suspension point is given by

$$\begin{aligned}
\boldsymbol{\rho}_l &= \mathbf{R}_y(\theta_l)\mathbf{R}_x(\phi_l)\begin{bmatrix} 0 \\ 0 \\ l \end{bmatrix} \\
&= \begin{bmatrix} \cos(\theta_l) & 0 & \sin(\theta_l) \\ 0 & 1 & 0 \\ -\sin(\theta_l) & 0 & \cos(\theta_l) \end{bmatrix}\begin{bmatrix} 1 & 0 & 0 \\ 0 & \cos(\phi_l) & -\sin(\phi_l) \\ 0 & \sin(\phi_l) & \cos(\phi_l) \end{bmatrix}\begin{bmatrix} 0 \\ 0 \\ l \end{bmatrix} \\
&= l\begin{bmatrix} \sin(\theta_l)\cos(\phi_l) \\ -\sin(\phi_l) \\ \cos(\theta_l)\cos(\phi_l) \end{bmatrix}
\end{aligned}$$

The absolute velocity of the payload, $\mathbf{v}_l$ is given by

$$\mathbf{v}_l = \mathbf{V}_B + \dot{\boldsymbol{\rho}}_l + \boldsymbol{\Omega} \times \boldsymbol{\rho}_l$$

where, $\mathbf{V}_B$ is the linear velocity of the quadcopter expressed in the body frame; $\boldsymbol{\Omega}$ is the angular velocity of the quadcopter expressed in the body frame.

The absolute acceleration of the payload is given by

$$\dot{\mathbf{v}}_l = \dot{\mathbf{V}}_B + \ddot{\boldsymbol{\rho}}_l + \dot{\boldsymbol{\Omega}} \times \boldsymbol{\rho}_l + 2\boldsymbol{\Omega} \times \dot{\boldsymbol{\rho}}_l + \boldsymbol{\Omega} \times (\boldsymbol{\Omega} \times \boldsymbol{\rho}_l)$$

The weight vector of the payload expressed in the hook coordinate frame is given by

$$\mathbf{w}_l = \mathbf{R}_{BI} \begin{bmatrix} 0 \\ 0 \\ m_l g \end{bmatrix} = m_l g \begin{bmatrix} -\sin(\theta) \\ \cos(\theta)\sin(\phi) \\ \cos(\theta)\cos(\phi) \end{bmatrix}$$

where m_l is the mass of the payload.

The wind velocity vector $\mathbf{V}_w$ is transformed into body frame and the relative wind velocity with respect to the payload in the body frame is expressed as,

$$\mathbf{V}_{rel_p} = \mathbf{v}_l - \mathbf{R}_{BI}\mathbf{V}_w$$

Using the relative velocity, the profile drag acting on the payload is computed as,

$$\mathbf{D}_l = \frac{1}{2} C_D \rho_{air} \left| \left(\mathbf{S}_l \cdot \mathbf{V}_{rel_p} \right) \right| \left(-\mathbf{V}_{rel_p} \right) \tag{3.9}$$

where, ρ_{air} is the air density, C_D is the drag coefficient and $\mathbf{S}_l$ is the reference area vector. Assuming the payload to be a sphere of radius R, the reference area vector is given by $\mathbf{S}_l = \begin{bmatrix} \pi R^2 & \pi R^2 & \pi R^2 \end{bmatrix}^T$ and $C_D \approx 1.20$ (see [53]). Note, even when there is no wind, the magnitude of the drag force $D_l \neq 0$ as it should be in reality.

The equations of motion for the payload can be obtained by enforcing the torque equilibrium about the suspension point

$$\mathbf{f}_l \left(m_Q, m_l, l, \phi_l, \dot{\phi}_l, \ddot{\phi}_l, \theta_l, \dot{\theta}_l, \ddot{\theta}_l, \mathbf{V}_B, \dot{\mathbf{V}}_B, \mathbf{\Theta}, \dot{\mathbf{\Theta}}, \mathbf{\Omega}, \dot{\mathbf{\Omega}} \right) = -\boldsymbol{\rho}_l \times (-m_l \dot{\mathbf{v}}_l + \mathbf{w}_l + \mathbf{D}_l) = 0 \tag{3.10}$$

The equations of motion for the cable suspended payload can be obtained in terms of $\ddot{\phi}_l$ and $\ddot{\theta}_l$ by solving eq. (3.10).

The force exerted on the quadcopter due to the motion of the payload is given by

$$\mathbf{F}_l = -m_l \dot{\mathbf{v}}_l + \mathbf{w}_l + \mathbf{D}_l$$

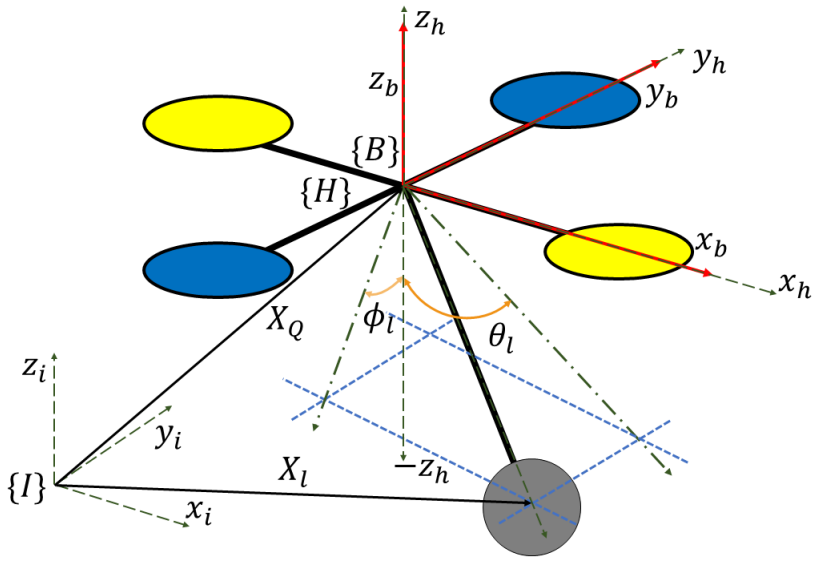

Figure 3.3: Description of coordinate frames associated with the quadcopter with cable suspended payload

3.4 Quadcopter Dynamics Using Euler-Lagrange Formulation

The equations of motion for the quadcopter with cable suspended payload can be represented in the alternative form using Euler-Lagrange formulation. The following assumptions are made for the dynamic analysis

- The cable is massless and has no slack
- The payload is approximated as a point mass
- The suspension point is the same as the center of mass of the quadcopter
- The suspension is frictionless

Figure 3.3 shows the coordinate frame assignment for the quadcopter with a cable suspended payload. Consider an inertial coordinate frame $\{\mathbf{I}\}$ and a body fixed frame $\{\mathbf{B}\}$ attached to the center of mass of the quadcopter. The generalized coordinates $\mathbf{q}$ and the generalized velocities $\dot{\mathbf{q}}$ are given by, $\mathbf{q} = \left[x_Q,\ y_Q,\ z_Q,\ \phi_l,\ \theta_l,\ \phi,\ \theta,\ \psi\right]^T$ and $\dot{\mathbf{q}} = \left[\dot{x}_Q,\ \dot{y}_Q,\ \dot{z}_Q,\ \dot{\phi}_l,\ \dot{\theta}_l,\ \dot{\phi},\ \dot{\theta},\ \dot{\psi}\right]^T$ respectively. Using the same notations used previously, let $\mathbf{X_Q} = \left[x_Q,\ y_Q,\ z_Q\right]^T$ denote the position of the quadcopter in the inertial frame; $[\phi,\ \theta,\ \psi]^T$ denote the Euler angles (roll, pitch, and yaw); $[\phi_l,\ \theta_l]^T$ denotes the

swing angle of the cable; m_Q is the mass of the quadcopter; m_l is the mass of the payload; l is the length of the cable.

The position of the center of mass of the payload $\mathbf{X}_l = [x_l,\ y_l,\ z_l]^T$ can be expressed in the inertial frame using the position of the center of mass of the quadcopter in the inertial frame, the payload cable swing angles and the length of the payload cable as,

$$\mathbf{X_l} = \begin{bmatrix} x_Q & y_Q & z_Q \end{bmatrix}^T + \mathbf{R}_y(\theta_l)\,\mathbf{R}_x(\phi_l) \begin{bmatrix} 0 & 0 & -l \end{bmatrix}^T, \tag{3.11}$$

where, $\mathbf{R}_x(\phi_l)$ and $\mathbf{R}_y(\theta_l)$ are the rotation matrices defined as,

$$\mathbf{R}_y(\theta_l) = \begin{bmatrix} \cos(\theta_l) & 0 & \sin(\theta_l) \\ 0 & 1 & 0 \\ -\sin(\theta_l) & 0 & \cos(\theta_l) \end{bmatrix}$$

$$\mathbf{R}_x(\phi_l) = \begin{bmatrix} 1 & 0 & 0 \\ 0 & \cos(\phi_l) & -\sin(\phi_l) \\ 0 & \sin(\phi_l) & \cos(\phi_l) \end{bmatrix}$$

Using eq. (3.11), the position of the payload can be expressed in terms of the quadcopter position and the swing angle of the cable as,

$$\begin{aligned} x_l &= x_Q - l\sin(\theta_l)\cos(\phi_l), \\ y_l &= y_Q + l\sin(\phi_l), \\ z_l &= z_Q - l\cos(\theta_l)\cos(\phi_l) \end{aligned} \tag{3.12}$$

Using eq. (3.12), the velocity of the payload in inertial frame is given as

$$\dot{\mathbf{X}}_l = \mathbf{J}_1(\theta_l, \phi_l) \begin{bmatrix} \dot{x}_Q & \dot{y}_Q & \dot{z}_Q & \dot{\phi}_l & \dot{\theta}_l \end{bmatrix}^T \tag{3.13}$$

where $\mathbf{J}_1$ is,

$$\mathbf{J}_1 = \begin{bmatrix} 1 & 0 & 0 & l\sin(\phi_l)\sin(\theta_l) & -l\cos(\theta_l)\cos(\phi_l) \\ 0 & 1 & 0 & l\cos(\phi_l) & 0 \\ 0 & 0 & 1 & l\cos(\theta_l)\sin(\phi_l) & l\cos(\phi_l)\sin(\theta_l) \end{bmatrix} \tag{3.14}$$

The body angular velocity of the quadcopter, $\mathbf{\Omega} = [p,\ q,\ r]^T$ is related to the rate of change of Euler angles as,

$$\begin{bmatrix} p \\ q \\ r \end{bmatrix} = \begin{bmatrix} 1 & 0 & -\sin(\theta) \\ 0 & \cos(\phi) & \cos(\theta)\sin(\phi) \\ 0 & -\sin(\phi) & \cos(\theta)\cos(\phi) \end{bmatrix} \begin{bmatrix} \dot{\phi} \\ \dot{\theta} \\ \dot{\psi} \end{bmatrix}. \tag{3.15}$$

and we denote,

$$\mathbf{J}_2 = \begin{bmatrix} 1 & 0 & \sin(\theta) \\ 0 & \cos(\phi) & \cos(\theta)\sin(\phi) \\ 0 & -\sin(\phi) & \cos(\theta)\cos(\phi) \end{bmatrix}. \tag{3.16}$$

This relation will be used further in the derivation of the equations of motion of the quadcopter with cable suspended load using Lagrange-Euler formulation [9, 35, 54].

The total kinetic energy of the quadcopter with a cable suspended load can be partitioned as sum of the quadcopter kinetic energy (T_Q),

$$T_Q = \frac{1}{2} m_Q \dot{x_Q}^2 + \frac{1}{2} m_Q \dot{y_Q}^2 + \frac{1}{2} m_Q \dot{z_Q}^2 + \frac{1}{2} \mathbf{\Omega}^T \mathbf{I}_Q \mathbf{\Omega}$$

and the kinetic energy of the cable suspended payload (T_l),

$$T_l = \frac{1}{2} m_l \dot{x_l}^2 + \frac{1}{2} m_l \dot{y_l}^2 + \frac{1}{2} m_l \dot{z_l}^2$$

where $\mathbf{I}_Q$ is the inertia matrix of the quadcopter.

Using the Jacobians derived in eq. (3.14) and (3.16), the total kinetic energy $T(\mathbf{q}, \dot{\mathbf{q}})$ can be written in terms of generalized coordinates as,

$$T(\mathbf{q}, \dot{\mathbf{q}}) = \frac{1}{2} \dot{\mathbf{q}}^T \mathbf{J}(\mathbf{q})^T \mathbf{M} \mathbf{J}(\mathbf{q}) \dot{\mathbf{q}}$$

with

$$\mathbf{M} = \begin{bmatrix} \mathbf{M}_Q & \mathbf{0}_{3\times 2} & \mathbf{0}_{3\times 3} \\ \mathbf{0}_{3\times 3} & \mathbf{M}_l & \mathbf{0}_{3\times 3} \\ \mathbf{0}_{3\times 3} & \mathbf{0}_{3\times 2} & \mathbf{I}_Q \end{bmatrix}$$

and

$$\mathbf{J} = \begin{bmatrix} \mathbf{I}_{3\times3} & \mathbf{0}_{3\times2} & \mathbf{0}_{3\times3} \\ & \mathbf{J}_1 & \mathbf{0}_{3\times3} \\ \mathbf{0}_{3\times3} & \mathbf{0}_{3\times2} & \mathbf{J}_2 \end{bmatrix}$$

where, $\mathbf{M}_Q = \text{diag}\left(m_Q,\ m_Q,\ m_Q\right)$ and $\mathbf{M}_l = \text{diag}\left(m_l, m_l, m_l\right)$.

The total potential energy function $V(\mathbf{q})$ of the system is the sum of the potential energy of the quadcopter and the payload and is given as,

$$V(\mathbf{q}) = m_Q g z_Q + m_l g\left(z_Q - l\cos(\theta_l)\cos(\phi_l)\right)$$

where, g is the acceleration due to gravity.

Using the expressions for the kinetic and potential energy, the Lagrangian is formulated as,

$$\mathscr{L} = T(\mathbf{q}, \dot{\mathbf{q}}) - V(\mathbf{q})$$

Using the Euler-Lagrange formulation, the mathematical model for the quadcopter with cable suspended load is obtained in the form of

$$\mathbf{M}(\mathbf{q})\ddot{\mathbf{q}} + \mathbf{C}(\mathbf{q}, \dot{\mathbf{q}})\dot{\mathbf{q}} + \mathbf{G}(\mathbf{q}) = \mathbf{F} \tag{3.17}$$

where, $\mathbf{F} = \begin{bmatrix} F_x + F_{Dx} & F_y + F_{Dy} & F_z + F_{Dz} & 0 & 0 & \tau_x & \tau_y & \tau_z \end{bmatrix}^T$ denotes the forces and torques acting on the quadcopter in the inertial frame. It is easily seen that,

$$\begin{bmatrix} F_x \\ F_y \\ F_z \end{bmatrix} = \mathbf{R}_{BI}^T \begin{bmatrix} 0 \\ 0 \\ T \end{bmatrix} \tag{3.18}$$

and

$$\begin{bmatrix} F_{Dx} \\ F_{Dy} \\ F_{Dz} \end{bmatrix} = \mathbf{R}_{BI}^T \boldsymbol{D} \tag{3.19}$$

where, $\mathbf{R}_{BI}^T$ is the rotation matrix transforming the force inputs from the quadcopter body frame $\{\mathbf{B}\}$ to the inertial frame $\{\mathbf{I}\}$ given in eq. (3.2); $T = -\sum_{i=1}^{i=4} T_i$ and T_i is the individual thust generated by

each propeller in the body frame; **D** is the drag force computed using eq. (3.8); τ_x, τ_y and τ_z are the roll, pitch and yaw moments respectively due to the propeller thrusts which is expressed using eq. (3.6)

3.5 Mathematical Modeling of a Quadcopter with a Payload Connected by a Flexible Cable

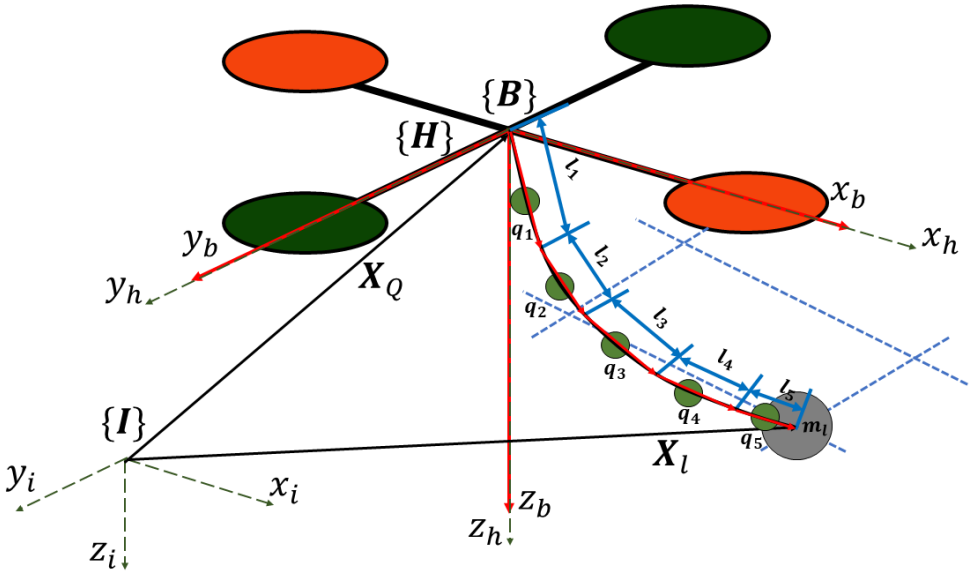

Figure 3.4: Description of coordinate frames associated with the quadcopter with a payload connected with a flexible cable

The mathematical model of the quadcopter with cable suspended payload presented in the sections 3.1, 3.3 and 3.4 assumed that the cable was rigid and massless. Hence, these models cannot be used to simulate cases when the cable is deformed. This section presents the mathematical model of the quadcopter with payload attached with a flexible cable. Figure 3.4 shows the coordinate frames associated with the quadcopter with a payload connected using a flexible cable. The flexible cable is modeled as a chain with n links. Consider an inertial coordinate frame $\{\mathbf{I}\}$ fixed to the ground and a body fixed frame attached to the center of mass of the quadcopter $\{\mathbf{B}\}$. Let $\mathbf{X}_Q =$

$\left[x_Q,\ y_Q,\ z_Q\right]^T$ denote the position vector of the quadcopter in the inertial frame; $\mathbf{V}_B = [u,\ v,\ w]^T$ represents the linear velocity of the quadcopter expressed in the body frame components; $\mathbf{\Theta} = [\phi,\ \theta,\ \psi]^T$ denote the Euler angles (roll, pitch, and yaw), i.e., the orientation of the quadcopter with respect to the Inertial frame; The body frame angular velocity of the quadcopter is represented by $\mathbf{\Omega} = [p,\ q,\ r]^T$; $\mathbf{R_{BI}} \in SO(3)$ is the direction cosine matrix representing the inertial frame to body frame transformation; m_Q be the mass of the quadcopter; $\mathbf{I}_Q$ is the inertia matrix of the quadcopter.

Let $\mathbf{q}_i$ $\left(\mathbf{q}_i \in \mathbb{R}^3 \text{ and } \|\mathbf{q}_i\| = 1\right)$ be the unit-vector representing the direction of the i-th link measured from the quadcopter towards the payload. The mass of each of the link is represented by m_i and it is concentrated at the center of each of the link. Let l_i be the length of each of the link, $\mathbf{x}_i$ corresponds to the location of the center of mass of each of the link and $\mathbf{X}_l$ be the location of the payload expressed in the inertial frame. The position of the center of mass of the i-th link and and the position of the center of mass of the payload can be expressed in terms of the position of the quadcopter and the unit vector $\mathbf{q}_i$ and the link length l_i as

$$\begin{aligned} \mathbf{x}_i &= \mathbf{X}_Q + \sum_{a=1}^{i-1} l_a \mathbf{q}_a + \frac{l_i}{2}\mathbf{q_i} \\ \mathbf{X}_l &= \mathbf{X}_Q + \sum_{a=1}^{n} l_a \mathbf{q}_a \end{aligned} \tag{3.20}$$

Let $\boldsymbol{\omega}_i$ represent the angular velocity of the i-th link represented in the inertial frame and is normal to the direction of the link i.e. $\mathbf{q}_i.\boldsymbol{\omega}_i = 0$. The kinematic equation for the i-th link is given by

$$\dot{\mathbf{q}}_i = \boldsymbol{\omega}_i \times \mathbf{q}_i \tag{3.21}$$

The equations of motion for the quadcopter with a payload connected by a flexible cable are derived using the Lagrangian mechanics. The kinetic energy of the quadcopter is given by

$$T_Q = \frac{1}{2} m_Q \|\dot{\mathbf{X}}_Q\|^2 + \frac{1}{2}\mathbf{\Omega}^T \mathbf{I}_Q \mathbf{\Omega} \tag{3.22}$$

The total kinetic energy of the flexible cable modeled as a chain with n links is given by

$$T_L = \frac{1}{2}\sum_{i=1}^{n} m_i \|\dot{\boldsymbol{X}}_Q + \sum_{a=1}^{i-1} l_i \dot{\mathbf{q}}_a + \frac{l_i}{2}\dot{\mathbf{q}}_i\|^2 \tag{3.23}$$

The total kinetic energy of the payload is given by

$$T_p = \frac{1}{2} m_l \|\dot{\mathbf{X}}_Q + \sum_{a=1}^{n} l_i \dot{\mathbf{q}}_a\|^2 \tag{3.24}$$

From eq. (3.22), (3.23) and (3.24), the total kinetic energy of the system is given as

$$T = \frac{1}{2}\dot{\mathbf{X}}_Q^T \mathbf{M}_{00} \dot{\mathbf{X}}_Q + \frac{1}{2}\boldsymbol{\Omega}^T \mathbf{I}_Q \boldsymbol{\Omega} + \dot{\mathbf{X}}_Q^T \sum_{i=1}^{n} \mathbf{M}_{0i} \dot{\mathbf{q}}_i + \frac{1}{2} \sum_{i,j=1}^{n} \dot{\mathbf{q}}_i^T \mathbf{M}_{ij} \dot{\mathbf{q}}_i \tag{3.25}$$

where,

$$\begin{aligned}
\mathbf{M}_{00} &= \mathbf{M}_Q + \mathbf{M}_l + \sum_{i=1}^{n} \mathbf{M}_L \\
\mathbf{M}_{0i} &= \left(\frac{2(n-i)+1}{2} \right) l_i \mathbf{M}_L + l_i \mathbf{M}_l \\
\mathbf{M}_{ij} &= \begin{cases} \left(\frac{4(n-i)+1}{4} \right) l_i^2 \mathbf{M}_L + l_i^2 \mathbf{M}_l, & \text{if } i = j \\ \left(\frac{2(n-a)+1}{2} \right) l_i^2 \mathbf{M}_L + l_i^2 \mathbf{M}_l, & \text{if } i \neq j \text{ and } a = max\{i, j\} \end{cases} \\
\mathbf{M}_Q &= \begin{bmatrix} m_Q & 0 & 0 \\ 0 & m_Q & 0 \\ 0 & 0 & m_Q \end{bmatrix} \\
\mathbf{M}_L &= \begin{bmatrix} m_i & 0 & 0 \\ 0 & m_i & 0 \\ 0 & 0 & m_i \end{bmatrix} \\
\mathbf{M}_l &= \begin{bmatrix} m_l & 0 & 0 \\ 0 & m_l & 0 \\ 0 & 0 & m_l \end{bmatrix}
\end{aligned}$$

The total potential energy of the system is given as

$$V = -\mathbf{M}_{00} g \mathbf{X}_Q \cdot \mathbf{e}_3 - \sum_{i=1}^{n} \left(\left(\frac{2(n-i)+1}{2} \right) l_i \mathbf{M}_L + l_i \mathbf{M}_l \right) g \mathbf{e}_3 . \boldsymbol{q}_i \tag{3.26}$$

where $\mathbf{e}_3 = \begin{bmatrix} 0 & 0 & 1 \end{bmatrix}^T$.

Using the expression for the total kinetic energy given in eq. (3.25) and total potential energy given in eq. (3.26), the Lagrangian is formulated as

$$\begin{aligned}\mathscr{L} =& \frac{1}{2}\dot{\mathbf{X}}_Q^T\mathbf{M}_{00}\dot{\mathbf{X}}_Q + \frac{1}{2}\boldsymbol{\Omega}^T\mathbf{I}_Q\boldsymbol{\Omega} + \dot{\mathbf{X}}_Q^T\sum_{i=1}^{n}\mathbf{M}_{0i}\dot{\mathbf{q}}_i + \frac{1}{2}\sum_{i,j=1}^{n}\dot{\mathbf{q}}_i^T\mathbf{M}_{ij}\dot{\mathbf{q}}_i \\ &+ \mathbf{M}_{00}g\mathbf{X}_Q.\mathbf{e}_3 + \sum_{i=1}^{n}\left(\left(\frac{2(n-i)+1}{2}\right)l_i\mathbf{M}_L + l_i\mathbf{M}_l\right)g\mathbf{e}_3.\mathbf{q}_i\end{aligned} \tag{3.27}$$

Let $\delta\mathbf{X}_Q$ and $\delta\dot{\mathbf{X}}_Q$ be the variation in $\mathbf{X}_Q$ and $\dot{\mathbf{X}}_Q$ respectively. From [55], the variation in the angular velocity of the quadcopter, $\boldsymbol{\Omega}$, and the variation of $\mathbf{q}_i$ is given as

$$\begin{aligned}\delta\boldsymbol{\Omega} &= \dot{\boldsymbol{\eta}} + \boldsymbol{\Omega}\times\boldsymbol{\eta} \\ \delta\mathbf{q}_i &= \boldsymbol{\xi}_i\times\mathbf{q}_i\end{aligned} \tag{3.28}$$

for $\boldsymbol{\eta}\in\mathbb{R}^3$ and $\boldsymbol{\xi}_i\in\mathbb{R}^3$. The variation of $\dot{\mathbf{q}}_i$ is given by

$$\delta\dot{\mathbf{q}}_i = \dot{\boldsymbol{\xi}}_i\times\mathbf{q}_i + \boldsymbol{\xi}_i\times\dot{\mathbf{q}}_i \tag{3.29}$$

Now, the derivatives of the Lagrangian $\mathscr{L}$ with respect to $\mathbf{X}_Q$, $\dot{\mathbf{X}}_Q$, $\boldsymbol{\Omega}$, $\mathbf{q}_i$ and $\dot{\mathbf{q}}_i$ are given by

$$\begin{aligned}\mathbf{D}_{\mathbf{X}_Q}\mathscr{L} &= \mathbf{M}_{00}g\mathbf{e}_3 \\ \mathbf{D}_{\dot{\mathbf{X}}_Q}\mathscr{L} &= \mathbf{M}_{00}\dot{\mathbf{X}}_Q + \sum_{i=1}^{n}\mathbf{M}_{0i}\dot{\mathbf{q}}_i \\ \mathbf{D}_{\boldsymbol{\Omega}}\mathscr{L} &= \mathbf{I}_Q\boldsymbol{\Omega} \\ \mathbf{D}_{\mathbf{q}_i}\mathscr{L} &= \left(\left(\frac{2(n-i)+1}{2}\right)l_i\mathbf{M}_L + l_i\mathbf{M}_l\right)g\mathbf{e}_3 \\ \mathbf{D}_{\dot{\mathbf{q}}_i}\mathscr{L} &= \dot{\mathbf{X}}_Q^T\mathbf{M}_{0i} + \sum_{j=1}^{n}\mathbf{M}_{ij}\dot{\mathbf{q}}_j\end{aligned} \tag{3.30}$$

Let $\mathfrak{B} = \int_{t_0}^{t_f}\mathscr{L}dt$ be the action integral. Using the derivatives of the Lagrangian in eq. (3.30) and the variation in $\mathbf{X}_Q$ and $\dot{\mathbf{X}}_Q$, the angular velocity of the quadcopter, $\boldsymbol{\Omega}$, and the variation of $\mathbf{q}_i$ and $\dot{\mathbf{q}}_i$ given in eq. (3.28) and (3.29), the variation of the action integral can be written as

$$\begin{aligned}\delta\mathfrak{B} = &\int_{t_0}^{t_f}\left(\mathbf{M}_{00}\dot{\mathbf{X}}_Q + \sum_{i=1}^{n}\mathbf{M}_{0i}\dot{\mathbf{q}}_i\right).\delta\dot{\mathbf{X}}_Q + \mathbf{M}_{00}g\mathbf{e}_3.\delta\mathbf{X}_Q + \mathbf{I}_Q\boldsymbol{\Omega}.\dot{\boldsymbol{\eta}} - \boldsymbol{\eta}.\left(\boldsymbol{\Omega}\times\mathbf{I}_Q\boldsymbol{\Omega}\right)\\ &+\sum_{i=1}^{n}\left(\hat{\mathbf{q}}_i\left(\dot{\mathbf{X}}_Q^T\mathbf{M}_{0i} + \sum_{j=1}^{n}\mathbf{M}_{ij}\dot{\mathbf{q}}_j\right) - \left(\frac{2(n-i)+1}{2}l_i\mathbf{M}_L + l_i\mathbf{M}_l\right)g\hat{\mathbf{e}}_3\mathbf{q}_i\right).\boldsymbol{\xi}_i\\ &+\sum_{i=1}^{n}\hat{\mathbf{q}}_i\left(\dot{\mathbf{X}}_Q^T\mathbf{M}_{0i} + \sum_{j=1}^{n}\mathbf{M}_{ij}\dot{\mathbf{q}}_j\right).\dot{\xi}_i dt\end{aligned} \tag{3.31}$$

Using Integration by parts and using the fact that the variations at the end points vanish [56] results in

$$\begin{aligned}\delta\mathfrak{B} = &\int_{t_0}^{t_f}\left(-\mathbf{M}_{00}\ddot{\mathbf{X}}_Q - \sum_{i=1}^{n}\mathbf{M}_{0i}\ddot{\mathbf{q}}_i + \mathbf{M}_{00}g\mathbf{e}_3\right).\delta\mathbf{X}_Q - \boldsymbol{\eta}.\left(\mathbf{I}_Q\dot{\boldsymbol{\Omega}} + \boldsymbol{\Omega}\times\mathbf{I}_Q\boldsymbol{\Omega}\right)\\ &+\sum_{i=1}^{n}\left(-\hat{\mathbf{q}}_i\left(\mathbf{M}_{0i}\ddot{\mathbf{X}}_Q + \sum_{j=1}^{n}\mathbf{M}_{ij}\ddot{\mathbf{q}}_j\right) - \left(\frac{2(n-i)+1}{2}l_i\mathbf{M}_L + l_i\mathbf{M}_l\right)g\hat{\mathbf{e}}_3\mathbf{q}_i\right).\boldsymbol{\xi}_i dt\end{aligned} \tag{3.32}$$

The virtual work done by the thrust and torques generated by the propellers is given by

$$\mathfrak{W} = \int_{t_0}^{t_f}\mathbf{R}_{BI}^T\mathbf{T}.\delta\mathbf{X}_Q + \boldsymbol{\tau}.\boldsymbol{\eta}\; dt \tag{3.33}$$

where, $\mathbf{T}$ is the total thrust acting on the quadcopter expressed in the body frame (ref. eq. (3.3)) and $\boldsymbol{\tau}$ is the torque acting on the quadcopter as given in eq. (3.4).

According to the Lagrange-d'Alembert principle, the variation of the action integral is equal to the negative of the virtual work done by the external force and moments. Hence,

$$\delta\mathfrak{B} = -\mathfrak{W} \tag{3.34}$$

From eq. (3.32), (3.33) and (3.34), the following equations of motion are obtained for the quadcopter with a payload connected using flexible cable

$$\mathbf{M}_{00}\ddot{X}_Q + \sum_{i=1}^{n}\mathbf{M}_{0i}\mathbf{q}_i = -\mathbf{R}_{BI}^T\mathbf{T} + \mathbf{M}_{00}g\mathbf{e}_3 \tag{3.35}$$

$$\mathbf{I}_Q\dot{\boldsymbol{\Omega}} + \boldsymbol{\Omega}\times\mathbf{I}_Q\boldsymbol{\Omega} = \boldsymbol{\tau} \tag{3.36}$$

$$\hat{\mathbf{q}}_i\left(\mathbf{M}_{0i}\ddot{\mathbf{X}}_Q + \sum_{j=1}^{n}\mathbf{M}_{ij}\ddot{\mathbf{q}}_j\right) = \left(\frac{2(n-i)+1}{2}l_i\mathbf{M}_L + l_i\mathbf{M}_l\right)g\hat{\mathbf{q}}_i e_3 \tag{3.37}$$

Eq. (3.37) can be rewritten to obtain an explicit expression for $\ddot{\mathbf{q}}_i$ as

$$-\hat{\mathbf{q}}_i^2\left(\mathbf{M}_{0i}\ddot{\mathbf{X}}_Q+\sum_{j=1}^{n}\mathbf{M}_{ij}\ddot{\mathbf{q}}_j\right)=-\left(\frac{2(n-i)+1}{2}l_i\mathbf{M}_L+l_i\mathbf{M}_l\right)g\hat{\mathbf{q}}_i^2e_3 \tag{3.38}$$

As $\mathbf{q}_i.\dot{\mathbf{q}}_i=0$,

$$\dot{\mathbf{q}}_i.\dot{\mathbf{q}}_i+\mathbf{q}_i.\ddot{\mathbf{q}}_i=0$$

Using this relation,

$$-\hat{\mathbf{q}}_i^2\ddot{\mathbf{q}}_i=-(\mathbf{q}.\ddot{\mathbf{q}}_i)\,\mathbf{q}_i+(\mathbf{q}_i.\mathbf{q}_i)\,\ddot{\mathbf{q}}_i=(\dot{\mathbf{q}}_i.\dot{\mathbf{q}}_i)\,\mathbf{q}_i+\ddot{\mathbf{q}}_i \tag{3.39}$$

Substituting eq. (3.39) in eq. (3.38), the explicit expression for $\ddot{\mathbf{q}}_i$ is obtained as

$$\mathbf{M}_{ii}\ddot{\mathbf{q}}_i-\hat{\mathbf{q}}_i^2\left(\mathbf{M}_{0i}\ddot{\mathbf{X}}_Q+\sum_{j=1}^{n}\mathbf{M}_{ij}\ddot{\mathbf{q}}_j\right)=-\|\dot{\mathbf{q}}_i\|^2\mathbf{M}_{ii}\mathbf{q}_i-\left(\frac{2(n-i)+1}{2}l_i\mathbf{M}_L+l_i\mathbf{M}_l\right)g\hat{\mathbf{q}}_i^2e_3 \tag{3.40}$$

In the matrix form, eq. (3.35) and (3.40) can be expressed as

$$\mathbf{M}\left(m_Q,m_l,m_L,\mathbf{q}_i\right)\ddot{\mathbf{X}}=\mathfrak{F}\left(m_Q,m_l,m_L,\mathbf{q}_i,l_i,g,\mathbf{R}_{BI},\mathbf{T}\right) \tag{3.41}$$

where, $\mathbf{M}\left(m_Q,m_l,m_L,\mathbf{q}_i\right)=\begin{bmatrix}\mathbf{M}_{00} & \mathbf{M}_{01} & \mathbf{M}_{02} & \cdots & \mathbf{M}_{0n}\\ -\hat{\mathbf{q}}_1^2\mathbf{M}_{10} & \mathbf{M}_{11} & -\mathbf{M}_{12}\hat{\mathbf{q}}_1^2 & \cdots & -\mathbf{M}_{1n}\hat{\mathbf{q}}_1^2\\ -\hat{\mathbf{q}}_2^2\mathbf{M}_{20} & -\mathbf{M}_{21}\hat{\mathbf{q}}_2^2 & \mathbf{M}_{22} & \cdots & -\mathbf{M}_{2n}\hat{\mathbf{q}}_2^2\\ \vdots & \vdots & \vdots & \ddots & \vdots\\ -\hat{\mathbf{q}}_n^2\mathbf{M}_{n0} & -\mathbf{M}_{n1}\hat{\mathbf{q}}_n^2 & -\mathbf{M}_{n2}\hat{\mathbf{q}}_n^2 & \cdots & \mathbf{M}_{nn}\end{bmatrix}$,

$\ddot{\mathbf{X}}=\begin{bmatrix}\ddot{\mathbf{X}}_Q & \ddot{\mathbf{q}}_1 & \ddot{\mathbf{q}}_2 & \cdots & \ddot{\mathbf{q}}_n\end{bmatrix}^T$, and

$\mathfrak{F}\left(m_Q,m_l,m_L,\mathbf{q}_i,l_i,g,\mathbf{R}_{BI},\mathbf{T}\right)=\begin{bmatrix}-\mathbf{R}_{BI}^T\mathbf{T}+\mathbf{M}_{00}g\mathbf{e}_3\\ -\|\dot{\mathbf{q}}_1\|^2\mathbf{M}_{11}\mathbf{q}_1-\left(\frac{2(n-1)+1}{2}l_1\mathbf{M}_L+l_1\mathbf{M}_l\right)g\hat{\mathbf{q}}_1^2e_3\\ -\|\dot{\mathbf{q}}_2\|^2\mathbf{M}_{22}\mathbf{q}_2-\left(\frac{2(n-2)+1}{2}l_2\mathbf{M}_L+l_2\mathbf{M}_l\right)g\hat{\mathbf{q}}_2^2e_3\\ \vdots\\ -\|\dot{\mathbf{q}}_n\|^2\mathbf{M}_{nn}\mathbf{q}_n-\left(\frac{1}{2}l_n\mathbf{M}_L+l_n\mathbf{M}_l\right)g\hat{\mathbf{q}}_n^2e_3\end{bmatrix}$

3.6 Propulsion System Model

The propulsion system consisting of a brushless DC motor and a propeller is modeled in this section. The dynamics of the current drawn by the brushless DC motor, i_m, and the motor shaft speed, ω_m, is expressed as,

$$\dot{i}_m = \frac{1}{L}\left[-Ri_m - K_e\omega_m + v_s\right] \tag{3.42}$$

$$\dot{\omega}_{mi} = \frac{1}{J_p + J_m}\left[K_T i_m - K_f\omega_m - \tau_m\right] \tag{3.43}$$

where, i_m is the current drawn by each of the motor, ω_m is the rotational speed of the motor, R is the phase resistance of the motor, L is the phase inductance of the motor, K_e is the electrical constant of the motor, K_f is the friction constant of the motor, K_T is the torque constant of the motor, $J_p + J_m$ is the combined propeller and motor shaft inertia, τ_m is the torque required to spin the propeller at a given speed ω_i, and v_s is the voltage supplied from the battery [57, 58].

Assuming a linear relation between the voltage supplied and the maximum voltage of the battery, the throttle input is given as,

$$\delta_t = \frac{v_s}{v_{max}}$$

Assuming that the propeller is a self-locking propeller attached directly to the motor without any gear mechanism between them, the propeller speed ω_i is equal to the motor speed ω_m. If the propeller is attached to the motor shaft with a gear mechanism between them, then the propeller speed is expressed in terms of motor speed as,

$$\omega_i = C_g\omega_m$$

where, C_g is the gear ratio of the mechanism. $C_g = 1$ if the propeller is directly attached to the motor shaft.

The thrust generated by a fixed pitch propeller and the torque required to turn the propeller, described in [59], is expressed as,

$$T_i = C_T\rho_{air}\left(\frac{N}{60}\right)^2 D_p^4$$

$$\tau_m = C_m\rho_{air}\left(\frac{N}{60}\right)^2 D_p^5$$

where T_i is the thrust generated by each of the propellers turning at N revolutions per minute; τ_m is the torque required to turn the propeller; C_T is the thrust coefficient; C_m is the torque coefficient; ρ_{air} is the air density and D_p is the propeller diameter.

The thrust coefficient, C_T, and the torque coefficient, C_m, are expressed as,

$$\begin{aligned} C_T &= 0.25\pi^3 \lambda \zeta^2 B_p K_0 \left(\frac{\varepsilon \theta_b - \alpha_0}{\pi A + K_0} \right) \\ C_m &= \frac{1}{8A} \pi^2 C_d \zeta^2 \lambda B_p^2 \end{aligned}$$

where, λ is the correction coefficient; ε is the correction factor due to downwash; B_p is the number of propeller blades; α_0 is the zero-lift angle of attack of the propeller airfoil; A is the aspect ratio; θ_b is the blade angle given by

$$\theta_b = \tan^{-1} \left(\frac{H_p}{\pi D_p} \right)$$

where, H_p is the pitch and D_P is the propeller diameter; and C_d is the drag coefficient (under the assumption that the induced drag has a quadratic dependence upon the local blade lift coefficient) expressed as,

$$C_d = C_{d0} + \frac{\pi A K_0^2}{e} \left(\frac{\varepsilon \theta_b - \alpha_0}{\pi A + K_0} \right)^2$$

where C_{d0} is the zero-lift drag coefficient and e is the Oswald factor.

The values of the parameters used in computing the thrust and the torque coefficients [59] are given in the table 3.1. Note, the in-plane drag due to the propeller motion is accounted for in the propeller motion equation (3.43) which in turn affects the amount of current drawn.

Table 3.1: Parameters to compute the Thrust and Torque coefficients

Parameter	Value
A	$5 \sim 8$
ε	$0.85 \sim 0.95$
λ	$0.7 \sim 0.9$
ζ	$0.4 \sim 0.7$
e	$0.7 \sim 0.9$
C_{d0}	0.015
α_0	$-\frac{\pi}{36} \sim 0$
K_0	6.11

3.7 Endurance and Battery Life

The battery capacity C_b, is defined as [60] the time integral of the current flow out of the battery from the beginning of the current flow $(t = 0)$ to a time (Δt) when it reaches a specified cut-off voltage, and can be expressed as

$$C_b = \int_{\Delta t} i_m \, dt$$

Hence, the endurance is given as,

$$E = \frac{C_b}{i_m}$$

where, i_m is the total current drawn by the motor over certain period. Hence the battery life percentage is computed as,

$$\%\text{Battery-life} = \left(100 - \frac{1}{E}\right) \times 100$$

CHAPTER 4

Extended State Observer Based Active Disturbance Rejection Controller Design

This chapter presents the design procedure for extended state observer based active disturbance rejection controller for the quadcopter with cable suspended payload and a verification into the controller's capacity both to control the states of the quadcopter (position and velocity) and attenuate the swing of the payload. The quadcopter model derived using the Newton-Euler method is used in the design procedure. The disturbance forces due to the oscillations of the payload are augmented in the mathematical model of the quadcopter. The design procedure contains two parts. First, an extended state observer is designed to estimate the disturbances induced in the system due to the oscillation of the payload as an additional state along with the states of the quadcopter. Using the Lyapunov analysis and the convergence rate analysis of the linear systems, it is proved that the errors in the estimates of the quadcopter state and the disturbance due to oscillation of the payload are bounded. Using the estimates of the disturbance, an active disturbance rejection controller is designed to control the trajectory of the quadcopter and attenuate the oscillation of the payload for stable operation.

To design an extended state observer, the concept of "total disturbance" is introduced. The term "total disturbance", its estimation and rejection was presented in [38]. To understand the concept, consider a second-order single input single output (SISO) system

$$\begin{aligned} \dot{y}_1 &= y_2 \\ \dot{y}_2 &= f\left(y_1, y_2, \omega(t), t\right) + bu \\ y &= y_1 \end{aligned} \tag{4.1}$$

where, y is the output which is measured and controlled; u is the control input; $f\left(y_1, y_2, \omega(t), t\right)$ is a function of both states and external disturbances $\omega(t)$ which is to be overcome and is denoted as the "total disturbance".

Treating $y_3 = f\left(y_1, y_2, \omega(t), t\right)$ as an additional state and $G(t) = \dot{f}\left(y_1, y_2, \omega(t), t\right)$, with $G(t)$ unknown, the plant dynamics is given by

$$\begin{aligned} \dot{y}_1 &= y_2 \\ \dot{y}_2 &= y_3 + bu \\ \dot{y}_3 &= G(t) \\ y &= y_1 \end{aligned} \tag{4.2}$$

The objective here is to control the output y using the control signal u. Here the total disturbance $f\left(y_1, y_2, \omega(t), t\right)$ does not need to be known and can be estimated along with the states of the system using an extended state observer with system output $y = y_1$ and control signal u as the input to the observer, which is constructed as follows

$$\begin{aligned} \dot{\hat{y}}_1 &= \hat{y}_2 - \beta_1(\hat{y}_1 - y) \\ \dot{\hat{y}}_2 &= \hat{y}_3 + bu - \beta_2(\hat{y}_1 - y) \\ \dot{\hat{y}}_3 &= -\beta_3(\hat{y}_1 - y) \end{aligned} \tag{4.3}$$

where, $\beta_1 = 3\omega_0$, $\beta_2 = 3\omega_0^2$ and $\beta_3 = \omega_0^3$ are the observer gains; ω_0 is the bandwidth of the observer; $\hat{y}_1$, $\hat{y}_2$ and $\hat{y}_3$ are the estimates of y_1, y_2 and $f\left(y_1, y_2, \omega(t), t\right)$ respectively.

Lemma: *Given that the system modeled by eq. (4.1) is locally observable, the extended state observer in eq. (4.3) for the model in eq. (4.1) ensures that the errors, $\|\hat{y}_i - y_i\| \leq \varepsilon$ are uniformly bounded as, $t \to \infty$, where $\varepsilon > 0$.*

Proof: Let $e_i = \hat{y}_i - y_i$ denote the estimation errors. The error dynamics is then obtained as,

$$\begin{aligned} \dot{e}_1 &= -\beta_1 s_1 + e_2 \\ \dot{e}_2 &= -\beta_2 s_2 + e_3 \\ \dot{e}_3 &= -\beta_3 s_3 - G(t) \end{aligned} \tag{4.4}$$

Choosing all $s_i = e_1$ and defining $\mathbf{e} = \begin{bmatrix} e_1 & e_2 & e_3 \end{bmatrix}^T$, the error dynamics can be written as

$$\dot{\mathbf{e}} = \mathbf{A}\mathbf{e} + \mathbf{B}G \tag{4.5}$$

where, $\mathbf{A} = \begin{bmatrix} -\beta_1 & 1 & 0 \\ -\beta_2 & 1 & 0 \\ -\beta_3 & 0 & 0 \end{bmatrix}$ and $\mathbf{B} = \begin{bmatrix} 0 \\ 0 \\ -1 \end{bmatrix}$. Thus, for all β_1, β_2 and $\beta_3 > 0$, $\mathbf{A}$ is Hurwitz. Thus, if $G(t)$ is bounded, i.e. $\|G(t)\| < \delta$, then the estimation errors, $\mathbf{e}(t)$ are also bounded.

Choosing a candidate Lyapunov function:

$$V = \frac{1}{2}\mathbf{e}^T\mathbf{P}\mathbf{e} \tag{4.6}$$

where, $\mathbf{P} = \mathbf{P}^T > 0$ and computing the derivative of V along the dynamics of eq. (4.5) we obtain,

$$\dot{V} = -\frac{1}{2}\mathbf{e}^T\mathbf{Q}\mathbf{e} + \mathbf{e}^T\mathbf{P}\mathbf{B}\mathbf{G} \tag{4.7}$$

where $\mathbf{Q} = \mathbf{Q}^T > 0$ and $\mathbf{P}\mathbf{A} + \mathbf{A}^T\mathbf{P} = -\mathbf{Q}$. The solution to this Lyapunov equation i.e. $\mathbf{P}$ for a chosen $\mathbf{Q}$ is guaranteed since $\mathbf{A}$ is Hurwitz.

Now,

$$\frac{\alpha}{2}\mathbf{e}^T\mathbf{e} + \frac{1}{2\alpha}\mathbf{G}^T\mathbf{B}^T\mathbf{P}\mathbf{P}\mathbf{B}\mathbf{G} \geq \mathbf{e}^T\mathbf{P}\mathbf{B}\mathbf{G} \tag{4.8}$$

Thus, from eq. (4.7) and eq. (4.8),

$$\begin{aligned} \dot{V} &\leq -\frac{1}{2}\mathbf{e}^T(\mathbf{Q} - \alpha\mathbf{I})\mathbf{e} + \frac{1}{2\alpha}\mathbf{G}^T\mathbf{B}^T\mathbf{P}\mathbf{P}\mathbf{B}\mathbf{G} \\ &\leq -\frac{1}{2}\mathbf{e}^T(\mathbf{Q} - \alpha\mathbf{I})\mathbf{e} + \frac{1}{2\alpha}\|\mathbf{B}^T\mathbf{P}\mathbf{P}\mathbf{B}\|\delta^2 \\ &\leq -\frac{1}{2}\mathbf{e}^T(\mathbf{Q} - \alpha\mathbf{I})\mathbf{e} + \frac{\lambda_{max}^2(\mathbf{P})}{2\alpha}\delta^2 \end{aligned} \tag{4.9}$$

From eq. (2.5) and (4.9),

$$\dot{V} \leq -\left(\frac{\lambda_{min}(\mathbf{Q} - \alpha\mathbf{I})}{\lambda_{max}(\mathbf{P})}\right)V + \frac{\lambda_{max}^2(\mathbf{P})}{2\alpha}\delta^2 \tag{4.10}$$

where $\lambda_{min}(.)$ and $\lambda_{min}(.)$ are the minimum and maximum eigenvalues of $(.)$ respectively. Clearly, the errors converge as per eq. (4.10) to a residual set given by eq. (4.10).

Thus, using the estimate of the total disturbance $\hat{y}_3$ for compensation and choosing u as

$$u = \frac{u_0 - \hat{y}_3}{b}$$

with

$$u_0 = -k_p\left(y_1 - y_{1d}\right) - k_d\left(\dot{y}_1 - \dot{y}_{1d}\right) + \ddot{y}_{1d}$$

where, $k_p > 0$ and $k_d > 0$ are the controller gains and y_{1d} as the desired values for the state y_1. This reduces the plant dynamics to

$$\begin{aligned} \dot{y}_1 &= y_2 \\ \dot{y}_2 &= -k_p\left(y_1 - y_{1d}\right) - k_d\left(\dot{y}_1 - \dot{y}_{1d}\right) + \ddot{y}_{1d} - e_3 \\ y &= y_1 \end{aligned} \tag{4.11}$$

which ensures $\|y_1 - y_{1d}\|$ is bounded (Note, e_3 is bounded as shown previously). This transforms the control problem to that of estimation and disturbance rejection.

Figure 4.1 gives the control architecture of the quadcopter with cable suspended payload us-

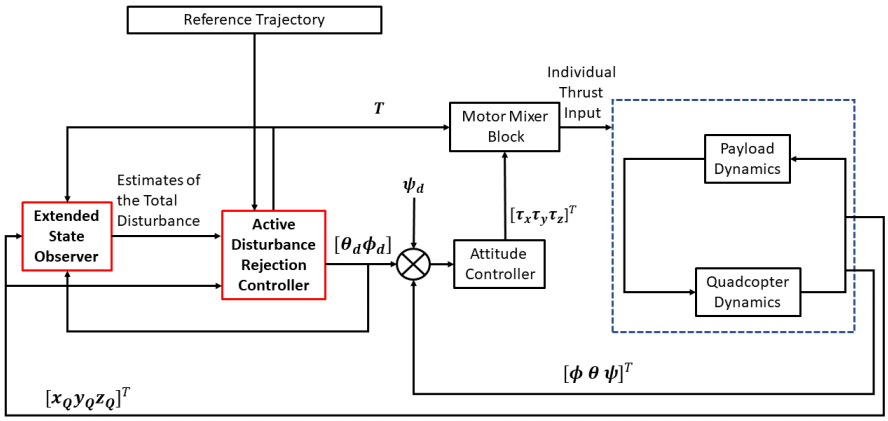

Figure 4.1: Control Architecture of the Quadcopter with Cable Suspended Payload Using Extended State Observer Based Active Disturbance Rejection Controller

ing the extended state observer based active disturbance rejection controller. The system is decoupled into an inner control loop to stabilize the attitude dynamics of the quadcopter and an outer loop to stabilize the translational dynamics of the quadcopter along with the cable suspended payload dynamics. The translational dynamics of the quadcopter is controlled using an active disturbance

rejection controller. An extended state observer is constructed to estimate the disturbances in the translational dynamics of the quadcopter with cable suspended payload. The input to the extended state observer includes the position of the quadcopter expressed in the inertial frame and the control inputs to the quadcopter. The disturbance estimates are used by the active disturbance rejection controller to control the position of the quadcopter while attenuating the payload oscillations. The extended state observer based active disturbance rejection controller design for the quadcopter with cable suspended payload is discussed in detail in the following sections.

4.1 Position Controller

Consider the translational kinematics and dynamics of the quadcopter given in eq. (3.1). Near hovering conditions and small roll, pitch angles and yaw angles, $\cos(\phi) = \cos(\theta) = \cos(\psi) \approx 1$, $\sin(\phi) \approx \phi$, $\sin(\theta) \approx \theta$ and $\sin(\psi) \approx \psi$. This reduces the translational kinematics and dynamics to

$$\begin{aligned}
\dot{x}_Q &= w(\phi\psi + \theta) - v(\psi - \phi\theta) + u \\
\dot{y}_Q &= -w(\phi - \psi\theta) + v(1 + \phi\psi\theta) + u\psi \\
\dot{z}_Q &= w - v\phi - u\theta \\
\dot{u} &= -g\theta + rv - qw + \frac{D_x}{m_Q} + \frac{F_{lx}}{m_Q} \\
\dot{v} &= g\phi + pw - ru + \frac{D_y}{m_Q} + \frac{F_{ly}}{m_Q} \\
\dot{w} &= qu - pv + \frac{T}{m_Q} + \frac{D_z}{m_Q} + \frac{F_{lz}}{m_Q}
\end{aligned} \tag{4.12}$$

where D_x, D_y and D_z are the components of the profile drag acting on the quadcopter along x_b, y_b and z_b axes in the body frame; F_{lx}, F_{ly} and F_{lz} are the components of the force exerted on the quadcopter due to the motion of the payload along x_b, y_b and z_b axes in the body frame; $T = -\sum_{i=1}^{i=4} T_i$ is the total thrust acting on the quadcopter and T_i is the individual thrust generated by each propeller in the body frame.

Let $\boldsymbol{X} = \begin{bmatrix} \boldsymbol{X}_Q^T & \boldsymbol{V}_B^T & \boldsymbol{\Theta}^T & \boldsymbol{\Omega}^T \end{bmatrix}$. The position of the quadcopter along x_i and y_i axes can only be controlled by commanding some desired roll and pitch angles θ_d and ϕ_d. The altitude

of the quadcopter is controlled using the thrust input. Linearizing the translational kinematics and dynamics of the quadcopter given in eq.4.12 at a certain hover position denoted as $\boldsymbol{X_T} = \begin{bmatrix} \overline{X}_Q^T & \mathbf{0}_{1\times3} & \mathbf{0}_{1\times3} & \mathbf{0}_{1\times3} \end{bmatrix}$ where, $\overline{X}_Q \in \mathbb{R}^3$ is any constant position and using the roll, pitch and thrust as control inputs results in

$$\begin{aligned} \dot{\boldsymbol{X}}_Q &= \boldsymbol{V}_B \\ \dot{\boldsymbol{V}}_B &= \boldsymbol{BU} + \boldsymbol{f} \\ \boldsymbol{y} &= \boldsymbol{X}_Q \end{aligned} \tag{4.13}$$

where, $\boldsymbol{U} = \begin{bmatrix} \theta_d & \phi_d & T \end{bmatrix}^T$; $\boldsymbol{B} = \begin{bmatrix} -g & 0 & 0 \\ 0 & g & 0 \\ 0 & 0 & \frac{1}{m_Q} \end{bmatrix}$; $\boldsymbol{f} = \frac{\boldsymbol{D}}{m_Q} + \frac{\boldsymbol{F_l}}{m_Q}$ is the total disturbance and $\boldsymbol{y}$ is the output which is measured and needs to be controlled.

Let $\boldsymbol{x}_1 = \boldsymbol{X}_Q$, $\boldsymbol{x}_2 = \boldsymbol{V}_B$ and treating $\boldsymbol{x}_3 = \boldsymbol{f}$ as an additional state, the state equations for the translational dynamics can be written as,

$$\begin{aligned} \dot{\boldsymbol{x}}_1 &= \boldsymbol{x}_2 \\ \dot{\boldsymbol{x}}_2 &= \boldsymbol{BU} + \boldsymbol{x}_3 \\ \dot{\boldsymbol{x}}_3 &= \boldsymbol{G}(t) \\ \boldsymbol{y} &= \boldsymbol{x}_1 \end{aligned}$$

where, $\dot{\boldsymbol{x}}_3 = \boldsymbol{G}(t)$ is the dynamics of the total disturbance which is unknown.

The extended state observer for the system is now constructed as

$$\begin{aligned} \dot{\hat{\boldsymbol{x}}}_1 &= \hat{\boldsymbol{x}}_2 - \boldsymbol{\beta}_1(\hat{\boldsymbol{x}}_1 - \boldsymbol{y}) \\ \dot{\hat{\boldsymbol{x}}}_2 &= \hat{\boldsymbol{x}}_3 - \boldsymbol{BU} - \boldsymbol{\beta}_2(\hat{\boldsymbol{x}}_1 - \boldsymbol{y}) \\ \dot{\hat{\boldsymbol{x}}}_3 &= -\boldsymbol{\beta}_3(\hat{\boldsymbol{x}}_1 - \boldsymbol{y}) \end{aligned}$$

where, $\boldsymbol{\beta}_1$, $\boldsymbol{\beta}_2$ and $\boldsymbol{\beta}_3$ are the observer gain matrices; $\hat{\boldsymbol{x}}_1$, $\hat{\boldsymbol{x}}_2$ and $\hat{\boldsymbol{x}}_3$ are the estimates of $\boldsymbol{x}_1$, $\boldsymbol{x}_2$ and $\boldsymbol{f}$ respectively.

Using the estimate of the total disturbance $\hat{\boldsymbol{x}}_3$ for compensation and choosing $\boldsymbol{U}$ as

$$\boldsymbol{U} = \boldsymbol{B}^{-1}\left(\boldsymbol{U}_0 - \hat{\boldsymbol{x}}_3\right)$$

with

$$\boldsymbol{U}_0 = -\boldsymbol{K}_p\left(\boldsymbol{x}_1 - \boldsymbol{x}_{1d}\right) - \boldsymbol{K}_d\left(\dot{\boldsymbol{x}}_1 - \dot{\boldsymbol{x}}_{1d}\right) + \ddot{\boldsymbol{x}}_{1d}$$

where, $\boldsymbol{K}_p$ and $\boldsymbol{K}_d$ are the controller gain matrices and $\boldsymbol{x}_{1d}$ is the desired value for $\boldsymbol{x}_1$.

This reduces the plant dynamics to

$$\begin{aligned}
\dot{\boldsymbol{x}}_1 &= \boldsymbol{x}_2 \\
\dot{\boldsymbol{x}}_2 &= -\boldsymbol{K}_p\left(\boldsymbol{x}_1 - \boldsymbol{x}_{1d}\right) - \boldsymbol{K}_d\left(\dot{\boldsymbol{x}}_1 - \dot{\boldsymbol{x}}_{1d}\right) + \ddot{\boldsymbol{x}}_{1d} - \Delta\boldsymbol{x}_3 \\
\boldsymbol{y} &= \boldsymbol{x}_1
\end{aligned}$$

where, $\Delta\boldsymbol{x}_3 = \hat{\boldsymbol{x}}_3 - \boldsymbol{x}_3$. The above ensures $\|\boldsymbol{x}_1 - \boldsymbol{x}_{1d}\|$ is bounded. The rate of decay and other transient characteristics of the tracking errors are controlled by tuning the positive gain matrices $\boldsymbol{K}_p$ and $\boldsymbol{K}_d$.

4.2 Attitude Controller

Using the desired roll, pitch and yaw angles, the desired attitude rates can be computed using a proportional controller as,

$$\begin{aligned}
\dot{\phi}_d &= k_{p,\phi}\left(\phi_d - \phi\right) \\
\dot{\theta}_d &= k_{p,\theta}\left(\theta_d - \theta\right) \\
\dot{\psi}_d &= k_{p,\psi}\left(\psi_d - \psi\right)
\end{aligned}$$

where $k_{p,\phi}$, $k_{p,\theta}$ and $k_{p,\psi}$ are the controller gains.

Using these attitude rates, a PI controller is used to generate the roll, pitch and yaw moment commands as,

$$\begin{aligned}
\tau_{roll} &= k_{p,\dot{\phi}}\left(\dot{\phi}_d - \dot{\phi}\right) + K_{I,\phi}\int_0^t \left(\dot{\phi}_d - \dot{\phi}\right) dt \\
\tau_{pitch} &= k_{p,\dot{\theta}}\left(\dot{\theta}_d - \dot{\theta}\right) + K_{I,\theta}\int_0^t \left(\dot{\theta}_d - \dot{\theta}\right) dt \\
\tau_{yaw} &= k_{p,\dot{\psi}}\left(\dot{\psi}_d - \dot{\psi}\right) + K_{I,\psi}\int_0^t \left(\dot{\psi}_d - \dot{\psi}\right) dt
\end{aligned}$$

where, $k_{p,\dot{\phi}}$, $k_{p,\dot{\theta}}$, $k_{p,\dot{\psi}}$, $K_{I,\phi}$, $K_{I,\theta}$ and $K_{I,\psi}$ are the controller gains.

Using these thrust input, roll, pitch and yaw moment commands, the pulse width modulated (PWM) signals for each motor, M_i is computed as,

$$\begin{aligned}
M_1 &= \left(\frac{\tau_{pitch} - \tau_{yaw}}{2}\right) \times T_{input} + T_{input} \\
M_2 &= \left(\frac{\tau_{roll} + \tau_{yaw}}{2}\right) \times T_{input} + T_{input} \\
M_3 &= \left(\frac{-\tau_{pitch} - \tau_{yaw}}{2}\right) \times T_{input} + T_{input} \\
M_4 &= \left(\frac{-\tau_{roll} + \tau_{yaw}}{2}\right) \times T_{input} + T_{input}
\end{aligned} \tag{4.14}$$

CHAPTER 5

Passivity Based Controller

This chapter presents the design procedure for a passivity based controller for the quadcopter with cable suspended payload and a verification into the controller's capacity both to control the states of the quadcopter (position and velocity) and attenuate the swing of the payload. The quadcopter model derived using the Euler-Lagrange formulation is used in the design procedure. The passivity based controller is an energy based approach. The idea is that every system has certain energy. By controlling this energy, the system can be stabilized [61].

First, the passivity based controller design procedure for the simplified model of the quadcopter with cable suspended payload with the dynamics restricted to the longitudinal plane has been presented. The controller requires the knowledge of the payload swing angle and its higher derivatives (primarily the angular velocity). Assuming that the measurements of the payload swing angle are available, a continuous-discrete Kalman filter is used to estimate the angular velocity of the payload cable. The design procedure is extended to the comprehensive model of the quadcopter with cable suspended payload derived using the Euler-Lagrange formulation.

5.1 Passivity Based Controller Design for a Planner Case

Consider the longitudinal plane restriction of the quadcopter with cable suspended payload in $x_i - z_i$ inertial plane. The simplified model can be obtained by applying constraints on the dynamic model obtained in eq. (3.17). The system dynamics for the quadcopter with cable suspended load in the $x_i - z_i$ plane is given by,

$$\left(m_Q + m_l\right)\left(\ddot{z}_Q + g\right) + m_l l\left(\cos\left(\theta_l\right)\dot{\theta}_l^2 - \sin\left(\theta_l\right)\ddot{\theta}_l\right) = F_z \tag{5.1}$$

$$\left(m_Q + m_l\right)\ddot{x}_Q + m_l l\left(\sin\left(\theta_l\right)\dot{\theta}_l^2 + \cos\left(\theta_l\right)\ddot{\theta}_l\right) = F_x \tag{5.2}$$

$$m_l l^2\ddot{\theta}_l + m_l l\sin\left(\theta_l\right)\ddot{z} - m_l l\cos\left(\theta_l\right)\ddot{x} + m_l g l\sin\left(\theta_l\right) = 0 \tag{5.3}$$

$$I_{yy}\dot{\omega}_y = \tau_y \tag{5.4}$$

where,

$$\begin{aligned} F_x &= \quad T\sin(\theta), \\ F_z &= \quad T\cos(\theta), \end{aligned} \tag{5.5}$$

are the control inputs and T is the sum of all individual thrusts provided by each propeller. Given the combined dynamics of the quadcopter and the cable suspended payload, control

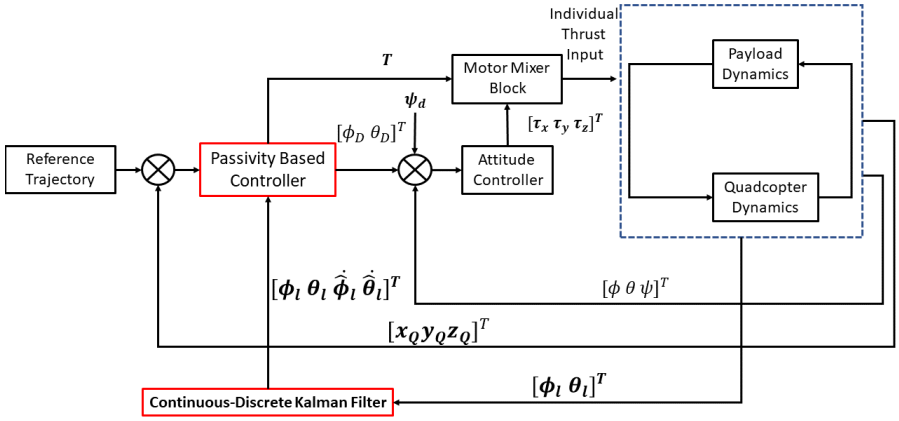

Figure 5.1: Control Architecture of the Quadcopter with Cable Suspended Payload Using Passivity Based Controller

functions are sought such that θ, θ_l, $\dot{\theta}$ and $\dot{\theta}_l \to 0$ as $t \to \infty$ for initial condition disturbances.

In this proposal, we adopt a similar control strategy as in [34] i.e. design a passivity based controller to stabilize the system by controlling the overall energy of the system. Figure 5.1 shows the control architecture of the quadcopter with cable suspended payload in $x_i - z_i$ plane using passivity based controller. The system is decoupled into an inner control loop to stabilize the attitude dynamics of the quadcopter and an outer loop to stabilize the translational dynamics of the quadcopter along with the payload dynamics [62]. The

outer loop is further decoupled to stabilize the altitude of the quadcopter (z_Q), longitudinal position of the quadcopter (x_Q), and the swing of the pendulum.

From eq. (5.1) and (5.2)

$$\ddot{z}_Q = \frac{T\cos(\theta)}{m_Q+m_l} - g - \frac{m_l l}{m_Q+m_l}\left[\cos(\theta_l)\,\dot{\theta}_l^2 + \sin(\theta_l)\,\ddot{\theta}_l\right] \tag{5.6}$$

$$\ddot{x}_Q = \frac{T\sin(\theta)}{m_Q+m_l} - \frac{m_l l}{m_Q+m_l}\left[\sin(\theta_l)\,\dot{\theta}_l^2 - \cos(\theta_l)\,\ddot{\theta}_l\right] \tag{5.7}$$

Using eq. (5.3), (5.6), and (5.7),

$$\ddot{\theta}_l = \frac{-\sin(\theta_l-\theta)\,T}{m_Q l} \tag{5.8}$$

Substituting eq. (5.8) in eq. (5.6) and (5.7),

$$\ddot{z}_Q = \frac{1}{m_Q+m_l}\left[\cos(\theta) + \frac{m_l}{2m_Q}\left(\cos(\theta) - \cos(\theta-2\theta_l)\right)\right]T - g - \frac{m_l l\cos(\theta_l)\,\dot{\theta}_l^2}{m_Q+m_l}$$

$$\ddot{x}_Q = -\frac{m_l l\sin(\theta_l)\,\dot{\theta}_l^2}{m_Q+m_l} + \frac{1}{m_Q+m_l}\left[\sin(\theta) + \frac{m_l}{2m_Q}\left(\sin(\theta) - \sin(\theta-2\theta_l)\right)\right]T$$

For hover conditions and small pitch angles of the quadcopter, the attitude dynamics can be approximated using $\cos(\theta)\approx 1$ and $\sin(\theta)\approx\theta$ and treating θ as the control input θ_d results into following dynamics for $\ddot{x}_Q$ and $\ddot{z}_Q$

$$\ddot{z}_Q = \frac{1}{m_Q+m_l}\left[1 + \frac{m_l}{2m_Q}\left(1-\cos(2\theta_l) - \theta_d\sin(2\theta_l)\right)\right]T - g - \frac{m_l l\cos(\theta_l)\,\dot{\theta}_l^2}{m_Q+m_l}$$

$$\ddot{x}_Q = -\frac{m_l l\sin(\theta_l)\,\dot{\theta}_l^2}{m_Q+m_l} + \frac{\theta_d}{m_Q+m_l} + \frac{1}{m_Q+m_l}\left[\frac{m_l}{2m_Q}\left(\theta_d - \theta_d\cos(2\theta_l) - \sin(2\theta_l)\right)\right]T$$

Near hovering condition, $T\approx\left(m_Q+m_l\right)g$ and longitudinal dynamics can only be controlled by θ_d. This results into the following for $\ddot{x}_Q$,

$$\ddot{x}_Q = \theta_d\left[g + \frac{gm_l}{2m_Q}\left(1-\cos(2\theta_l)\right)\right] - \frac{m_l l\sin(\theta_l)\,\dot{\theta_l}^2}{m_l+m_Q} - \frac{m_l g\sin(2\theta_l)}{2m_Q}$$

Thus, choosing the control inputs θ_d and T as,

$$\begin{aligned}
\theta_d &= \frac{u_x + \frac{m_l l \sin(\phi_l) \dot{\phi_l}^2}{m_l + m_Q} + \frac{m_l g \sin(2\phi_l)}{2m_Q}}{\left[g + \frac{g m_l}{2m_Q} \left(1 - \cos\left(2\phi_l\right) \right) \right]} \\
T &= \frac{\left(m_Q + m_l\right) \left(g + \frac{m_l l \cos(\phi_l) \dot{\phi_l}^2}{m_Q + m_l} + u_z \right)}{\left[1 + \frac{m_l}{2m_Q} \left(1 - \cos\left(2\phi_l\right) - \theta_d \sin\left(2\phi_l\right) \right) \right]}
\end{aligned}$$

and with

$$\begin{aligned}
u_z &= -k_p^z (z_Q - z_d) - k_d^z \left(\dot{z}_Q - \dot{z}_d \right) + \ddot{z}_d \\
u_x &= -k_p^x (x_Q - z_d) - k_d^x \left(\dot{x}_Q - \dot{x}_d \right) + \ddot{x}_d
\end{aligned}$$

the closed loop position tracking dynamics of the quadcopter are reduced to,

$$\begin{aligned}
\ddot{z}_Q &= -k_p^z (z_Q - z_d) - k_d^z \left(\dot{z}_Q - \dot{z}_d \right) + \ddot{z}_d \\
\ddot{x}_Q &= -k_p^x (x_Q - x_d) - k_d^x \left(\dot{x}_Q - \dot{x}_d \right) + \ddot{x}_d
\end{aligned}$$

which ensures $x_Q \to x_d$ and $z_Q \to z_d$. The rate of decay and other transient characteristics of the tracking errors are controlled by tuning the positive gains k_p^z, k_d^z, k_p^x, and k_d^x.

The pitch controller can be designed using the pitch tracking error e_θ, which is defined as,

$$e_\theta = \theta - \theta_d$$

and

$$\dot{e}_\theta = \dot{\theta} - \dot{\theta}_d$$

We seek a very tightly controlled pitch loop, so the pitch errors are prescribed to converge to zero exponentially with a decay rate of λ_θ. Thus, the pitch error dynamics takes the form,

$$\dot{e}_\theta = -\lambda_\theta e_\theta$$

The desired pitch rate

$$\omega_{yd} = -\lambda_\theta e_\theta + \dot{\theta}_d$$

ensures that $e_\theta \to 0$, as $t \to \infty$.

The pitch rate error (e_ω) is then obtained as,

$$e_\omega = \omega_y - \omega_{yd}$$

The pitch rate errors are also prescribed to converge to zero exponentially with a decay rate of λ_ω. Thus, the desired pitch rate error dynamics takes the form,

$$\dot{e}_\omega = -\lambda_\omega e_\omega$$

Thus, $\dot{\omega}_y - \dot{\omega}_{yd} = -\lambda_\omega e_\omega$ and the control law for the pitch dynamics is determined as,

$$\tau_y = I_{yy}\left(-\lambda e_\omega + \dot{\omega}_{yd}\right)$$

It is noted that the above procedure is a nested backstepping process [63].

Clearly, the passivity based controller requires several higher derivatives of the payload swing angle. The measurement of all swing angle and all its higher order derivatives is a challenging task. Specifically at the hover state, the dynamics of the swinging payload can be assumed to be equivalent to the dynamics of a simple pendulum linearized about some angle θ_l, is given by,

$$\ddot{\theta}_l \approx -\frac{g}{l}\theta_l$$

Thus, if the swing angle is measured, using this approximation, the angular velocity as well as the acceleration of the swinging payload can be estimated. Also, under these assumptions all higher order derivatives are successively obtained. Assuming that the angle measurements for the cable are available, the angular velocity of the swinging cable can be estimated using a Continuous-Discrete Kalman Filter (CDKF) driven by the cable angle measurements.

In our specific implementation, the propagation is continuous while the measurement updates happen at discrete instants (every 0.01 s). The CDKF utilizes the simplified one degree-of-freedom dynamics

$$\ddot{\theta}_l = -\frac{g}{l}\theta_l + w_\theta(t)$$

where $w_\theta(t)$ is a zero mean white noise process with covariance 0.25 rad^2/s^4.
The measurement equation is

$$\tilde{\theta}_l = \theta_l + v_\theta(t)$$

The measurement error $v_\theta(t)$ is also assumed to be a zero-mean white noise process with variance 0.01 rad^2. Additionally, $w_\theta(t)$, and $v_\theta(t)$ are assumed to be uncorrelated. The derivation of the CDKF is straightforward and can be found in [64]. The mechanism of the filter approach is tabulated in table D.1.

5.2 Passivity Based Controller Design for the Comprehensive Quadcopter Model with Cable Suspended Payload

The design procedure described in section 5.1 for a simplified case when the dynamics of the quadcopter with cable suspended payload were restricted to the longitudinal plane is extended for the comprehensive dynamic model.

The translational dynamics of the quadcopter with cable suspended payload given in eq. (3.17) can be written as

$$\ddot{x}_Q = \frac{F_x}{m_Q + m_l} + f_x\left(\phi_l, \theta_l, \dot{\phi}_l, \dot{\theta}_l, \ddot{\phi}_l, \ddot{\theta}_l\right) \tag{5.9}$$

$$\ddot{y}_Q = \frac{F_y}{m_Q + m_l} + f_y\left(\phi_l, \theta_l, \dot{\phi}_l, \dot{\theta}_l, \ddot{\phi}_l, \ddot{\theta}_l\right) \tag{5.10}$$

$$\ddot{z}_Q = \frac{F_z}{m_Q + m_l} - g + f_z\left(\phi_l, \theta_l, \dot{\phi}_l, \dot{\theta}_l, \ddot{\phi}_l, \ddot{\theta}_l\right) \tag{5.11}$$

where F_x, F_y and F_z are the control inputs to the quadcopter given in eq. (3.18). Using eq. (5.9), (5.10), (5.11), the dynamics of the payload from eq. (3.17) can be written as

$$\ddot{\phi}_l = \frac{f_{\phi_l 1}(\phi,\theta,\psi,\phi_l,\theta_l)\,T}{m_Q l} + f_{\phi_l 2}\left(\phi_l,\theta_l,\dot{\phi}_l,\dot{\theta}_l\right) \tag{5.12}$$

$$\ddot{\theta}_l = \frac{f_{\theta_l 1}(\phi,\theta,\psi,\phi_l,\theta_l)\,T}{m_Q l} + f_{\theta_l 2}\left(\phi_l,\theta_l,\dot{\phi}_l,\dot{\theta}_l\right) \tag{5.13}$$

For hover conditions and small roll, pitch and yaw angles of the quadcopter, the attitude dynamics can be approximated using $\cos(\phi)\approx 1$, $\cos(\theta)\approx 1$, $\cos(\psi)\approx 1$, $\sin(\phi)\approx \phi$, $\sin(\theta)\approx\theta$ and $\sin(\psi)\approx\psi$. Now, if the desired yaw angle is fixed to zero, then the dynamics of the quadcopter along x and y axes can only be controlled by controlling the roll and pitch angles. Thus θ and ϕ are treated as the control inputs θ_d and ϕ_d. Also, near hovering condition, $T\approx\left(m_Q+m_l\right)g$. Using these assumptions and substituting eq. (5.12) and (5.13) in eq. (5.9), (5.10) and (5.11) results into following dynamics for $\ddot{x}_Q$, $\ddot{y}_Q$ and $\ddot{z}_Q$

$$\ddot{x}_Q = g\theta_d f_{x1}\left(m_Q,m_l,\psi,\phi_l,\theta_l\right) + f_{x2}\left(m_Q,m_l,g,\phi,\psi,\phi_l,\theta_l,\dot{\phi}_l,\dot{\theta}_l\right) \tag{5.14}$$

$$\ddot{y}_Q = g\phi_d f_{y1}\left(m_Q,m_l,\psi,\phi_l,\theta_l\right) + f_{y2}\left(m_Q,m_l,g,\theta,\psi,\phi_l,\theta_l,\dot{\phi}_l,\dot{\theta}_l\right) \tag{5.15}$$

$$\ddot{z}_Q = \frac{T}{m_Q+m_l} - g + f_{z1}\left(m_Q,m_l,g,\phi,\theta,\psi,\phi_l,\theta_l\right) + f_{z2}\left(m_Q,m_l,\phi_l,\theta_l,\dot{\phi}_l,\dot{\theta}_l\right) \tag{5.16}$$

Thus, choosing the control inputs θ_d, ϕ_d and T as,

$$\theta_d = \frac{u_x - f_{x2}\left(m_Q,m_l,g,\phi,\psi,\phi_l,\theta_l,\dot{\phi}_l,\dot{\theta}_l\right)}{g f_{x1}\left(m_Q,m_l,\psi,\phi_l,\theta_l\right)}$$

$$\phi_d = \frac{u_y - f_{y2}\left(m_Q,m_l,g,\theta,\psi,\phi_l,\theta_l,\dot{\phi}_l,\dot{\theta}_l\right)}{g f_{y1}\left(m_Q,m_l,\psi,\phi_l,\theta_l\right)}$$

$$T = \left(m_Q+m_l\right)\left(u_z + g - f_{z1}\left(m_Q,m_l,g,\phi,\theta,\psi,\phi_l,\theta_l\right) - f_{z2}\left(m_Q,m_l,\phi_l,\theta_l,\dot{\phi}_l,\dot{\theta}_l\right)\right)$$

and with

$$u_x = -k_p^x(x_Q - x_d) - k_d^x\left(\dot{x}_Q - \dot{x}_d\right) + \ddot{x}_d$$

$$u_y = -k_p^y(y_Q - y_d) - k_d^y\left(\dot{y}_Q - \dot{y}_d\right) + \ddot{y}_d$$

$$u_z = -k_p^z(z_Q - z_d) - k_d^z\left(\dot{z}_Q - \dot{z}_d\right) + \ddot{z}_d$$

and x_d, y_d and z_d as the desired quadcopter position, the closed loop position tracking dynamics of the quadcopter is reduced to,

$$\begin{aligned}
\ddot{x}_Q &= -k_p^x(x_Q - x_d) - k_d^x\left(\dot{x}_Q - \dot{x}_d\right) + \ddot{x}_d \\
\ddot{y}_Q &= -k_p^y(y_Q - y_d) - k_d^y\left(\dot{y}_Q - \dot{y}_d\right) + \ddot{y}_d \\
\ddot{z}_Q &= -k_p^z(z_Q - z_d) - k_d^z\left(\dot{z}_Q - \dot{z}_d\right) + \ddot{z}_d
\end{aligned}$$

which ensures $x_Q \to x_d$, $y_Q \to y_d$ and $z_Q \to z_d$. The rate of decay and other transient characteristics of the tracking errors are controlled by tuning the positive gains k_p^x, k_d^x, k_p^y, k_d^y, k_p^z and k_d^z.

The attitude of the quadcopter is controlled using the backstepping controller which is designed using the procedure described in section 5.1. Again, the passivity based controller designed for the comprehensive quadcopter model with cable suspended payload requires the knowledge of the payload cable swing angles and its angular velocity. At the hover state, the dynamics of the swinging payload can be assumed to be equivalent to the dynamics of a spherical pendulum linearized about some ϕ_l and θ_l and is given by

$$\begin{aligned}
\ddot{\phi}_l &\approx -\frac{g}{l}\phi_l \\
\ddot{\theta}_l &\approx -\frac{g}{l}\theta
\end{aligned}$$

Thus, assuming that the swing angles of the payload cable are measured, a Continuous-Discrete Kalman Filter driven by the cable angle measurements is used to estimate the angular velocity of the payload cable angle.

The continuous-discrete Kalman filter utilizes simplified dynamics of the spherical pendulum given as

$$\begin{aligned}
\ddot{\phi}_l &= -\frac{g}{l}\phi_l + w_\phi(t) \\
\ddot{\theta}_l &= -\frac{g}{l}\theta_l + w_\theta(t)
\end{aligned}$$

where $w_\phi(t)$ and $w_\theta(t)$ are assumed to be zero mean white noise processes with covariance 0.25 rad^2/s^4.

The measurement equations are

$$\tilde{\phi}_l = \phi_l + v_\phi(t)$$

$$\tilde{\theta}_l = \theta_l + v_\theta(t)$$

The measurement errors $v_\phi(t)$ and $v_\theta(t)$ are also assumed to be a zero-mean white noise processes with variance 0.01 rad^2. Additionally, $w_\phi(t)$, $v_\phi(t)$, $w_\theta(t)$, and $v_\theta(t)$ are assumed to be uncorrelated.

CHAPTER 6

Simulation Results

This chapter presents the implementation of the passivity based controller and the extended state observer based active disturbance rejection controller in the simulation environment developed in chapter 2. A comparison between the two controllers is performed first. The passivity based controller is implemented on the mathematical model developed using the Euler-Lagrange formulation (ref. subsection 3.4). The extended state observer based active disturbance rejection controller is implemented on the mathematical model of the quadcopter developed using the Newton-Euler approach (ref. subsection 3.1 and 3.3). Furthermore, the efficacy of the extended state observer based active disturbance rejection controller is demonstrated in the simulations using the mathematical model of the quadcopter attached to a payload using a flexible cable modeled (ref. subsection 3.5).

6.1 Comparison Between the Performance of the Passivity Based Controller and the Extended State Observer Based Active Disturbance Rejection Controller

The simulation environment developed in the chapter 2 is used to demonstrate the performance of the extended state observer based active disturbance rejection controller and the passivity based controller. The specifications of the propulsion system and the mass, inertia and geometric parameters of the quadcopter model used in the simulation are tabulated in table A.1. The observer and controller gains are tabulated in table B.1. The following cases are used to compare the performance of the controllers

1. Quadcopter in Hover Mode and the Payload is Perturbed

2. Quadcopter Moving with a Constant Speed along the inertial x axis is commanded to go in the Hover Mode

Finally, the controller performance for both the extended state observer and the passivity based controller under reduced maximum available thrust will be demonstrated to show that the desired control is well within the limits of the original available control authority.

6.1.1 Case 1: Quadcopter in Hover Mode and the Payload is Perturbed

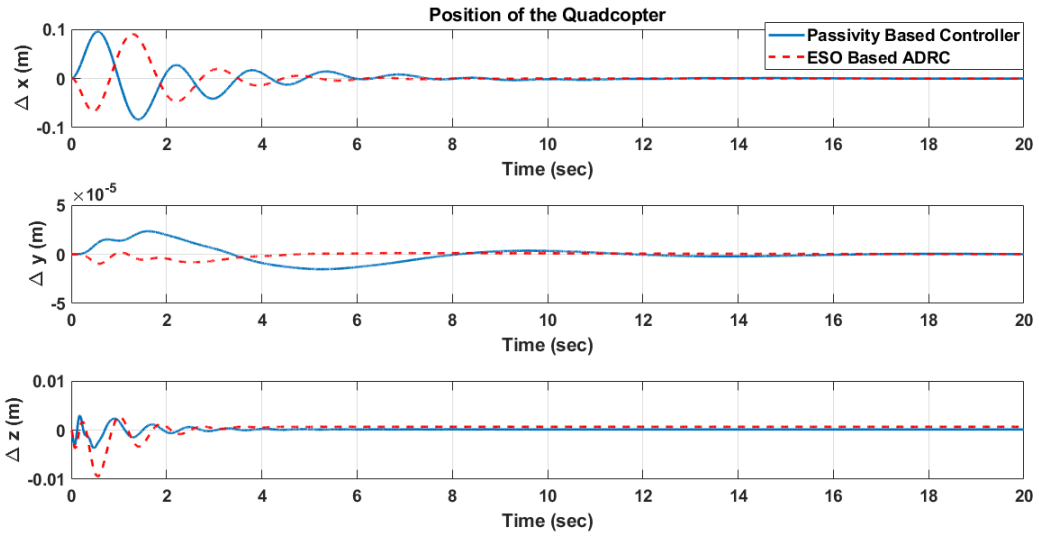

Figure 6.1: Position of the quadcopter

The quadcopter is in a hovering state at the start of the simulation. The payload cable angle, θ_l, at the start of the simulation is 30°. Figures 6.1, 6.2 and 6.3 compares the performance of the controllers. At the start of the simulation, there are disturbances introduced in the system due to the oscillations of the payload. As shown in figures 6.1, 6.2 and 6.3, the controllers try to reject these disturbances while trying to maintain the inertial position of the quadcopter and damp out the oscillations of the cable slung payload. From figure 6.3,

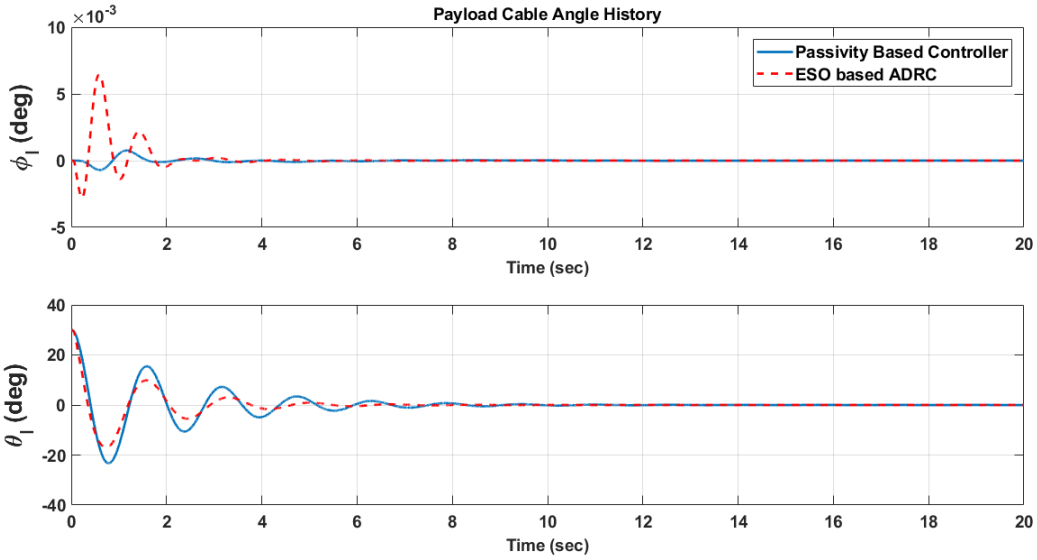

Figure 6.2: Payload Cable angle history

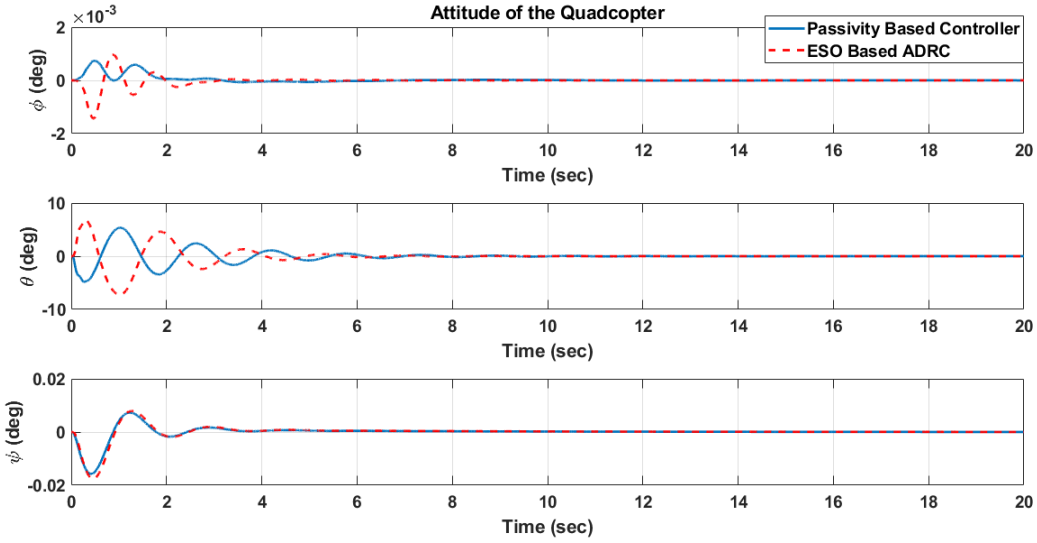

Figure 6.3: Attitude of the quadcopter

it can be observed that the attitude controller tries to control the pitch angle of the quadcopter, thus providing necessary force to control the longitudinal position of the quadcopter (position along inertial x axis) and damp the oscillations of the payload. The pitch angle has an oscillatory behavior and it decays to zero as the payload oscillations decay and the

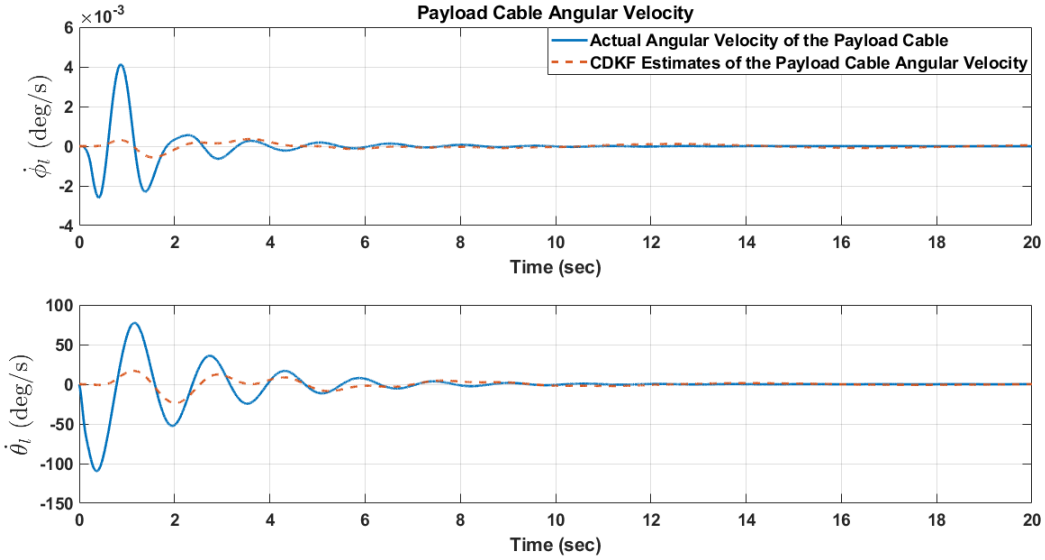

Figure 6.4: Comparison between the Actual and the Estimated Angular Velocity of the Payload Cable Using Kalman Filter

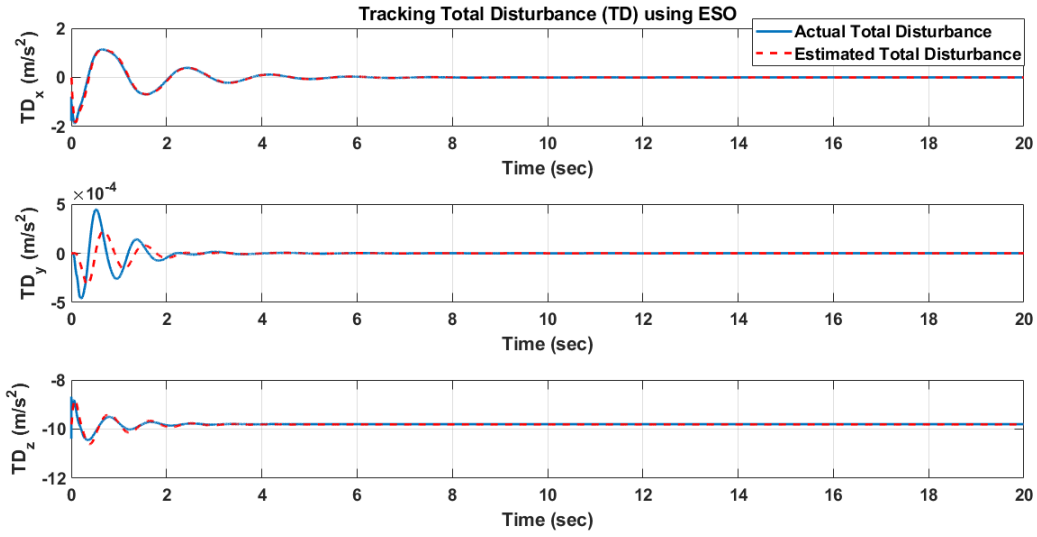

Figure 6.5: Comparison between the Actual and the Estimated Total Disturbance Using Extended State Observer

quadcopter goes back to the initial hover pose.

From the above results, it can be deduced that the extended state observer based ac-

tive disturbance rejection controller gives a better performance by damping the oscillations of the payload and controlling the inertial position of the quadcopter faster than the passivity based controller. It can be seen from figure 6.5 that the extended state observer is able to track the total disturbances TD_x, TD_y, and TD_z induced in the system in x, y, and z direction respectively in the body frame. These estimates are used by the active disturbance rejection controller to control the position of the quadcopter and damp the oscillations of the slung payload. The total disturbance in the z direction (TD_z) converges to a value of -9.81 m/s^2 as the system is stabilized indicates that the only disturbance acting on the system is the acceleration due to gravity as the quadcopter goes back to the desired hover position.

The passivity based controller requires the knowledge of the payload swing angle and its higher derivatives. Assuming the payload to have the dynamics of a spherical pendulum and the measurements of the payload cable angle are available, a continuous-discrete Kalman filter was used to estimate the angular velocity of the payload cable. It can be seen from figure 6.4 that the continuous-discrete Kalman filter is able to track the angular velocity states of the payload cable and the passivity based controller provides a reasonable performance.

6.1.2 Case 2: Quadcopter Moving with a Constant Speed along the inertial x axis is commanded to go in the Hover Mode

At the start of the simulation, the quadcopter is in the hover mode and the payload is in a stable configuration. The quadcopter is commanded to follow a straight line trajectory along the inertial x axis with a constant speed of 10.8 kmph $\left(3 \text{ m/s}\right)$ and fixed altitude. At 50 s, the quadcopter is commanded to go back to the hover mode. Figures 6.6, 6.7, and 6.8 compare the performance of the passivity based controller and the extended state observer

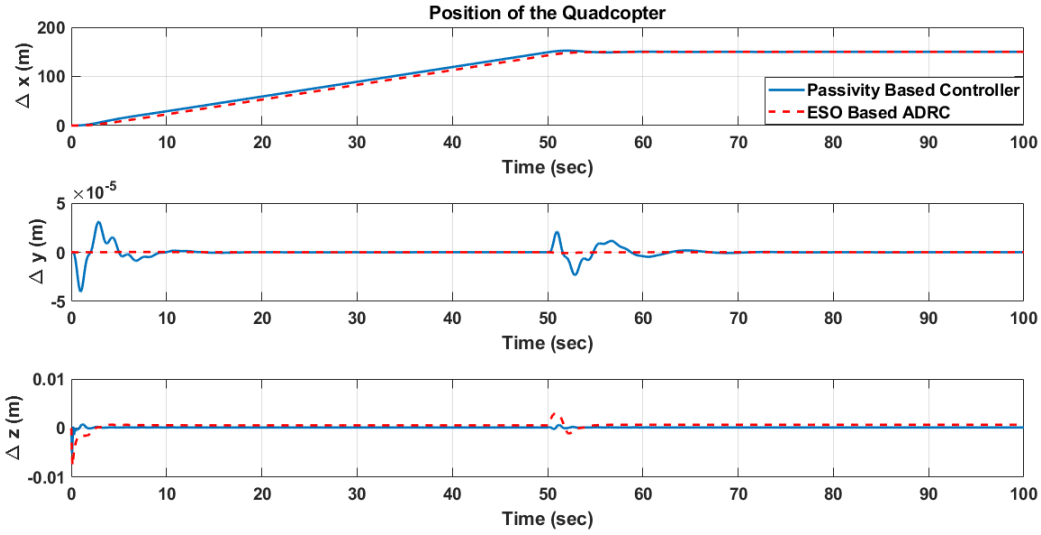

Figure 6.6: Position of the quadcopter

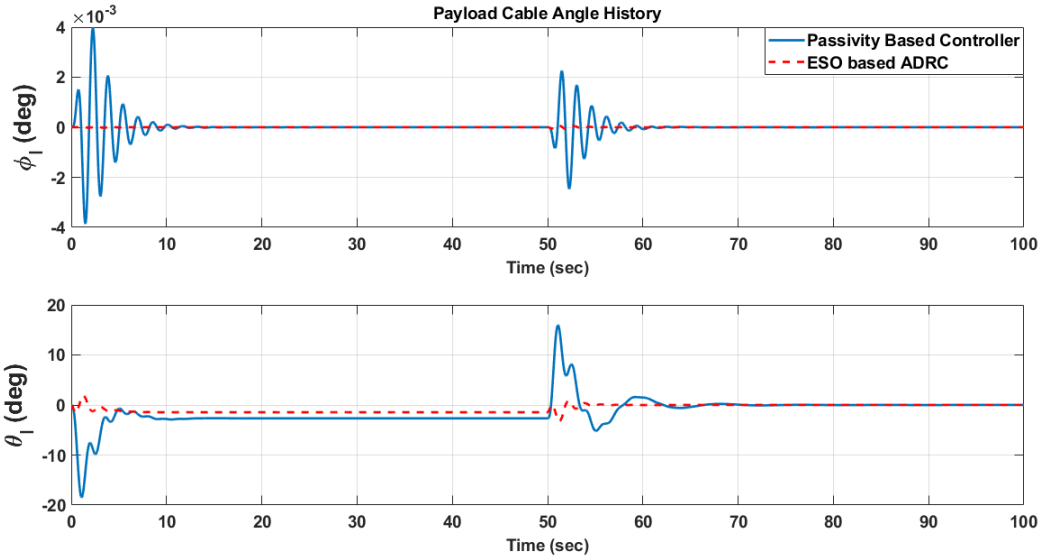

Figure 6.7: Payload Cable angle history

based active disturbance rejection controller. From figure 6.6, it can be observed that the controllers are able to maintain the quadcopter altitude as well as the trajectory along the inertial x axis and the desired position when commanded to go back to the hover mode. From figure 6.7, it can be seen that the payload is perturbed due to changes in the quad-

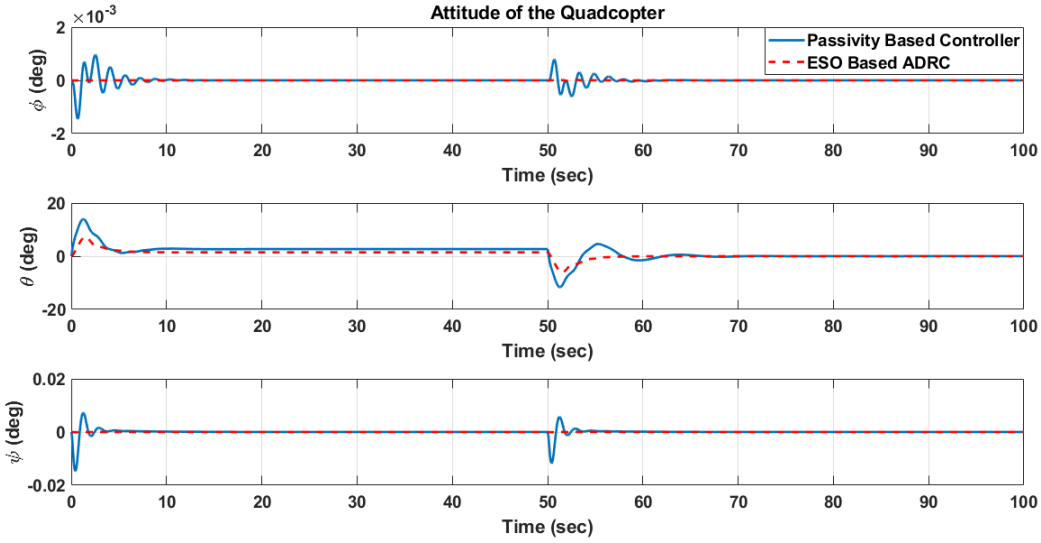

Figure 6.8: Attitude of the quadcopter

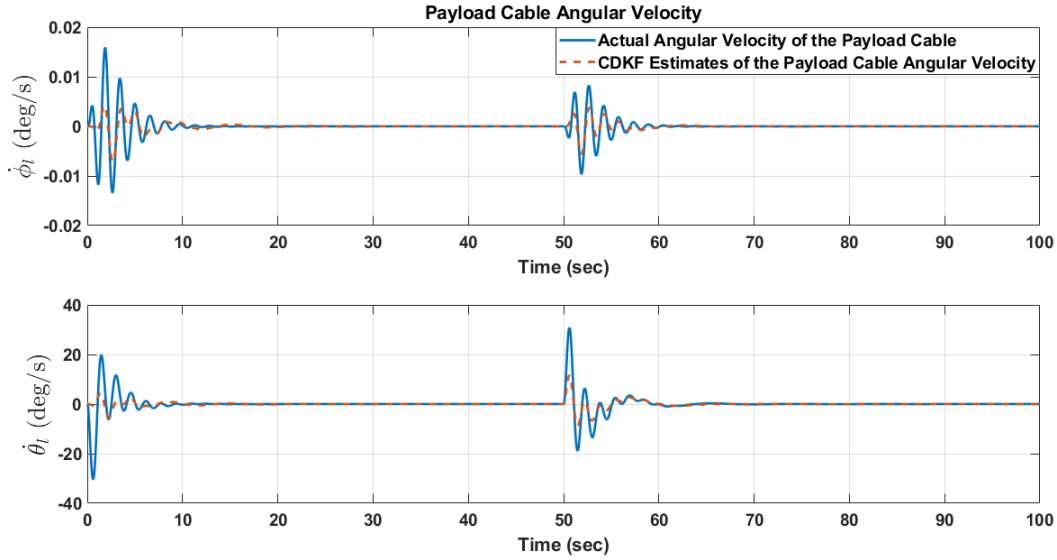

Figure 6.9: Comparison between the Actual and the Estimated Angular Velocity of the Payload Cable Using Kalman Filter

copter states at the start of the simulation and the controllers stabilize the payload while the quadcopter is in motion. The payload is perturbed again when the quadcopter goes back to the hover mode and the controllers are able to stabilize the system. The quadcopter

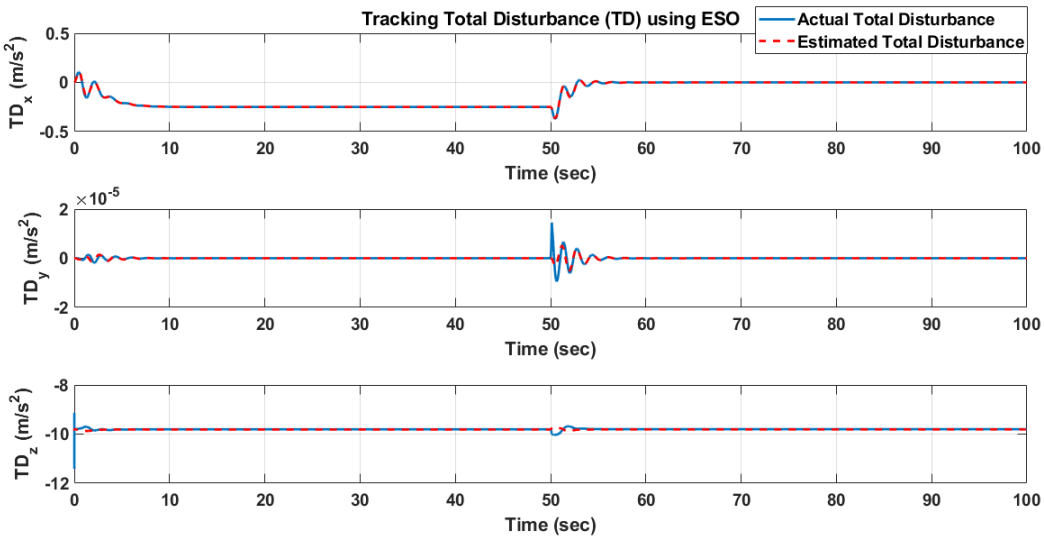

Figure 6.10: Comparison between the Actual and the Estimated Total Disturbance Using Extended State Observer

position and velocity along the inertial x axis is maintained by controlling the pitch angle. From figure 6.8, it is observed that the pitch angle has a decaying oscillatory behavior as the controllers try to maintain the constant speed straight line trajectory of the quadcopter while attenuating the oscillations of the payload due to the changes in the quadcopter states. When the quadcopter is commanded to go back to the hover mode at 50 s, the controllers try to maintain the position of the quadcopter along the inertial x and attenuate the oscillations of the payload due to the changes in the quadcopter states using the pitch angle. A decaying oscillatory behavior in the pitch angle of the quadcopter is observed again as the payload oscillations decay and quadcopter goes back to the desired hover pose.

It can be seen that the extended state observer based active disturbance rejection controller gives a better performance by damping the oscillations of the payload and tracking the position of the quadcopter faster than the passivity based controller. It can be seen from figure 6.10 that the extended state observer is able to track the total disturbance. These estimates are used by the active disturbance rejection controller to control the position

of the quadcopter and damp the oscillations of the slung payload. Note, the wind speed $V_w = 0$ kmph for the simulation case but the drag force acting on the quadcopter $\mathbf{D} \neq 0$. Hence, the total disturbance in the x direction (TD_x) in figure (6.10) has a non-zero value even when the payload oscillations are damped out and the quadcopter is moving along a straight line with a constant speed. Again, the total disturbance along the z direction (TD_z), converges to a value of -9.81 m/s^2, indicating that the disturbance force acting on the system when the quadcopter is either moving along the inertial x axis with constant speed or when the quadcopter goes back in the hover mode and the cable slung payload is in the equilibrium position, is due to the acceleration due to gravity.

It can be seen from figure 6.9 that the continuous-discrete Kalman filter is able to estimate the angular velocity states of the payload cable and the passivity based controller still provides a reasonable performance.

6.1.3 Controller Performance under Reduced Maximum Available Thrust

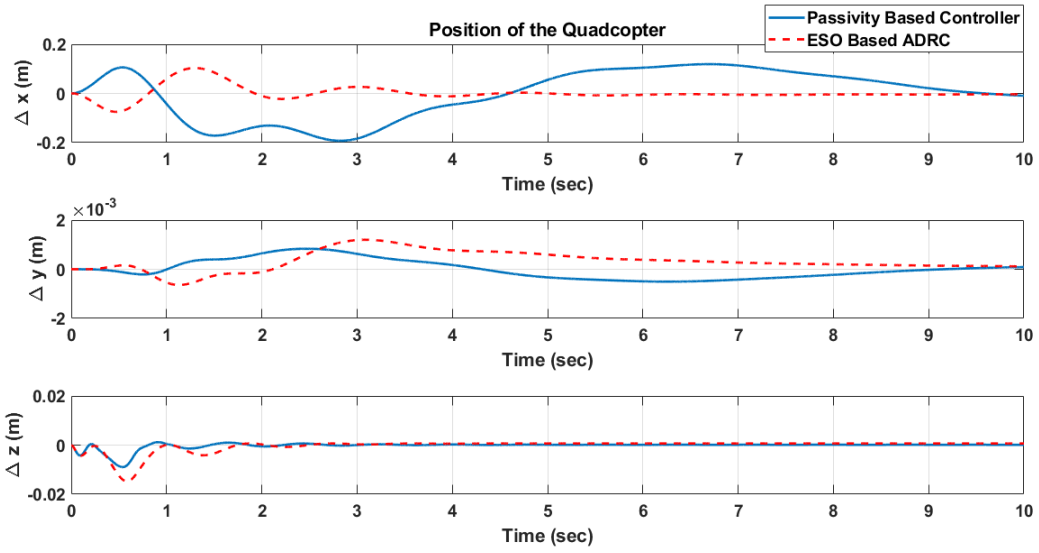

Figure 6.11: Position of the quadcopter

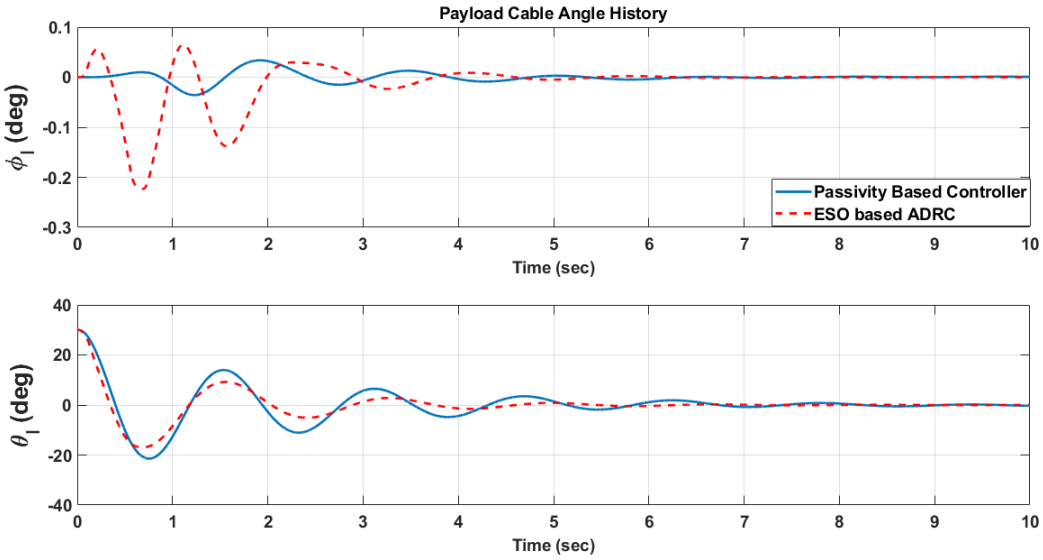

Figure 6.12: Payload Cable angle history

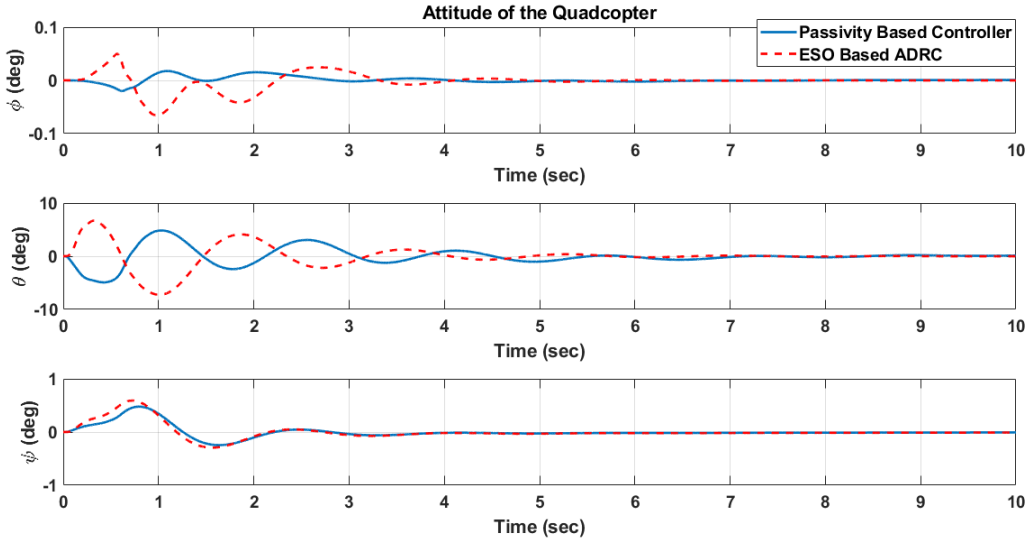

Figure 6.13: Attitude of the quadcopter

The maximum thrust available for a given propeller and motor tabulated in table (A.1) is 9 N. The controller performance were compared for the case when maximum available

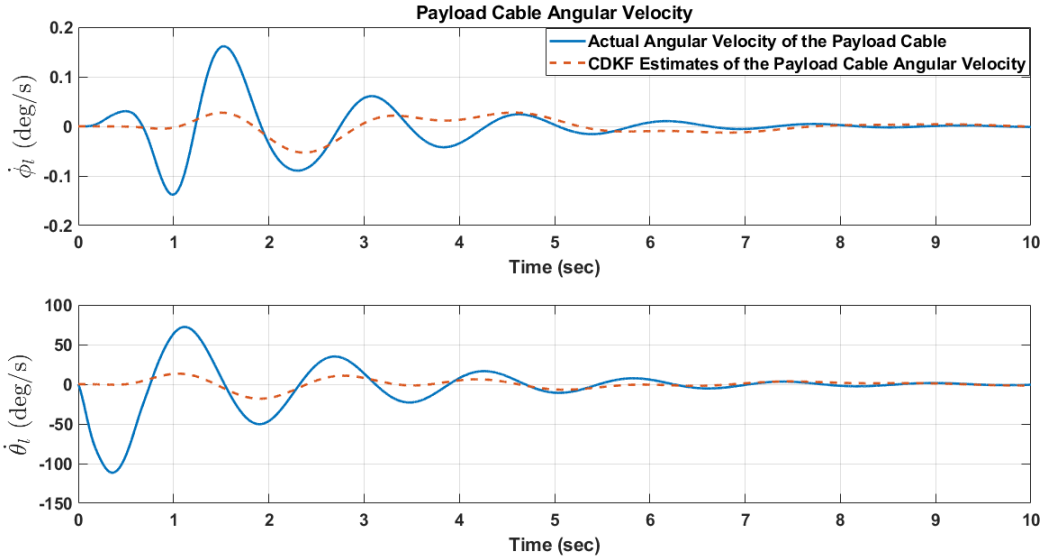

Figure 6.14: Comparison between the Actual and the Estimated Angular Velocity of the Payload Cable Using Kalman Filter

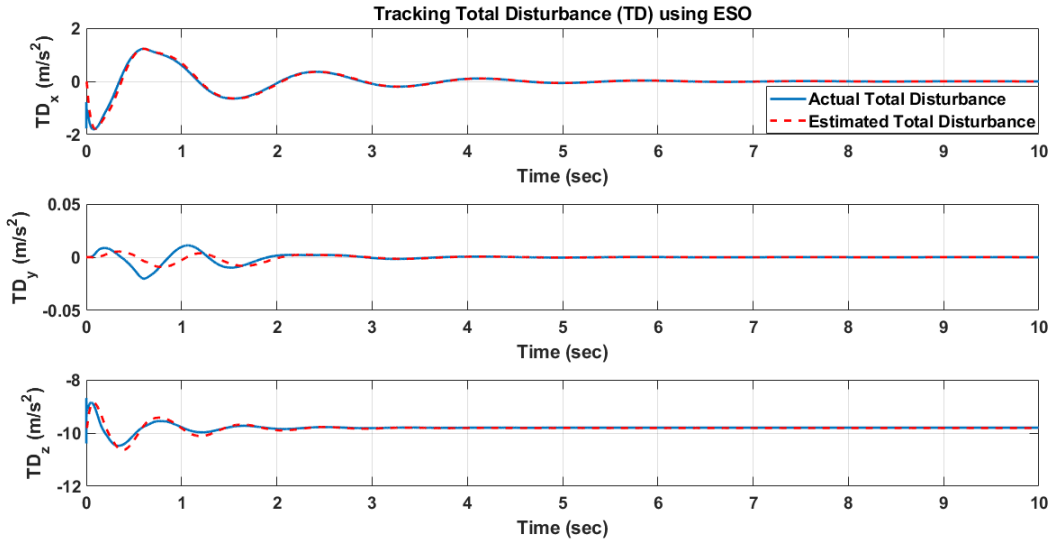

Figure 6.15: Comparison between the Actual and the Estimated Total Disturbance Using Extended State Observer

thrust is reduced by 50%. Initially, the quadcopter is in a hovering state at the start of the simulation. The payload cable angle, θ_l, at the start of the simulation is 30°. Figures 6.11,

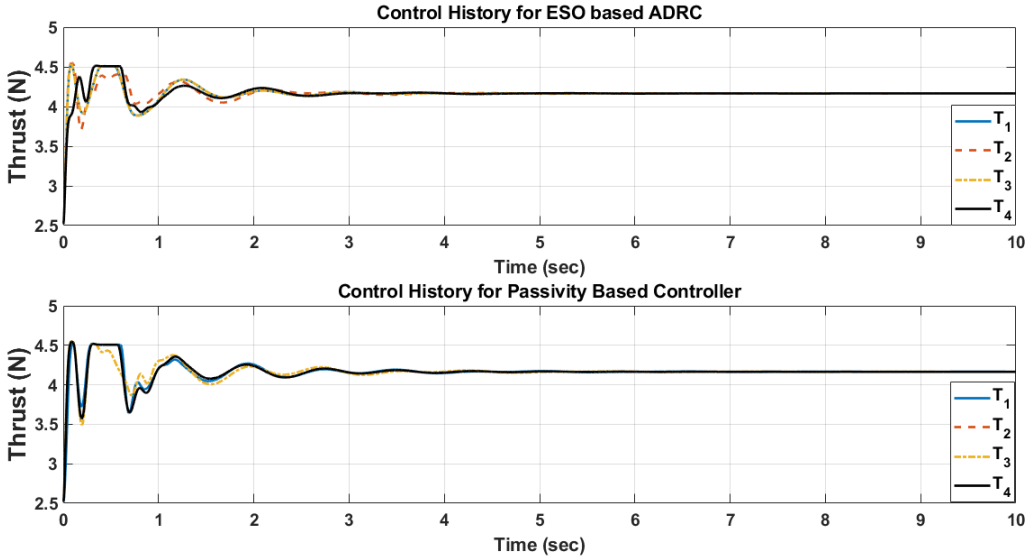

Figure 6.16: Control History

6.12, and 6.13 compares the performance of the passivity based controller and the extended state observer based active disturbance rejection controller for the case when the maximum control limit is reduced.

The extended state observer based active disturbance rejection controller gives a better performance by damping the oscillations of the payload and stabilizing and controlling the altitude and the position of the quadcopter faster than the passivity based controller.

It can be seen from the figure 6.16 that the available thrust is saturated at 4.5 N as the controllers try to control the position of the quadcopter and damp the oscillations of the payload. The thrust values converge to the value required to hover (4.16 N), which is less than the reduced maximum limit as the payload oscillations are damped and the quadcopter goes back to the desired position.

6.1.4 Concluding Remarks

The passivity based controller was implemented to achieve the control objective of controlling the trajectory of the quadcopter and stabilize the swing of the payload cable.

The controller depends upon the knowledge of the payload swing angle and its derivatives. A state estimator is utilized to estimate the angular velocity of the payload assuming that the payload swing angle is measured. Since it is difficult to measure the payload swing angle or additional sensors are required to measure this angle during the actual hardware implementation, an extended state observer based active disturbance rejection controller strategy was proposed and implemented effectively in the simulation environment. Since the extended state observer requires just the state information about the quadcopter states, additional on-board sensors are not required to estimate the disturbances due to the motion of the cable suspended payload during actual hardware implementation.

6.2 Extended State Observer Based Active Disturbance Rejection Controller Implemented on a Quadcopter attached to a Payload using a Flexible Cable

This section presents the implementation of the extended state observer based active disturbance rejection controller for the stabilization and control of a quadcopter with payload connected by a flexible cable. The specifications of the propulsion system and the mass, inertia and geometric parameters of the quadcopter model used in the simulation are tabulated in table A.1. The observer and controller gains are tabulated in table B.1. The cable is modeled using 5 identical serially connected links and the total mass of the cable is 20 g. Hence, the link length is 0.15 m and mass of each link is 4 g. The following cases are used to demonstrate the efficacy of the controller

1. Quadcopter in Hover Mode and the Payload is Perturbed
2. Quadcopter Moving with a Constant Speed along the inertial x axis is commanded to go in the Hover Mode

6.2.1 Quadcopter in Hover Mode and the Payload is Perturbed

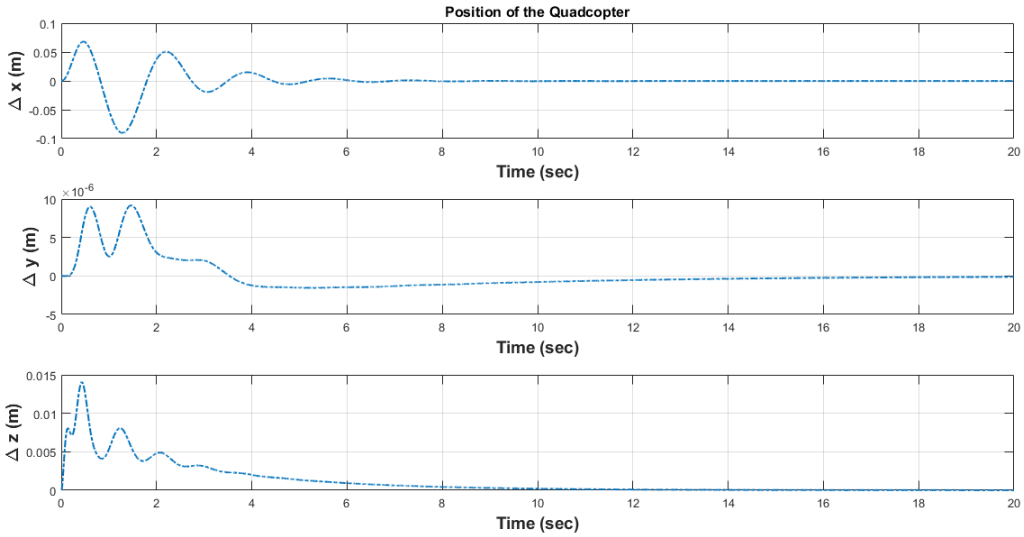

Figure 6.17: Position of the quadcopter

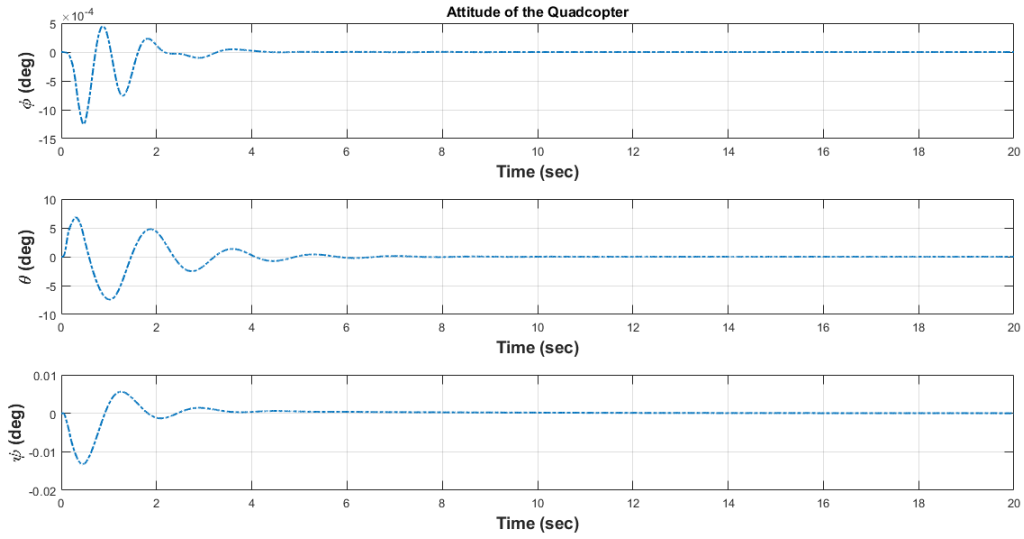

Figure 6.18: Attitude of the quadcopter

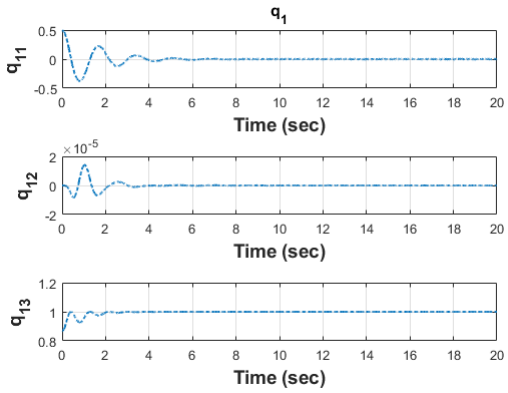

(a) $\mathbf{q}_1$

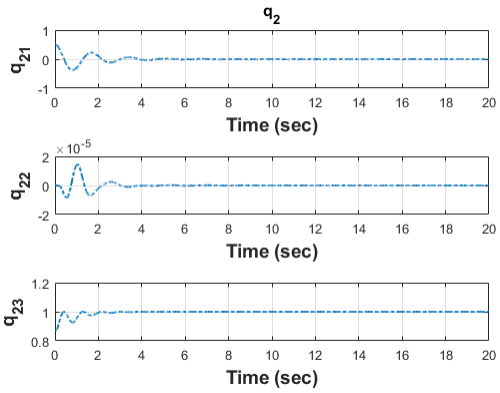

(b) $\mathbf{q}_2$

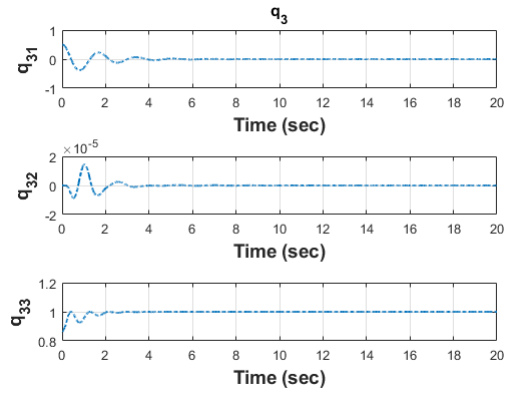

(c) $\mathbf{q}_3$

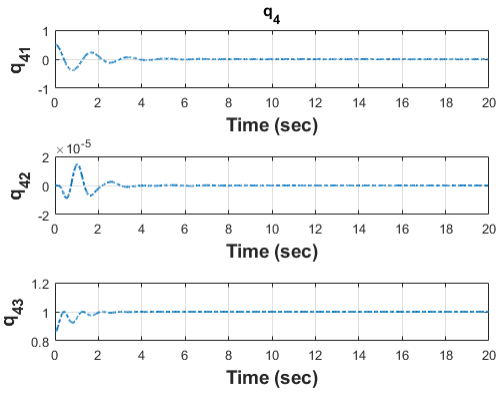

(d) $\mathbf{q}_4$

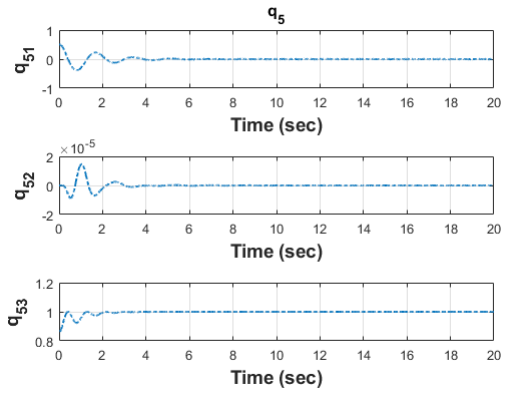

(e) $\mathbf{q}_5$

Figure 6.19: Unit Vector Representing the Direction of each Cable Link $\mathbf{q}_i$

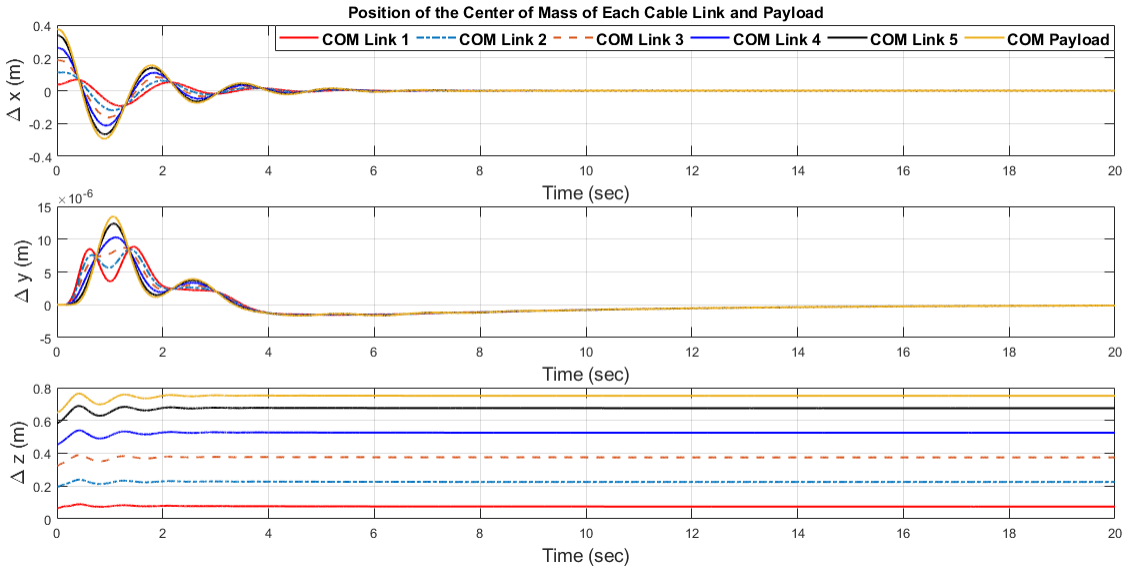

Figure 6.20: Position of the Payload and the Center of Mass (COM) of Each Cable Link in the Inertial Frame

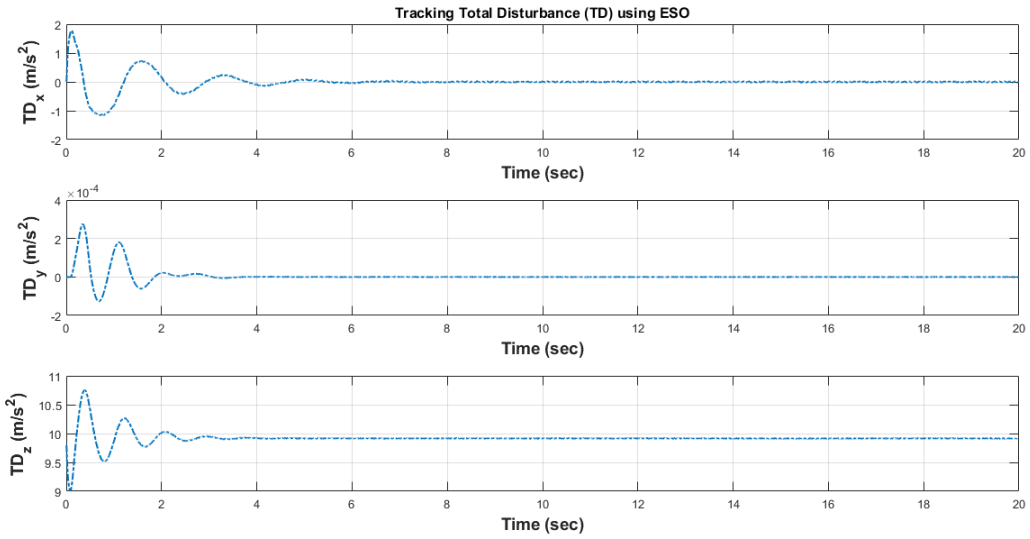

Figure 6.21: Comparison between the Actual and the Estimated Total Disturbance Using Extended State Observer

The quadcopter is in a hovering state at the start of the simulation. The initial angle for each link in the longitudinal plane ($x-z$ plane) is 30° w.r.t the quadcopter. Hence, the initial condition of the unit vector representing the direction of each link is $\mathbf{q}_i = \begin{bmatrix} \sin(\pi/6) & 0 & \cos(\pi/6) \end{bmatrix}^T$. The control objective is to ensure that as time $t \to \infty$, the quadcopter position, $\mathbf{X}_Q \to \mathbf{X}_{Q\_desired}$ and $\mathbf{q}_i \to [0\ 0\ 1]$.

At the start of the simulation, there are disturbances introduced in the system due to the oscillations of the payload. As shown in figures 6.17 6.18, and 6.19, the controller tries to reject these disturbances while trying to achieve the control objective. From figure 6.18 it can be observed that the attitude controller tries to control the pitch angle of the quadcopter, thus providing necessary force to control the longitudinal position of the quadcopter (position along inertial x axis) and damp the oscillations of the payload. The pitch angle has an oscillatory behavior as well and it decays to zero as the payload oscillations decay and the quadcopter goes back to the initial hover pose.

Figure 6.20 shows the position of center of mass of the each cable link and the position of the payload in the inertial frame. The position of the payload and the center of mass of each cable link has a decaying oscillatory behavior in the inertial $x-z$ plane as the controller achieves the control objective.

It can be seen from figure 6.21 that the extended state observer tracks the total disturbances $\mathrm{TD_x}$, $\mathrm{TD_y}$, and $\mathrm{TD_z}$ induced in the system, in x, y, and z directions respectively. These estimates are used by the active disturbance rejection controller to control the position of the quadcopter and damp the oscillations of the slung payload. The total disturbance in the z direction ($\mathrm{TD_z}$) converges to a value of 9.81 $\mathrm{m/s^2}$ as the system is stabilized indicates that the only disturbance acting on the system is the acceleration due to gravity as the quadcopter goes back to the hover position.

6.2.2 Quadcopter Moving with a Constant Speed along the inertial x axis is commanded to go in the Hover Mode

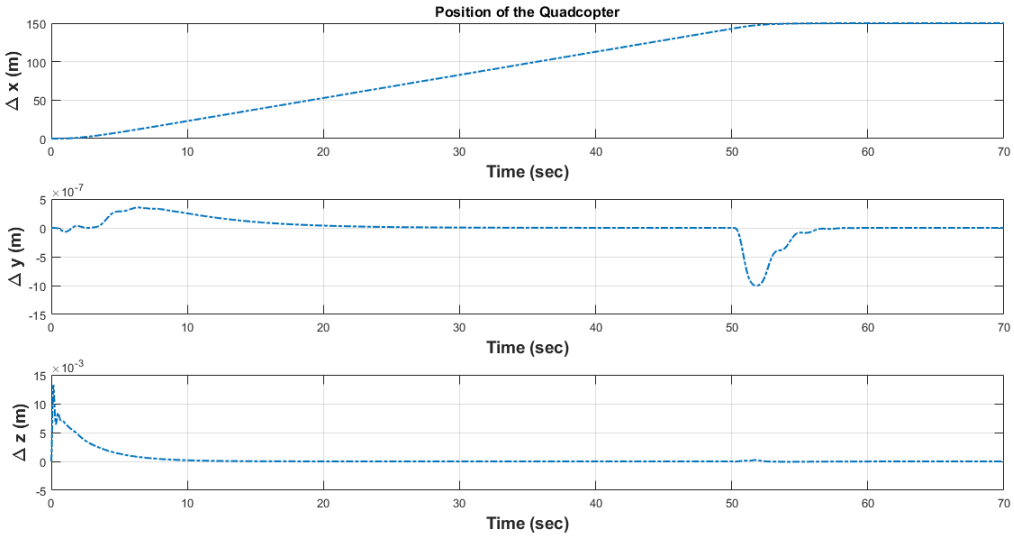

Figure 6.22: Position of the quadcopter

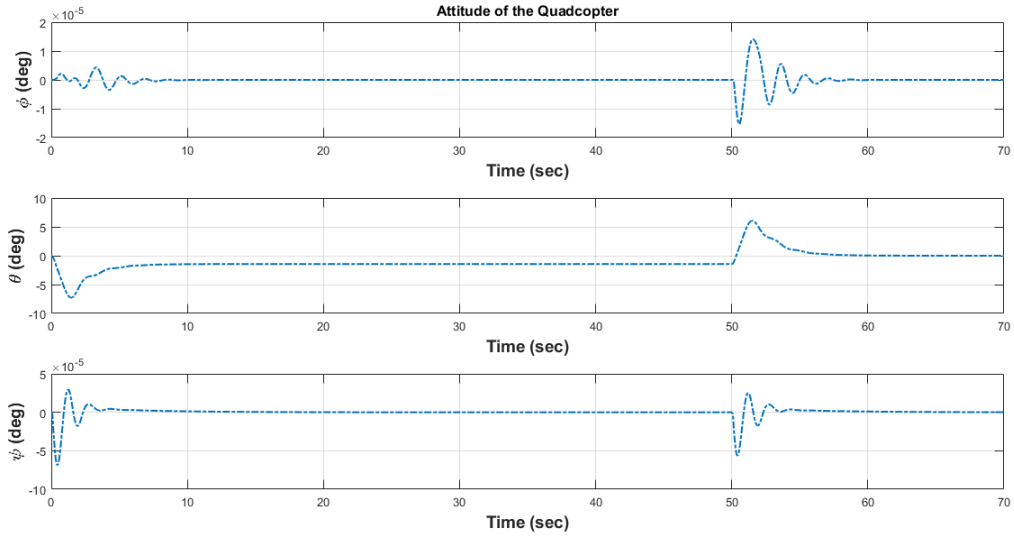

Figure 6.23: Attitude of the quadcopter

At the start of the simulation, the quadcopter is in the hover mode and the payload is in a stable configuration. The quadcopter is commanded to follow a straight line trajectory along the inertial x axis with a constant speed of 10.8 kmph $\left(3\ \mathrm{m/s}\right)$ and fixed altitude. At 50 s, the quadcopter is commanded to go back to the hover mode. From figure 6.22, it can be observed that the controller is able to maintain the quadcopter altitude as well as the trajectory along the inertial x axis and the desired position when commanded to go back to the hover mode. From figure 6.24, it can be seen that the payload is perturbed due to the changes in the quadcopter states at the start of the simulation and the controller stabilizes the payload while the quadcopter is in motion. The payload is perturbed again when the quadcopter goes back to the hover mode and the controller is able to stabilize the system. The quadcopter position and velocity along the inertial x axis is maintained by controlling the pitch angle. From figure 6.23, it is observed that the pitch angle has a decaying oscillatory behavior as the controllers try to maintain the constant speed straight line trajectory of the quadcopter while attenuating the oscillations of the payload due to the changes in the quadcopter states. When the quadcopter is commanded to go back to the hover mode at 50 s, the controller tries to maintain the position of the quadcopter along the inertial x axis and attenuate the oscillations of the payload due to the changes in the quadcopter states using the pitch angle. A decaying oscillatory behavior in the pitch angle of the quadcopter is observed again as the payload oscillations decay and quadcopter goes back to the desired hover pose.

It can be seen from figure 6.25 that the extended state observer is able to track the total disturbances. These estimates are used by the active disturbance rejection controller to control the position of the quadcopter and damp the oscillations of the slung payload. Note, the wind speed $V_w = 0$ kmph for the simulation case but the drag force acting on the quadcopter $\mathbf{D} \neq 0$. Hence, the total disturbance in the x direction ($\mathrm{TD_x}$) in figure (6.10) has

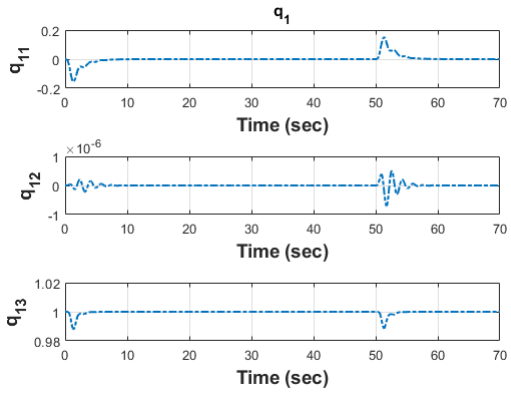

(a) $\mathbf{q}_1$

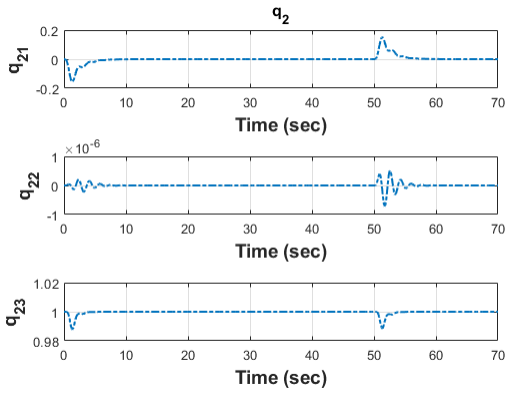

(b) $\mathbf{q}_2$

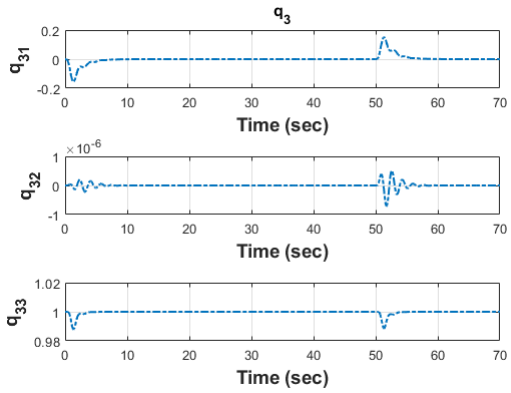

(c) $\mathbf{q}_3$

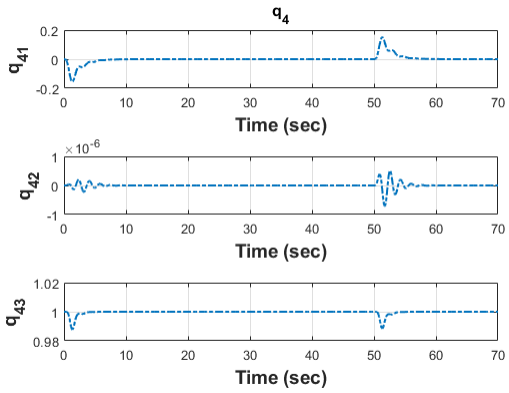

(d) $\mathbf{q}_4$

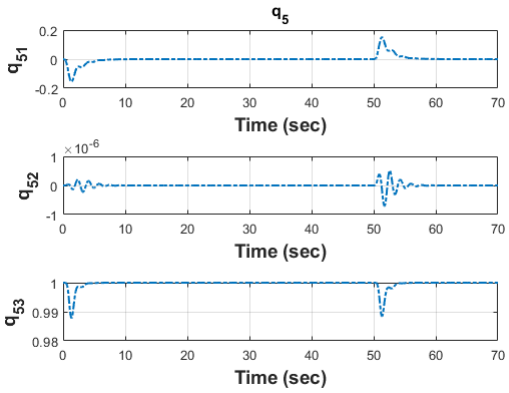

(e) $\mathbf{q}_5$

Figure 6.24: Unit Vector Representing the Direction of each Cable Link $\mathbf{q}_i$

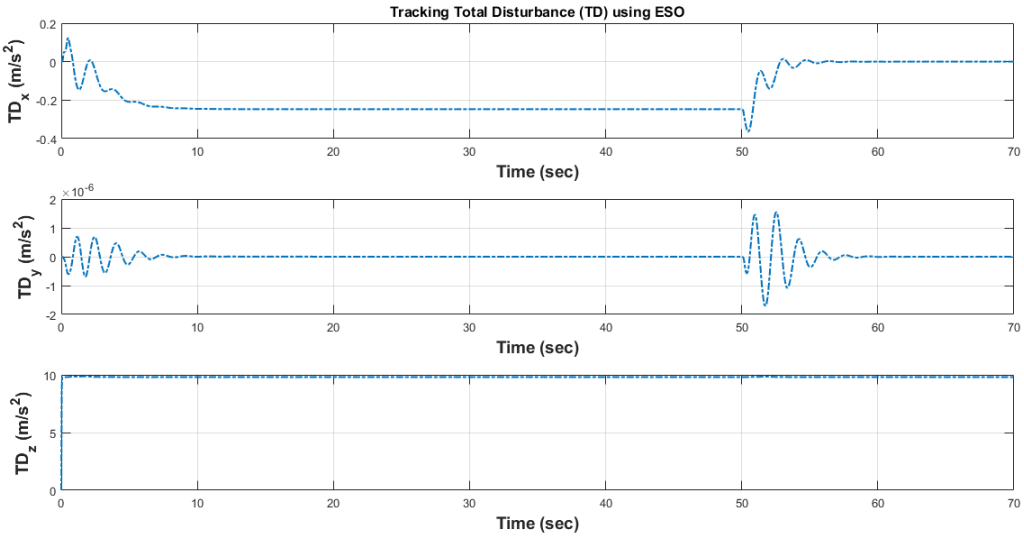

Figure 6.25: Comparison between the Actual and the Estimated Total Disturbance Using Extended State Observer

a non-zero value even when the payload oscillations are damped out and the quadcopter is moving along a straight line with a constant speed. Again, the total disturbance along the z direction (TD_z) converges to a value of 9.81 $\mathrm{m/s^2}$, indicating that the disturbance force acting on the system when the quadcopter is either moving along the inertial x axis with constant speed or when the quadcopter goes back in the hover mode and the cable slung payload is in the equilibrium position, is due to the acceleration due to gravity.

CHAPTER 7

Experimental Setup

Figure 7.1 shows the quadcopter platform that is used to perform the experimental validation of the extended state observer based active disturbance rejection controller. The physical parameters for the quadcopter platform nicknamed 'ASL-Garud', and the specifications of the sub-components are tabulated in table (A.1).

The quadcopter platform contains an onboard autopilot, Pixhawk [65], containing a sensor suite, an onboard computer to communicate with the ground station, and a mount to attach the cable suspended payload. The platform has the DJI F450 chassis, DJI 2212/920 kV motor, 9443 ABS self-locking propellers, and DJI E300 15 A electronic speed controllers (ESC). The sensor suite on the Pixhawk autopilot board is used to extract the state information of the quadcopter. The quadcopter platform uses Raspberry Pi 3 Model B, an onboard computer to collect the sensor data from the Pixhawk sensor suite, relay information and commands from the ground-station computer to the quadcopter. The sensor suite contains a GPS and the experiments can be performed outdoors to capture the effect of wind gusts and evaluate the performance of the extended state observer based active disturbance rejection controller. Since the experiments are performed indoors, the Vicon motion capture system is used for getting the position and the orientation feedback for the quadcopter platform. Note, the Vicon system is just used as an alternative to the GPS for the indoor experiments and the payload states are not measured or utilized by the controller. A radio transmitter and receiver pair is used as a kill switch to overrride the motor commands in case any control failure occurs to ensure safety. The Robot Operating System (ROS) [66], MATLAB, and Simulink software platforms are employed to accomplish the implementa-

Figure 7.1: ASL-Garud, Quadcopter Platform for the Experiments

tion of the extended state observer based active disturbance rejection controller.

Apart from the on-board computer installed on the quadcopter platform, three additional computers are used for the experiments. The first computer (PC1) serves as a ground station which receives all the quadcopter state information, generates the control commands and relays them to the on-board computer. The second computer (PC2) is connected to the Vicon system which collects the data from the Vicon cameras and sends the processed data to the third computer (PC3) dedicated to receive the Vicon data and relay this information to the ground station and the on-board computer over the ROS network. Figure 7.2 shows the communication network between all the four computers used in the experimental setup. The flow of information within the cyber-physical network used for the given tasks, parameter settings on the Pixhawk, and ROS network setup will be explained in detail in section 7.3 and 7.4.

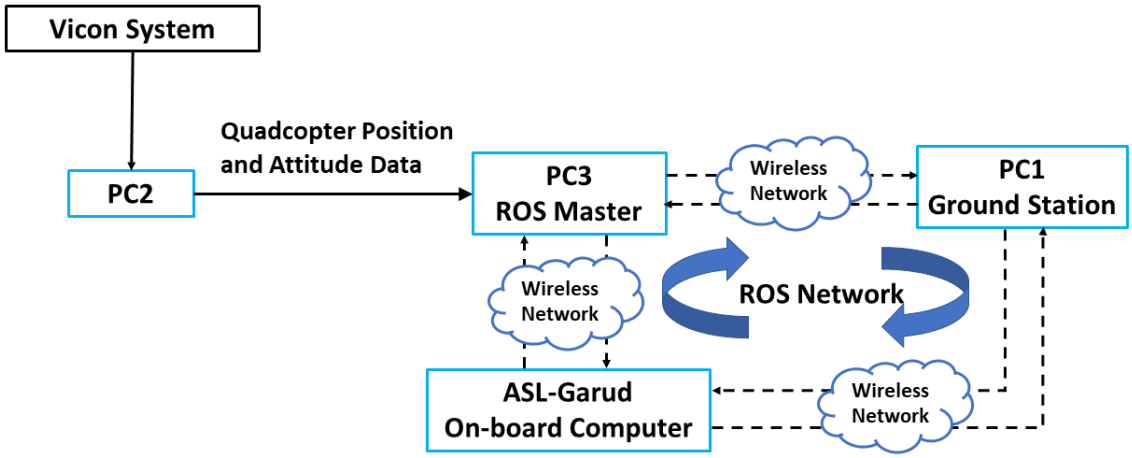

Figure 7.2: Communication Network between the Computers used in the Experimental Setup

7.1 On-board Sensors

The quadcopter is equipped with an autopilot containing different sensors and an on-board computer. These components are explained in the following subsections.

7.1.1 Pixhawk

Pixhawk is an independent open-hardware autopilot designed for high-quality and low cost robotic applications. The ASL-Garud quadcopter platform uses the Pixhawk4 mini board [67]. It uses the PX4 flight stack [68], which provides flexible set of tools for drone developers to create tailored solutions for drone applications. The QGroundControl application [69] is used to flash the PX4 firmware, set the parameters on the Pixhawk, perform sensor and radio calibration, plan missions for any MAVLink [70] enabled drones.

The data from the sensors inside Pixhawk can be accessed and routed to other soft-

Figure 7.3: Pixhawk4 mini Autopilot and ublox Neo-M8N GPS/GLONASS receiver with integrated magnetometer IST8310 used on the ASL-Garud Quadcopter
Source: http://www.holybro.com/product/pixhawk4-mini/

ware modules using the MAVLink protocol and an on-board computer. This makes it ideal for testing custom algorithms on the fly without re-writing the internal flight stack module.

The Pixhawk autopilot system does come with an internal 3-axis gyroscope, 3-axis accelerometer and a magnetometer. Additionally, the Pixhawk has various communication ports to attach an external GPS/Compass module, on-board computer, R/C input, telemetry radio, etc.

Together GPS and Compass are indespensible tools when it comes to the navigation of the quadcopter platform in an outdoor environment.

7.1.2 Raspberry Pi 3 Model B

The Raspberry Pi 3 Model B is a single-board computer installed on the ASL-Garud quadcopter platform which is used to collect the sensor data from the Pixhawk autopilot, process it and send the state feedback to the ground station computer. Additionally, it is

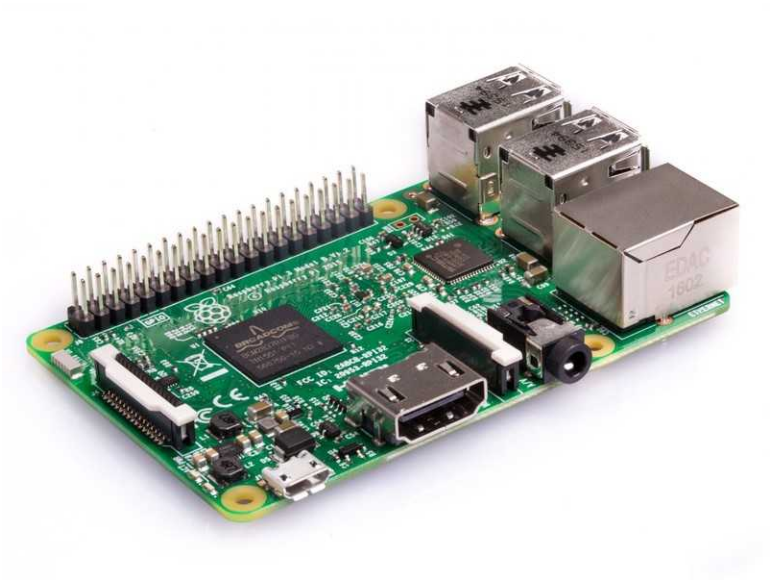

Figure 7.4: On-board Computer on ASL-Garud Quadcopter
Source: https://www.raspberrypi.org/products/raspberry-pi-3-model-b/

used to receive the control signals from the ground station computer and relay them to the Pixhawk autopilot running in the offboard mode to control the platform. The offboard mode of the Pixhawk autopilot will be will be explained in the section 7.5.
The Raspberry Pi 3 Model B has Ubuntu MATE 16.04 operating system and ROS Kinetic Kame installed on it.

7.2 Vicon Motion Capture System

Motion capture or mocap is the process of recording the movement of objects [71]. There are several approaches to the motion capture but the approach which is used here is optical-passive approach. This technique uses retroreflective markers that are tracked by infrared cameras.

Figure 7.5 shows the Vicon motion capture system setup. The system consists of several infrared cameras tracking the retroreflective marker laden objects in space called as capture volume. These cameras send the data to a computer (PC2 shown in figure 7.2) with

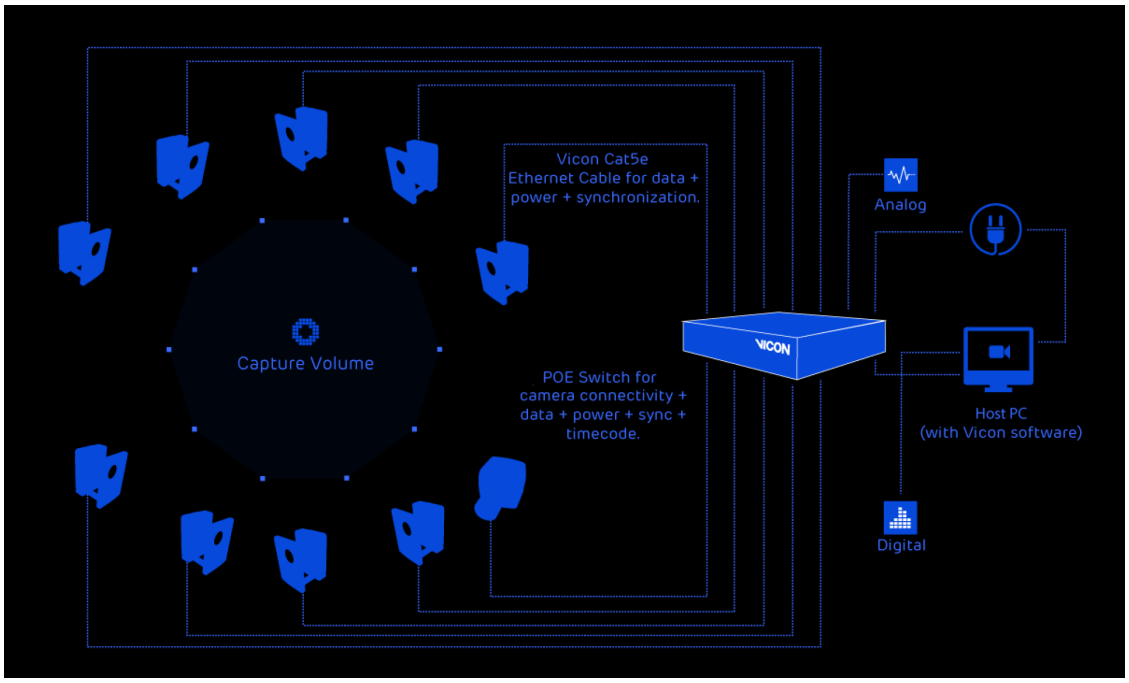

Figure 7.5: Vicon Motion Capture System
Source: https://www.vicon.com/what-is-motion-capture

Windows 10 operating system and a motion capture software through the sync box. The sync box provides a single communication point between the cameras and the computer. The motion capture software is a key component not only because it is a main point of interaction with cameras and all other components like the computer running the ROS Master (PC3), but also it is the main processing tool for all the data. By connecting the ground station computer (PC1) and the computer running ROS Master (PC3) to the same network as the computer connected to the Vicon system, the position and orientation data of the object being tracked can be accessed by the ROS network using a driver which will be explained in subsection 7.3.1.

7.3 Software and Communication Network Setup

This section gives an introduction to the software packages and the communication network setup that is used for the implementation of the extended state observer based active disturbance rejection controller on the quadcopter with cable suspended payload.

7.3.1 Robot Operating System (ROS) and ROS Packages

Robot Operating System (ROS) is a flexible framework for writing robot software. It is a framework with collection of tools, libraries, and conventions that aim to simplify the task of creating complex and robust robot behavior across a wide variety of robotic platforms. The following concepts explain the structure of ROS briefly [72]:

- **ROS File-System:** Similar to an operating system, a ROS program is divided into folders, and these folders have some files that describe their functionality.
  - Packages: These are the basic unit of the ROS software. it contains all the runtime processes called nodes, libraries, package configuration etc.
  - Messages: Messages are the type of information that is sent from one ROS process to other ROS process. These are usually located inside ROS package with the file extension ".msg". These files are located inside the package as,

    `ros_package_name/msg/<message-name>.msg`
  - Services: Services are kind of a request/reply interaction between processes. The service information is usually stored with the file extension ".srv". These files are located inside the package as,

    `ros_package_name/srv/<service-name>.srv`
- **ROS Computation-Graph Level:** This is the level where communication between processes and systems happen. ROS creates a network where all the processes are connected. Any node in the system can access this network, interact with other nodes,

see the information that they are sending, and transmit data to the network. The basic concepts in this level are

- Nodes: These are the processes that performs the computation.
- Master: The ROS Master provides the registration and lookup to the rest of the nodes. Nodes will not be able to find each other, exchange messages, or invoke services without a ROS Master.
- Parameter Server: The parameter server allows you to keep the data to be stored in a central location. This is part of the ROS Master.
- Topics: Each message in ROS is transported using named buses called topics. When a node sends a message through a topic, then we can say the node is publishing a topic. When a node receives a message through a topic, then we can say that the node is subscribing to a topic.
- Bags: Bags are a format for saving and playing back ROS message data. Bags are an important mechanism for storing data, such as sensor data, which can be difficult to collect but is necessary for developing and testing robot algorithms.

7.3.2 Robot Operating System (ROS) Support from Robotics System Toolbox in Simulink

The Robotics System Toolbox [73] provides an interface between MATLAB and Simulink and the ROS network. The key feature of this toolbox are

- Simulink models that work with a ROS network can be created and a communication network can be setup which can enable the users to interactively explore robot capabilities, and visualize sensor data
- ROS nodes, publishers, and subscribers can be created directly from MATLAB and Simulink
- ROS Custom Messages can be created and sent from MATLAB and Simulink

- ROS functionality can be used on any operating system (Windows, Linux, Mac) running MATLAB and Simulink
- A standalone ROS C++ node can be generated from a Simulink model

7.3.3 Communication Setup between Pixhawk and On-board Computer

To access the sensor data from the Pixhawk autopilot and send the control commands to the flight control unit, the Serial port or the Telemetry Port of the Pixhawk is used. A MAVLink [70] enabled software package that performs the serialization with minimum configuration is used. The reason to use the MAVLink enabled software package is that, Pixhawk internally uses the MAVLink supported firmware (PX4). The package called MAVROS [74], which is an open-source ROS package is designed to communicate between Pixhawk and the on-board computer through an FTDI-cable.

To connect the FTDI cable to the serial port, the wiring is done as follows

Table 7.1: `TELEM1` to FTDI Cable Wiring

`TELEM1`		FTDI	
1	+5V(red)		DO NOT CONNECT!
2	Tx(out)	5	FTDI RX (yellow) (in)
3	Rx(in)	4	FTDI TX (orange) (out)
4	CTS(in)	6	FTDI RTS (green) (out)
5	RTS(out)	2	FTDI CTS (brown) (in)
6	GND	1	FTDI GND (black)

To interface the on-board computer with Pixhawk4 mini, we have to configure the `TELEM1` port to enable MAVLink using the following parameters in the Pixhawk Parameter list

- `MAV_1_CONFIG` = `TELEM1`
- `MAV_1_MODE` = `Onboard`

- SER_TEL1_BAUD = 921600

Once the MAVROS package is installed and the Pixhawk is connected to the on-board computer using an FTDI cable, the next step is to configure the MAVROS package as follows

- Get the port number that the Pixhawk is connected to, let's say that the port number is /dev/ttyUSB0
- Now open the "px4.launch" file by navigating to the launch folder of the MAVROS package and change the fcu_url parameter to /dev/ttyUSB0:921600
- Once the "px4.launch" file is launched, the on-board computer will be able to access the sensor data from the Pixhawk and send the control commands as ROS topics

7.3.4 Network Communication Setup

A ROS system can have several nodes running across multiple machines on a network. Depending on the system configuration, any node may need to communicate with other nodes across the network. ROS has certain requirements for setting up this communication [75]

- There must be complete, bi-directional connectivity between all pairs of machines, on all ports
- Each machine must advertise itself by a name that all other machines can resolve

Let us assume a ROS network with two systems, System1 and System2 with IP addresses as System1-IP and System2-IP respectively. Before setting up the network, one of the machine is chosen to run the ROS Master. Let System1 be the machine chosen to run ROS Master. Hence, System2 will be connected to System1.

Before launching the ROS Master on System1, two variables are needed to be declared on all the machines

- `ROS_MASTER_URI`: IP address of the machine chosen as ROS Master. The syntax for setting this variable is

  `export ROS_MASTER_URI=http://<MASTER-IP>:11311`

- `ROS_IP`: IP address of the current machine. The syntax for setting this variable is

  `export ROS_IP=<system-IP>`

For connecting System1 and System2 with ROS-Master running on system1,

On System1

```
export ROS_IP=<System1-IP>
export ROS_MASTER_URI=https://<System1-IP>:11311
```

On System2

```
export ROS_IP=<System2-IP>
export ROS_MASTER_URI=https://<System1-IP>:11311
```

Setting up these variables enables the communication between System1 and System2 and both the systems will be able to access the data over the network.

7.3.5 Network Communication between ROS network and Simulink

To setup the communication between the simulink model running the extended state observer and the position controller and the ROS network, the ROS Master URI and the Node Host (IP of the machine running simulink) needs to be specified using the "Configure ROS Network Addresses" dialog. This menu can be accessed under the `Tools>Robot Operating System (ROS)` by selecting "Configure ROS Network Addresses" [76].

Figure 7.6 shows the menu to set the `ROS_MASTER_URI` and the IP of the machine running the simulink which will be used by other ROS nodes to connect to the simulink model. Using the Custom option under the "Network Address" drop down menu under ROS Master, the `ROS_MASTER_URI` variable can be set. This will enable us to setup the

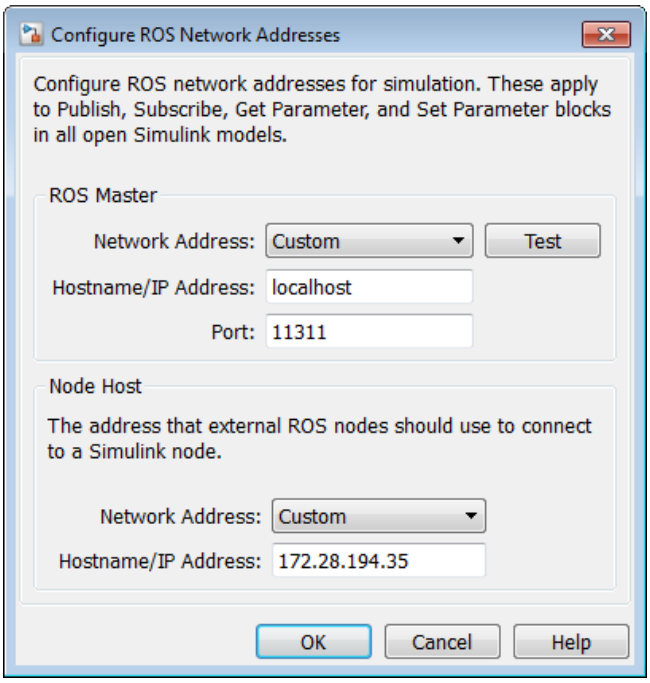

Figure 7.6: Configuration of Network Addresses for Simulink
Source: https://www.mathworks.com/help/robotics/ug/configure-ros-network-addresses.html

communication between the ROS Network and the simulink model where the simulink model will show up as a node in the network.

7.4 Flow of Information

The flow of information within the given GNC framework for the ASL-Garud quadcopter platform is illustrated in the figure 7.7. The experimental setup makes use of the cyber-physical system architecture. As seen in the figures 7.7 and 7.2, the ground station computer (PC1) receives the state feedback and the control commands are generated. PC1 has the MATLAB and Simulink installed along with the Robotics System Toolbox. The extended state observer and the active disturbance rejection controller run as Simulink model on PC1 and communicate with the ROS network using the Robotics System Toolbox.

The ROS Master is run of the computer PC3 as shown in figure 7.2. The computer connected to the Vicon system (PC2) sends the quadcopter position and attitude information to a computer (PC3) which runs the ROS Master over a wired network. PC3 has the Ubuntu 16.04 LTS operating system, ROS Kinetic Kame and vicon_bridge driver [77] installed on it. The vicon_bridge driver enables the PC3 to receive the quadcopter position and attitude information and advertise it over the ROS network.

On the ASL-Garud quadcopter platform, the onboard computer has MAVROS and a custom ROS package which extracts and processes the sensor data from the Pixhawk and advertises it to the ROS network. The custom ROS package also has a ROS node which receives the control commands from the ground station, switches the Pixhawk to the OFFBOARD mode and relays the setpoint attitude commands to the Pixhawk.

The flow of information between hardware components of the ASL-Garud quadcopter platform is illustrated in figure 7.8. The information is exchanged between different computers (ground station, ROS Master and the on-board computer) over the ROS network through a wireless network.

Figure 7.9 shows the `rqt_graph` of various ROS nodes and ROS topics, and the flow of information between them. The nodes are represented inside the ellipses and the topics are represented in the rectangular boxes. The `vicon` node publishes data to the

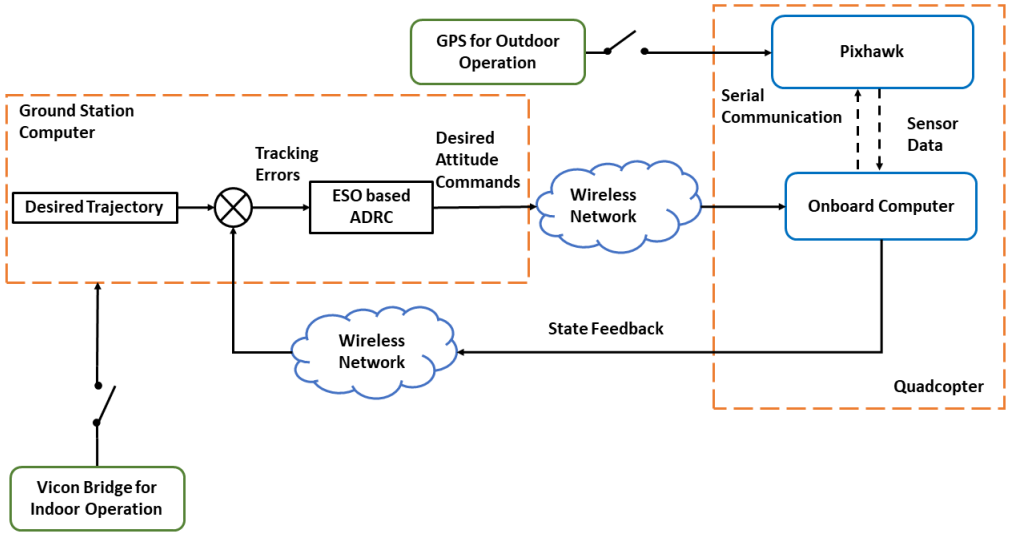

Figure 7.7: Flow of information within the GNC framework for the quadcopter platform

pixhawk for pose estimation and to the controller node which is running the extended state obsrever based active disurbance rejection controller. The `mavros` node publishes the imu data to the controller node. The battery voltage information, arming status of the pixhawk and the individual motor commands are subscribed by the `/TotalThrustFeedback` node to estimate the total thrust generated by all the propellers. This information is further utilized by the controller node. The desired thrust and the attitude commands published by the controller node are subscribed by the setpoint plugins of MAVROS.

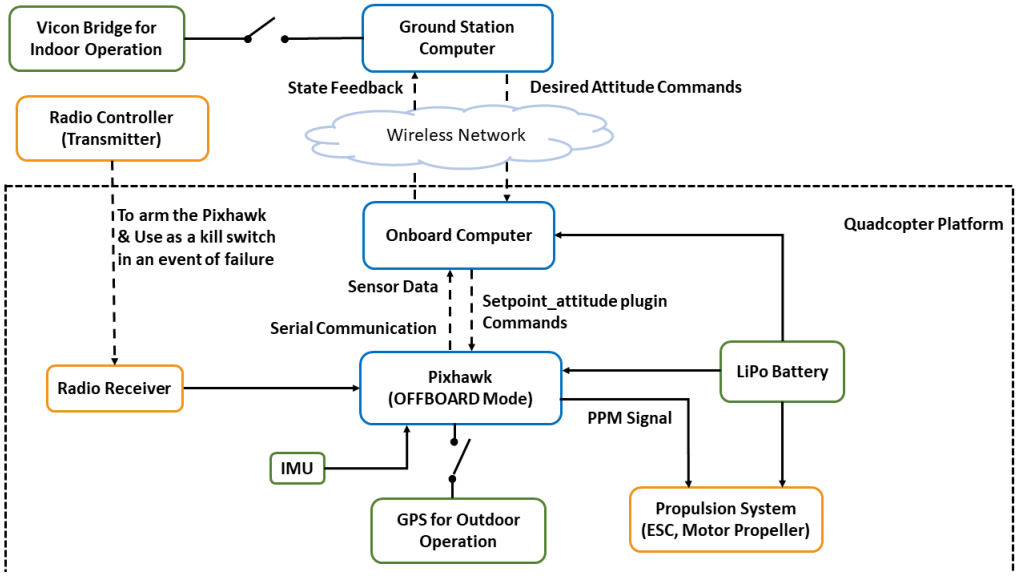

Figure 7.8: Flow of information between hardware components of the quadcopter platform

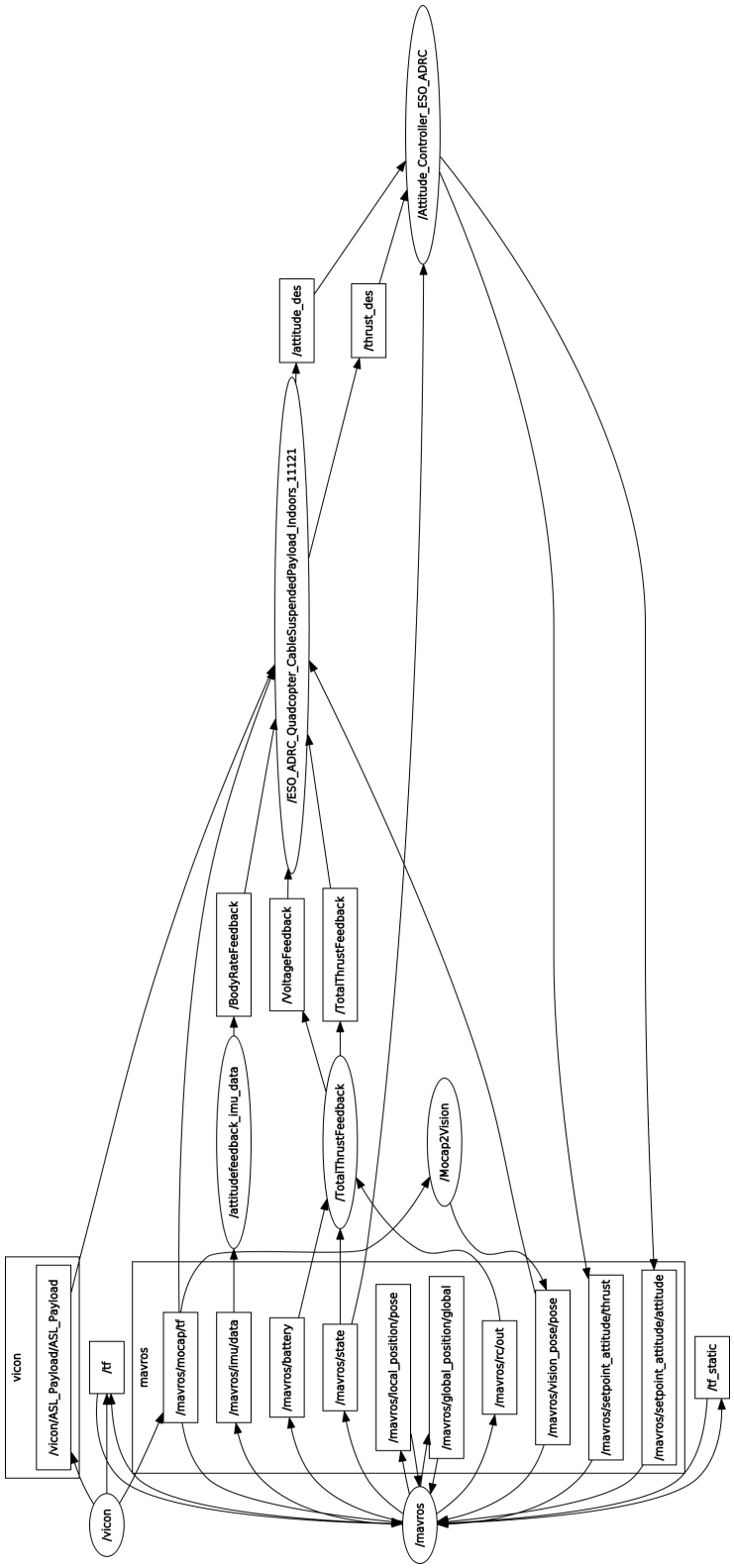

Figure 7.9: Visualization of the ROS Computation Graph

7.5 Offboard Mode and Pixhawk Parameter Setup

The following section explains the Offboard mode of the Pixhawk autopilot, its implementation and the Pixhawk parameter setup.

7.5.1 Offboard Mode

The Offboard mode is used for controlling the vehicle movement and the attitude using some setpoints provided by the MAVLink API running on a companion computer [78]. This mode requires position and attitude information feedback usually available through the on-board sensors or through the visual inertial odometry or motion capture. This mode is automatic and RC control is disabled except to change to different modes or as a kill switch. The Pixhawk must be already be receiving a stream of target setpoints before the autopilot can be switched to this mode. The autopilot will exit this mode if the target setpoints are not received at a rate $>$ 2Hz.

The MAVLink commands can be used to control the

- Position, Velocity, or Thrust (`SET_POSITION_TARGET_LOCAL_NED`)
- Vehicle attitude/orientation (`SET_ATTITUDE_TARGET`)

The desired attitude and thrust commands generated by the controller are streamed as the attitude and thrust target setpoints to the `/mavros/setpoint_attitude/attitude` and `/mavros/setpoint_attitude/thrust` mavros topics to achieve the control objective. The thrust value is scaled between $[0-1]$ where, the thrust value equal to 0 corresponds to 0% throttle and 1 corresponds to 100% throttle.

The ideal total thrust of the quadcopter to maintain the hover position [18] is given by

$$T = \left(m_Q + m_l\right) g - k_{pz} e_z - k_{dz} \dot{e}_z - k_{iz} \int_0^t e_z dt \tag{7.1}$$

where, T is the desired thrust, $\left(m_Q + m_l\right)$ is the total mass of the quadcopter and the payload, e_z is the error in the altitude, k_{pz}, k_{iz}, and k_{dz} are the controller gains. Near hover condition, the total desired thrust, $T \approx \left(m_Q + m_l\right) g$. Let $\left(m_Q + m_l\right) g$ be the nominal thrust value which is mapped to the throttle value. The throttle value depends on the battery voltage and needs to be adaptive to maintain the altitude. The nominal throttle value required to maintain the altitude were obtained experimentally for a range of the battery voltage values. Using these values, a 4^{th} order polynomial curve fit was obtained (ref. figure7.10) to express the nominal thrust value as a function of battery voltage as

$$T_{nom}(v) = -814.4 + 313.99v - 45.208v^2 + 2.8842v^3 - 0.069918v^4 \tag{7.2}$$

where, T_{nom} is the nominal throttle value and v is the battery voltage. Note, this polynomial

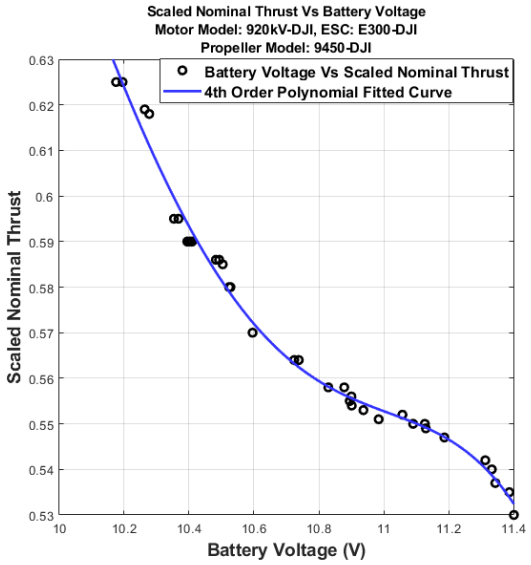

Figure 7.10: Nominal Thrust Vs Battery Voltage Curve Fit

fit is only valid for the DJI 221/920 kV motor, DJI 9443 ABS self locking propeller and DJI E300, 15 A ESC combination. The experiment will have to be repeated if any of these component is substituted.

7.5.2 Using Motion Capture for Position Estimation

To switch the Pixhawk to the Offboard mode, it requires the position and attitude information of the vehicle and a continuous stream of the target setpoints. This section gives the setup for configuring the PX4-based system to get the Vicon motion capture system (via ROS) for position and attitude estimation. PX4 uses the `VISION_POSITION_ESTIMATE` MAVLink messages to get the external position information. These messages should be streamed between 30Hz and 50Hz.

The following parameters must be set to use the external position information with the EKF2. These parameters can be set by connecting the Pixhawk to the QGroundControl software under `Vehicle Setup>Parameters>EKF2` tab as shown in table 7.2.

The quadcopter position and attitude information which is available on the ROS network is first remapped to the `/mavros/mocap/tf` MAVROS topic and is then remapped again to the `/mavros/vision_pose/pose` MAVROS topic which is then utilized by the EKF2 pose estimator running on the Pixhawk. More information about the reference frames, and relaying the position information from other motion capture and visual inertial odometry systems to the PX4-based systems can be found at [79]

Table 7.2: Settings for External Position Estimation

Parameter	Setting for External Position Estimation
`EKF2_AID_MASK`	Set vision position fusion and vision yaw fusion
`EKF2_HGT_MODE`	Set Vision to use the vision as a primary source for altitude estimation
`EKF2_EV_DELAY`	Set to the difference between the timestamp of the measurement and the "actual" capture time. It is the Vision Position Estimator Delay relative to IMU measurements.

Table 7.3: Coefficients for the Surface to Estimate the Thrust On-board

Coefficient	Value
p_{00}	2418
p_{10}	-2.912
p_{01}	-139.1
p_{20}	7.806×10^{4}
p_{11}	0.1145

7.6 Thrust Estimation Using the PPM Signal and Battery Voltage

To perform the estimation of the thrust generated by the propellers on-board, a test bench (ref. figure7.11) developed at the Aerospace Systems Laboratory at The University of Texas at Arlington was used [80]. The test bench consists of a motor mounted on a load cell which measures the thrust produced by the propellers. Along with the load cell there are additional sensors to record various quantities like the battery voltage, current drawn by the motor, infra red temperature sensor to measure the temperature of the motor and an optical sensor to measure the RPM of the motor. These sensors are connected to an Arduino microcontroller which sends the data to the MATLAB through serial communication. The thrust as a funtion of the battery voltage and the PPM signal was fitted to a surface of the form

$$T(s,v) = p_{00} + p_{10}s + p_{01}v + p_{20}s^2 + p_{11}sv \tag{7.3}$$

where, T is the thrust measured in grams, s is the PPM signal in μs, and v is the battery voltage in volts. Using the test bench, the coefficients of the surface polynomial were obtained for the DJI 221/920 kV motor, DJI 9443 ABS self locking propeller and DJI E300, 15 A ESC combination. The coefficients are tabulated in table 7.3

Since the motor input i.e. the PPM signal and the battery voltage are available as ROS topics in the MAVROS package, an on-board thrust estimation can be performed. These

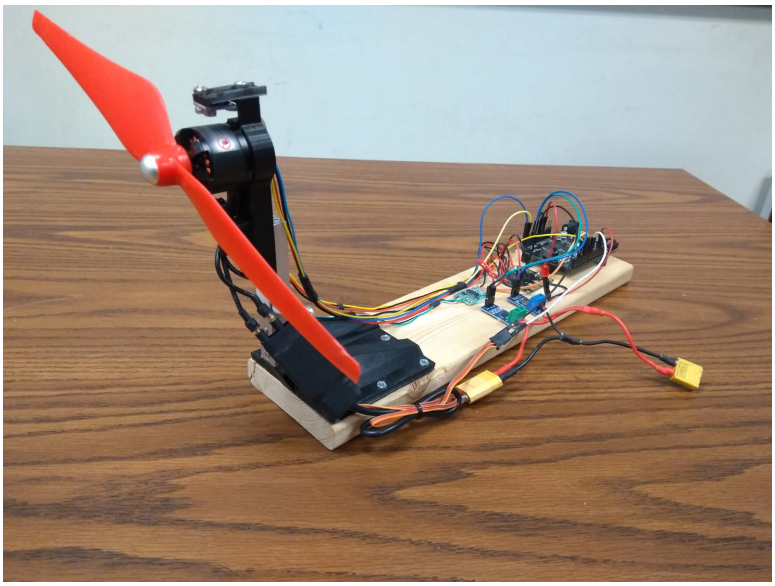

Figure 7.11: Test Bench for Thrust Estimation as a Function of Battery Voltage and PPM Signal

thrust estimates are used by the extended state observer to estimate the total disturbance along the z direction.

CHAPTER 8

Experimental Results

This chapter presents the experimental validation and performance analysis of the extended state observer based active disturbance rejection controller developed in chapter 4 using the experimental setup discussed in chapter 7. As discussed earlier in chapter 4 and 7, the extended state observer based active disturbance rejection controller running on the ground station generates three control inputs which are desired thrust, T, desired roll and pitch angles, ϕ_d and θ_d, respectively. These control inputs, along with the desired yaw angle, ψ_d, are sent to the on-board computer which relays these inputs to the Pixhawk in the "Offboard Mode". An internal PID controller and the motor mixing block running inside the Pixhawk generates individual motor commands using these inputs.

The following three cases are used to conduct experiments to analyze the performance of the extended state observer based active disturbance rejection controller

1. Quadcopter in Hover mode and the payload is perturbed
2. Quadcopter in Hover mode and the payload is perturbed but the disturbance estimates are not available to the controller
3. Quadcopter is commanded to follow a point to point minimum-jerk trajectory

Results for each of these experiments are described in the sequence.

8.1 Experiment 1: Quadcopter in Hover mode and the payload is perturbed

The quadcopter is in a hovering state at the start of the experiment and the payload is in the stable configuration. The desired altitude at which the quadcopter is commanded to hover is 1.5 m and the initial x and y location of the quadcopter in the Vicon capture

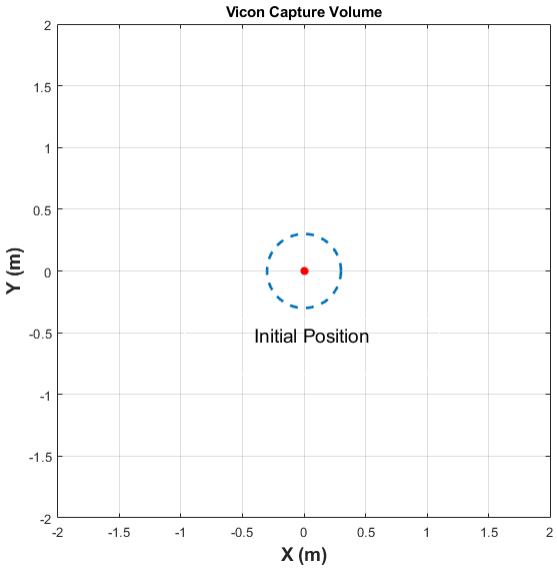

Figure 8.1: Waypoint Setup for Experiment 1 and 2

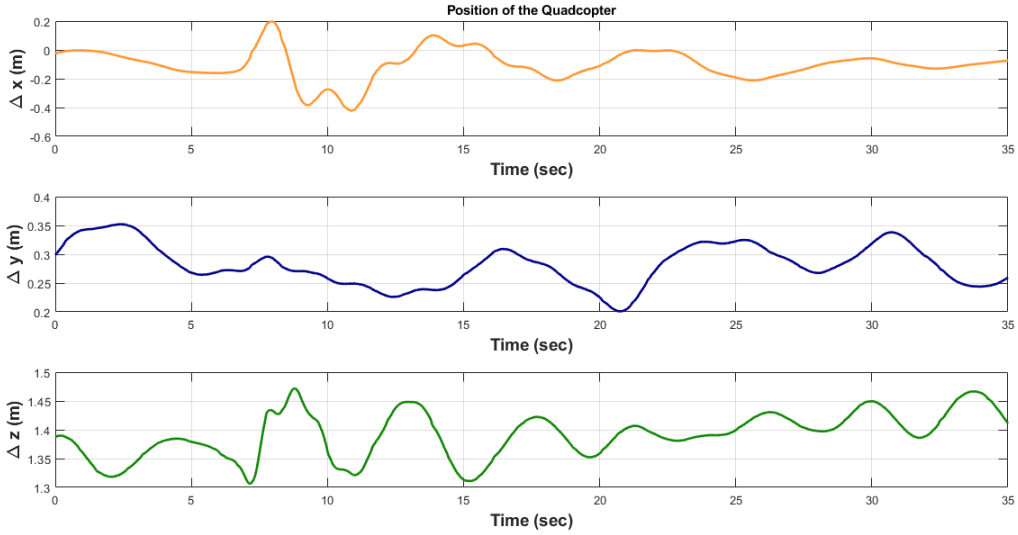

Figure 8.2: Position History of the quadcopter for Experiment 1

volume is illustrated in figure 8.1. Approximately 6 seconds after the experiment is initiated, the payload is perturbed manually in the $x-z$ longitudinal plane and disturbances are introduced in the system due to the oscillation of the payload. The control objective of this

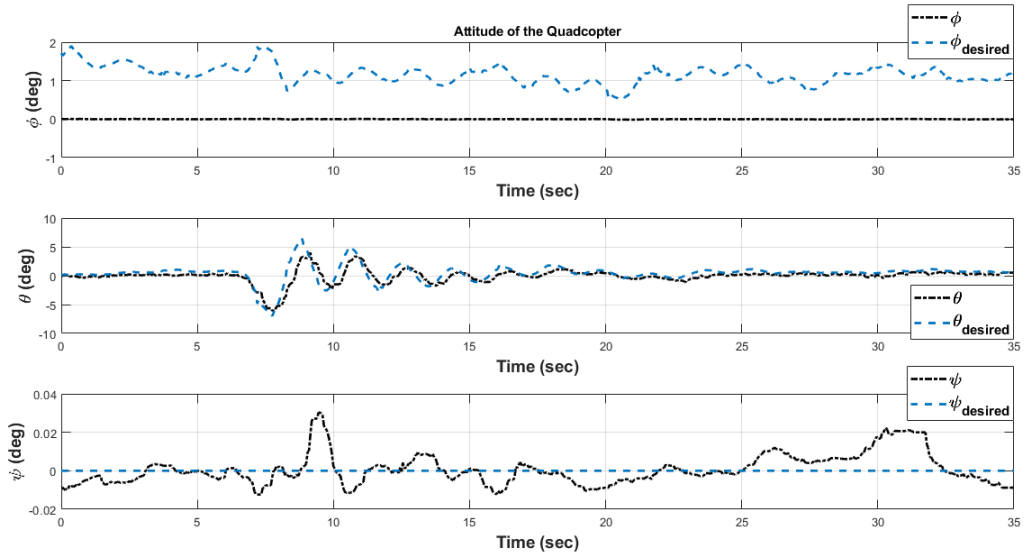

Figure 8.3: Attitude of the quadcopter for Experiment 1

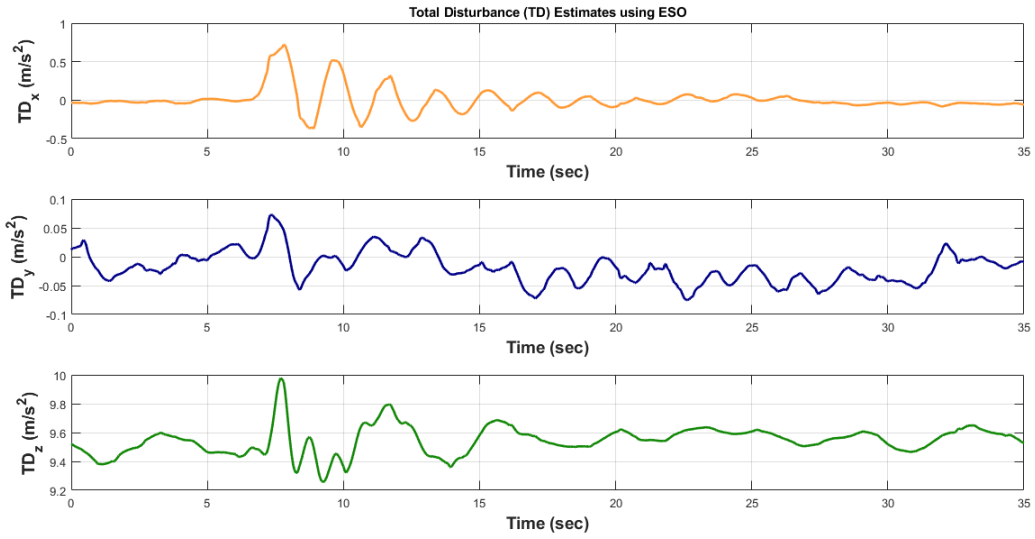

Figure 8.4: Estimated value of the Total Disturbance acting on the Quadcopter for Experiment 1

experiment is to maintain the hover position and stabilize the perturbed payload. As seen in figures 8.2, 8.3 and 8.4, the extended state observer based active disturbance rejection controller tries to reject these disturbances and achieves its task.

From figure 8.3 it can be observed that the attitude controller tries to control the pitch angle of the quadcopter, thus providing necessary force to control the longitudinal position of the quadcopter (position along inertial x axis) and damp the oscillations of the payload. The desired pitch angle has an oscillatory behavior and it decays to zero as the total disturbance estimates decay and the quadcopter goes back to the initial hover pose.

The state information about the swing of the payload is unavailable and the extended state observer is employed to estimate the disturbances induced in the system due to the oscillations of the cable suspended payload. No additional sensors are required to estimate these disturbances since the only inputs required by the observer are the quadcopter states. These estimates are used by the active disturbance rejection controller to achieve its objective. It can be seen from figure 8.4 that the extended state observer is able to estimate the total disturbances TD_x, TD_y, and TD_z induced in the system in x, y, and z direction respectively. The total disturbance along x and y direction converge to a value around 0 m/s^2 as the quadcopter goes back to the initial hover pose. The estimates of the total disturbance in the z direction (TD_z) converges to a value around 9.6 m/s^2 as the system is stabilized. This indicates that the only disturbance acting on the system is the acceleration due to gravity as the quadcopter goes back to the hover position. The average settling time for the system to be stabilized after the payload is perturbed is approximately 15 seconds.

Additional information about the system can be obtained from these experimental results. The dominant damped natural frequency of the total disturbance along x direction (ω_{dx_exp}) is obtained using the Fast Fourier Transform of the estimate history (figure 8.5). From figure 8.5, the dominant damped natural frequency of the total disturbance along x direction is obtained as 0.54 Hz.

The time domain solution for the impulse response for a second order system is

$$y(t) = Ae^{(-\zeta\omega_n t)}\cos(\omega_d t) \tag{8.1}$$

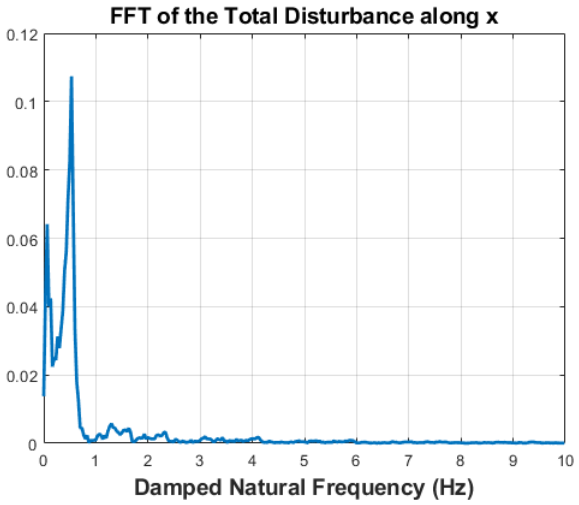

Figure 8.5: Fast Fourier Transform of the Total Disturbance along x direction for Experiment 1

where, A is the amplitude of the impulse, ζ is the damping ratio of the second order system, ω_n is the natural frequency of the system, ω_d is the damped natural frequency of the system, and y is the solution for the impulse response for the second order system. Let y_1 and y_2 be the impulse responses for a second order system at time t_1 and t_2 respectively. From eq. (8.1)

$$\begin{aligned} y_1 &= Ae^{(-\zeta\omega_n t_1)}\cos(\omega_d t_1) \\ y_2 &= Ae^{(-\zeta\omega_n t_2)}\cos(\omega_d t_1) \end{aligned} \tag{8.2}$$

Using the ratio of y_1 and y_2, the following relation is obtained

$$\delta = \left|\frac{y_1\sec(\omega_d t_1)}{y_2\sec(\omega_d t_2)}\right| = e^{(\zeta\omega_n(t_2-t_1))} \tag{8.3}$$

Using the natural log on both the sides,

$$\ln|\delta| = \zeta\omega_n(t_2-t_1) \tag{8.4}$$

For a given second order underdamped system, the damped natural frequency is related to the natural frequency as

$$\omega_d = \sqrt{1-\zeta^2}\omega_n \tag{8.5}$$

Using eq. (8.4) and (8.5), the damping ratio for the system is obtained as

$$\zeta = \frac{\left(\frac{\ln|\delta|}{\omega_d(t_2-t_1)}\right)^2}{1+\left(\frac{\ln|\delta|}{\omega_d(t_2-t_1)}\right)^2} \tag{8.6}$$

From eq. (8.5) and (8.6), the natural frequency of the system can be computed.

Near hover condition, the dynamics of the payload can be approximated as the dynamics of the simple pendulum which is a second order system. The oscillation of the payload induces disturbance in the system. Hence, the estimates of the total disturbance can be used to estimate the frequency of the oscillation of the payload since the frequency of the disturbance will be equal to the frequency of the oscillating payload. The estimates of the total disturbance along x direction(TD_x), the damped natural frequency of the total disturbance obtained using the Fast Fourier Transform (ω_{dx_exp}), and the expression for the damping ratio (ζ) of the system (ref. eq. (8.6)) are used to obtain the natural frequency of the oscillating payload. Table 8.1 shows the comparison between the natural frequency of the oscillating payload obtained from the experimental results and the natural frequency of the oscillating payload approximated as a simple pendulum. Here, y_1 and y_2 are the estimates of the total disturbance along x axis at time t_1 and t_2 respectively. The percentage error between the natural frequency of the payload obtained using the experimental results, and obtained by approximating it as a simple pendulum, is computed as

$$\%error = \frac{\omega_{n\_exp} - \omega_{n\_act}}{\omega_{n\_act}} \times 100$$

It can be seen from the table 8.1 that the natural frequency of the payload and the damping can be estimated using the estimates of the total disturbance. These estimates of the natural frequency and damping can be used to obtain the information like the the velocity and

acceleration of the swinging payload if the cable angle measurements are available. This information can be utilized by the passivity based controller developed in chapter 5.

Table 8.1: Comparison of the Natural Frequency of the Payload Approximated as a Simple Pendulum with the Natural Frequency of the Payload Computed Using Total Disturbance Estimates

t_1	t_2	$y_1\ (m/s^2)$	$y_2\ (m/s^2)$	ζ	ω_{n_exp}(Hz)	ω_{n_act}(Hz)	$\%\ error$
7.85	9.6	0.712	0.5188	0.1093	0.5433	0.4985	8.99
9.6	11.75	0.5188	0.31	0.0133	0.5400	0.4985	8.32
11.75	13.4	0.31	0.1362	0.0328	0.5403	0.4985	8.39

8.2 Experiment 2: Quadcopter in Hover mode and the payload is perturbed but the disturbance estimates are not available to the controller

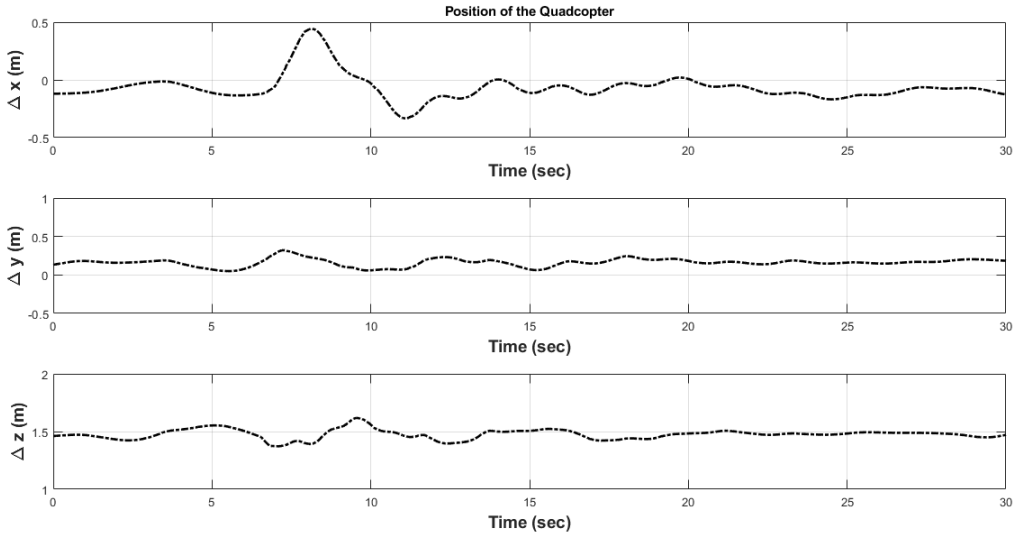

Figure 8.6: Position History of the quadcopter for Experiment 2

This experiment is performed to evaluate the performance of the controller when the disturbance estimates are not available. In the experimental setup the total disturbance is

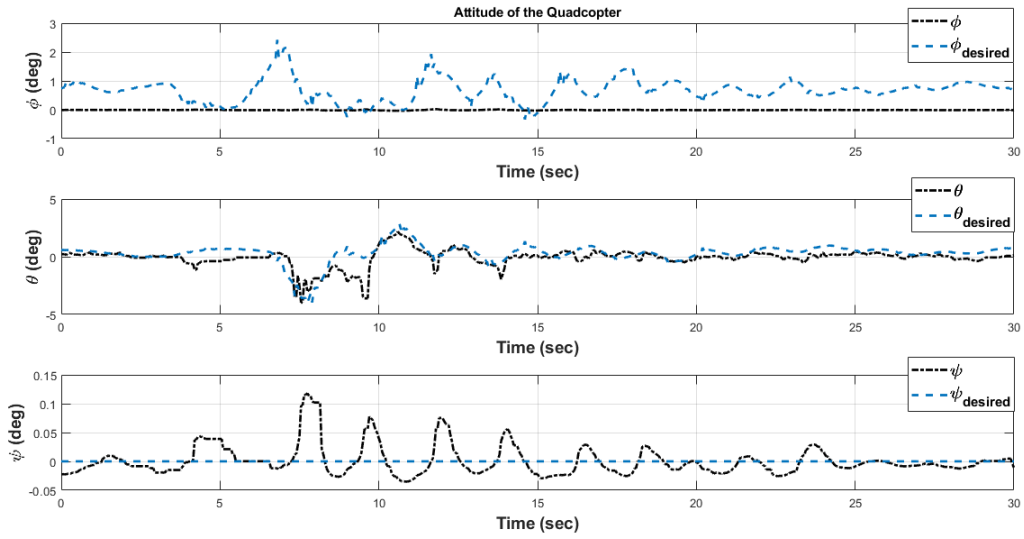

Figure 8.7: Attitude of the quadcopter for Experiment 2

estimated for the performance evaluation of the controller but the information is not provided to the controller. The quadcopter is in a hovering state at the start of the experiment and the payload is in the stable configuration. The desired altitude at which the quadcopter is commanded to hover is 1.5 m and the initial x and y location of the quadcopter in the Vicon capture volume as illustrated in figure 8.1. Approximately at 5 seconds after the experiment is initiated, the payload is perturbed manually in the $x_i - z_i$ longitudinal plane and disturbances are introduced in the system due to the oscillation of the payload. As seen in figures 8.6, 8.7 and 8.8, the controller tries to reject these disturbances while trying to maintain the inertial position of the quadcopter and damp out the oscillations of the cable slung payload.

From figure 8.7 it can be observed that the attitude controller tries to control the pitch angle of the quadcopter, thus providing necessary force to control the longitudinal position of the quadcopter (position along inertial x axis) and damp the oscillations of the payload. The desired pitch angle has an oscillatory behavior and it decays to zero as the quadcopter

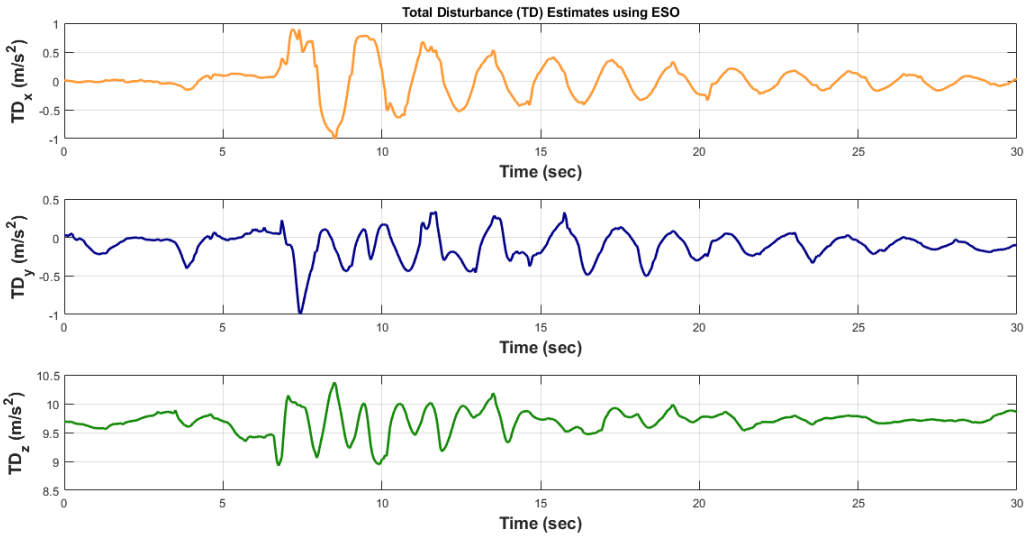

Figure 8.8: Estimated value of the Total Disturbance acting on the Quadcopter for Experiment 2

goes back to the initial hover pose.

Even though the extended state observer is estimating the disturbances, this information is not provided to the controller. These estimates are used to compare the performance of the controller with the case when the disturbance estimate information is available to the controller. It can be seen from figure 8.8 that the extended state observer estimates the total disturbances $\mathrm{TD_x}$, $\mathrm{TD_y}$, and $\mathrm{TD_z}$ induced in the system in x, y, and z direction respectively. The total disturbance along x and y direction converge to a value around 0 $\mathrm{m/s^2}$ as the quadcopter goes back to the initial hover pose. The estimates of the total disturbance in the z direction ($\mathrm{TD_z}$) converges to a value around 9.6 $\mathrm{m/s^2}$ as the system is stabilized. This indicates that the only disturbance acting on the system is the acceleration due to gravity as the quadcopter goes back to the hover position.

The average settling time for the system to be stabilized after the payload is perturbed is approximately $20-25$ seconds. It can be deduced from figure 8.8 that the settling time for the cable suspended payload is more in this case as compared to the case when

these disturbance estimates are available to the controller, since it takes more time for the disturbance estimates along x and y direction to converge to a value around 0 $\mathrm{m/s^2}$.

8.3 Controller Performance Comparison (with and without the Disturbance Estimates)

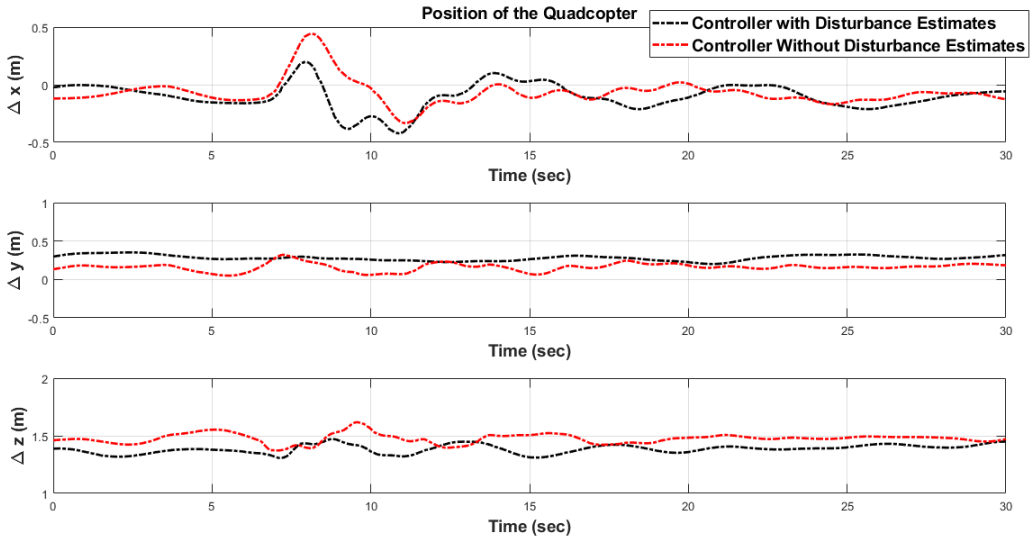

Figure 8.9: Position History Comparison for Experiment 1 and 2

This section compares the performance of the controller when the estimates of the total disturbance acting on the quadcopter due to the motion of the payload are provided (ref. section 8.1) and when the disturbance estimates are unavailable (ref. section 8.2). From figure 8.9, it can be seen that the amplitude of the perturbation along the x direction is more when the payload is perturbed and the disturbance estimates are unavailable. The position control of the quadcopter is dependent on the desired attitude of the quadcopter and how well the attitude (pitch angle in this case) is controlled. This is reflected in the attitude history of the quadcopter for both the experiments as shown in figure 8.10 since the desired attitude is dependent on the estimates of the total disturbance. The total disturbance

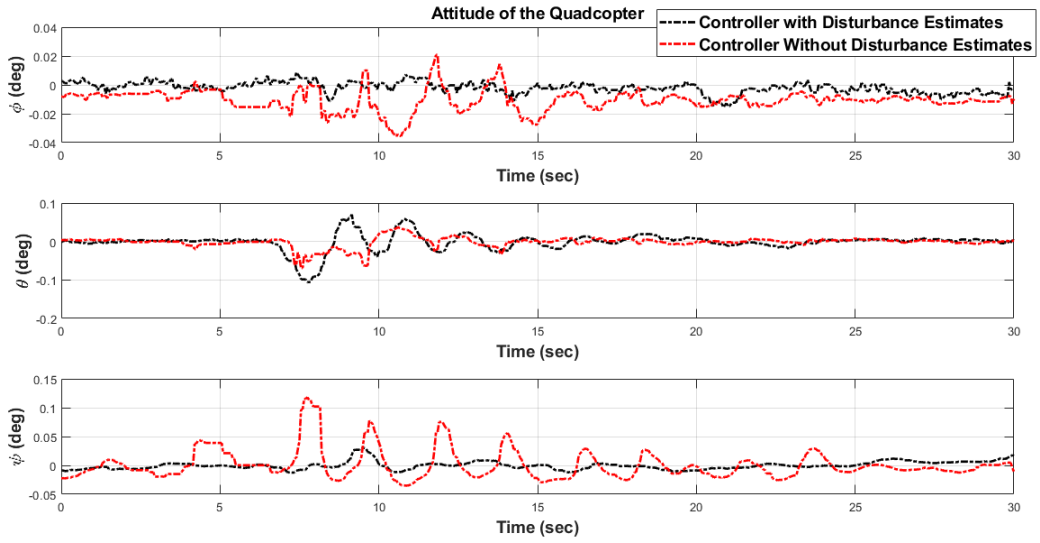

Figure 8.10: Attitude History Comparison for Experiment 1 and 2

estimates, shown in figure 8.11, gives an idea about the swing of the payload cable. Since there are no additional disturbances acting on the quadcopter, the only disturbance is due to the oscillation of the payload. As seen in the figure 8.9 and 8.11, the quadcopter settles and goes in the hover mode at the desired position, approximately in the same time after the payload is perturbed in both the cases but the payload stabilizes faster when the total disturbance estimates are provided to the controller.

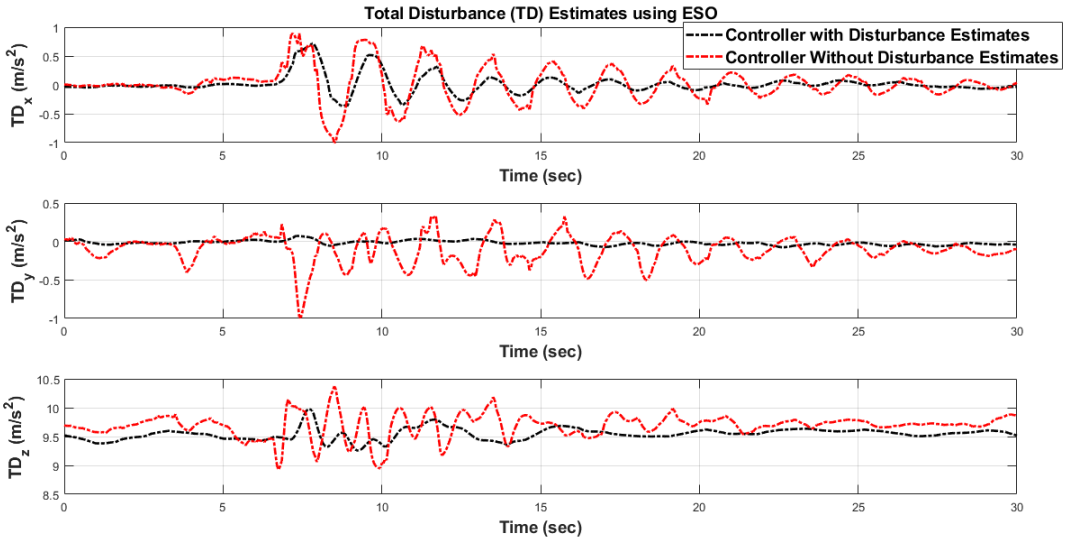

Figure 8.11: Comparison of Estimated value of the Total Disturbance acting on the Quadcopter for Experiment 1 and 2

8.4 Experiment 3: Quadcopter is Commanded to Follow a Point to Point Minimum-Jerk Trajectory

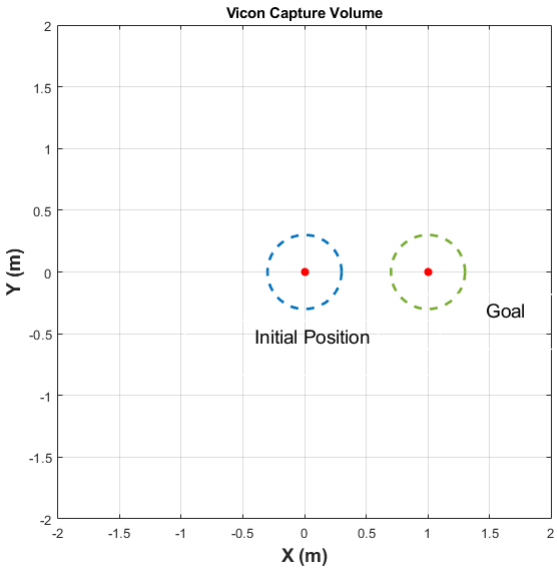

Figure 8.12: Waypoint Setup for Experiment 3

For this experiment case, the quadcopter with cable suspended payload is commanded to hover at an altitude of 1.6 m and the payload is in a stable configuration at the start of the experiment. The initial x and y position of the quadcopter and the goal location are illustrated in figure 8.12. Approximately at 5 seconds after the experiment is initiated, the quadcopter is commanded to follow a point to point minimum-jerk trajectory with constrained acceleration [49] from the initial position to the goal.

The desired trajectory is defined as as follows

$$\begin{aligned} x_{des}(t) &= a_0 + a_1 t + a_2 t^2 + a_3 t^3 + a_4 t^4 + a_5 t^5 \\ \dot{x}_{des}(t) &= a_1 + 2a_2 t + 3a_3 t^2 + 4a_4 t^3 + 5a_5 t^4 \\ \ddot{x}_{des}(t) &= 2a_2 + 6a_3 t + 12a_4 t^2 + 20a_5 t^3 \end{aligned} \tag{8.7}$$

where, x_{des}, $\dot{x}_{des}$ and $\ddot{x}_{des}$ are the desired position, velocity and acceleration of the quadcopter along inertial x axis respectively and $a_0,\ a_1,\ a_2,\ a_3,\ a_4,\ a_5$ are the coefficients of the polynomial. The initial conditions at time $t = 0$ and the final conditions at $t = t_f$ are

$$\begin{aligned} x_{des}(0) &= 0 \\ x_{des}(t_f) &= 1 \\ \dot{x}_{des}(0) = \dot{x}_{des}(t_f) &= 0 \\ \ddot{x}_{des}(0) = \ddot{x}_{des}(t_f) &= 0 \end{aligned} \tag{8.8}$$

Note, time $t = 0$ is the time at which the trajectory is initiated and it is not equal to the time at which the experiment is initiated. Also, $t = t_f$ is the final time of the trajectory and not the time when the experiment is terminated.

From [49], the final time t_f is obtained in terms of the maximum acceleration (a_{max}) and the coefficients of the polynomial are computed as function t_f and boundary conditions as

$$
\begin{aligned}
t_f &\geq \sqrt{\frac{10\left(x_{des}\left(t_f\right)-x_{des}\left(t_f\right)\right)}{\sqrt{3}a_{max}}} \\
a_0 &= x_{des}\left(0\right) \\
a_1 &= 0 \\
a_2 &= 0 \\
a_3 &= 10\left(\frac{\left(x_{des}\left(t_f\right)-x_{des}\left(0\right)\right)}{t_f^3}\right) \\
a_4 &= -15\left(\frac{\left(x_{des}\left(t_f\right)-x_{des}\left(0\right)\right)}{t_f^4}\right) \\
a_5 &= 6\left(\frac{\left(x_{des}\left(t_f\right)-x_{des}\left(0\right)\right)}{t_f^5}\right)
\end{aligned} \tag{8.9}
$$

Using the boundary conditions and choosing the maximum acceleration, $a_{max} = 0.5\text{m/s}^2$, the final time, t_f, and the coefficients are computed as

$$
\begin{aligned}
t_f &\geq 3.3981 \\
a_0 &= 0 \\
a_1 &= 0 \\
a_2 &= 0 \\
a_3 &= 0.2549 \\
a_4 &= -0.1125 \\
a_5 &= 0.0132
\end{aligned} \tag{8.10}
$$

It can be seen from figure 8.13 that the quadcopter follows the desired trajectory with a lag and the system response converges with a steady state error approximately equal to 0.2 m. From figure 8.14 it is observed that the pitch angle has a decaying oscillatory behav-

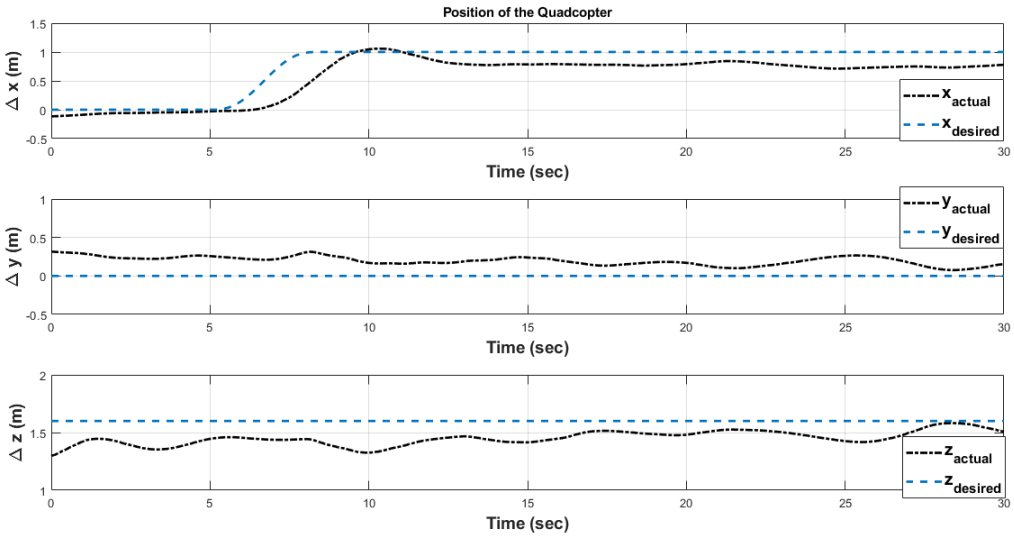

Figure 8.13: Position of the quadcopter for Experiment 3

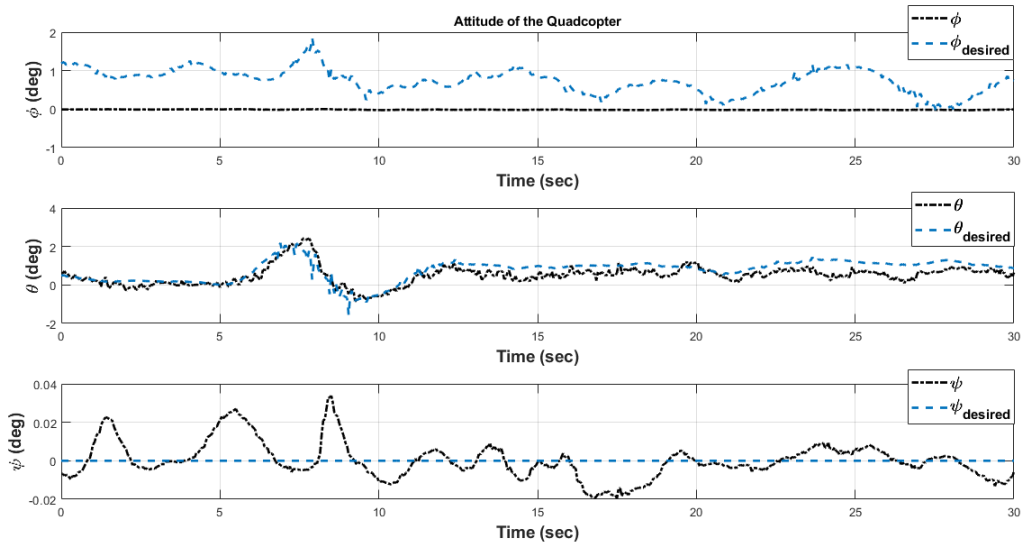

Figure 8.14: Attitude of the quadcopter for Experiment 3

ior as the controller tries to track the desired trajectory while attenuating the oscillations of the cable slung payload.

From the disturbance estimates in figure 8.15, it can be seen that the payload is perturbed as the quadcopter starts tracking the desired trajectory. The estimates of the total

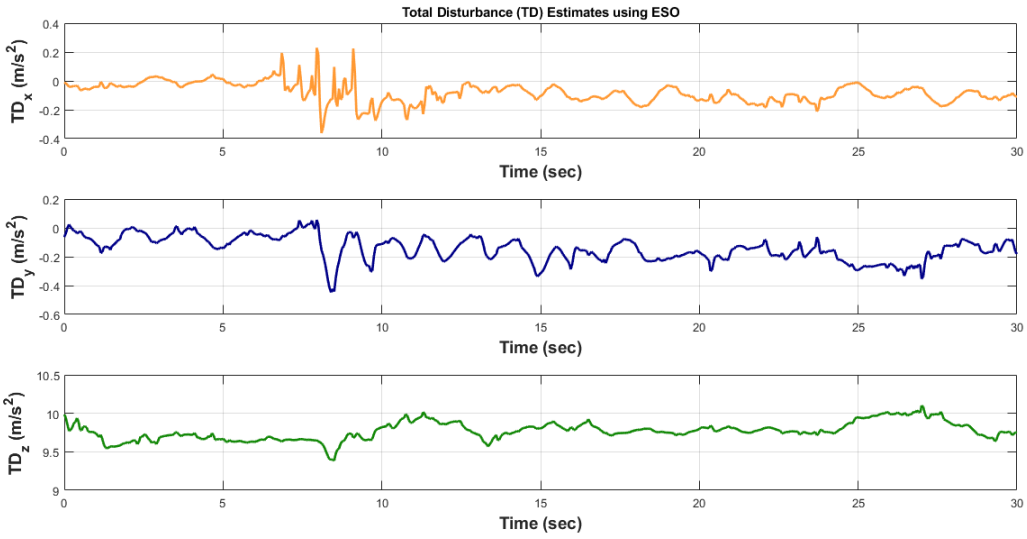

Figure 8.15: Estimated value of the Total Disturbance acting on the Quadcopter for Experiment 3

disturbance along x and y direction converge to a value around 0 $\mathrm{m/s^2}$ and the total disturbance along z direction to a value around 9.6 $\mathrm{m/s^2}$ as the quadcopter goes in the hover mode at the goal location. The average settling time after the quadcopter reaches the goal and goes in the hove mode is approximately 3 seconds.

CHAPTER 9

Cooperative Control Design for Multiple Quadcopters Transporting a Cable Suspended Payload

This chapter presents the mathematical modeling of a multi-agent system consisting of multiple quadcopters connected to a rigid body payload via cables. A distributed extended state observer based active disturbance rejection controller is implemented on this system to achieve the cooperative control task of safely transporting the payload while attenuating the swing of the payload and maintaining the trajectory of the payload along a prescribed path. The following assumptions are made for the dynamic modeling of this multi-agent interconnected and underactuated mechanical system

- The suspension point is same as the center of mass for each of the quadcopter
- The payload is assumed to be a rigid body
- The cable is assumed to be massless and rigid
- The suspension is frictionless

9.1 Equations of Motion

Figure 9.1 shows the coordinate frames associated with the multi-agent system of n quadcopters connected to a rigid body payload via rigid and massless cables. Throughout this chapter, the variables related to the payload are denoted by the subscript "0" and the variables for the i^{th} quadcopter by the subscript "i". Consider an inertial coordinate frame $\{\mathbf{I}\}$, fixed to the ground, a body fixed frame $\{\mathbf{B}_i\}$, attached to the center of mass of each quadcopter, and a body fixed frame $\{\mathbf{O}\}$, attached to the center of mass of the payload. Let $\mathbf{X}_{Qi} \in \mathbb{R}^3$ denote the position of the i^{th} quadcopter in the inertial frame and $\mathbf{X}_0 \in \mathbb{R}^3$

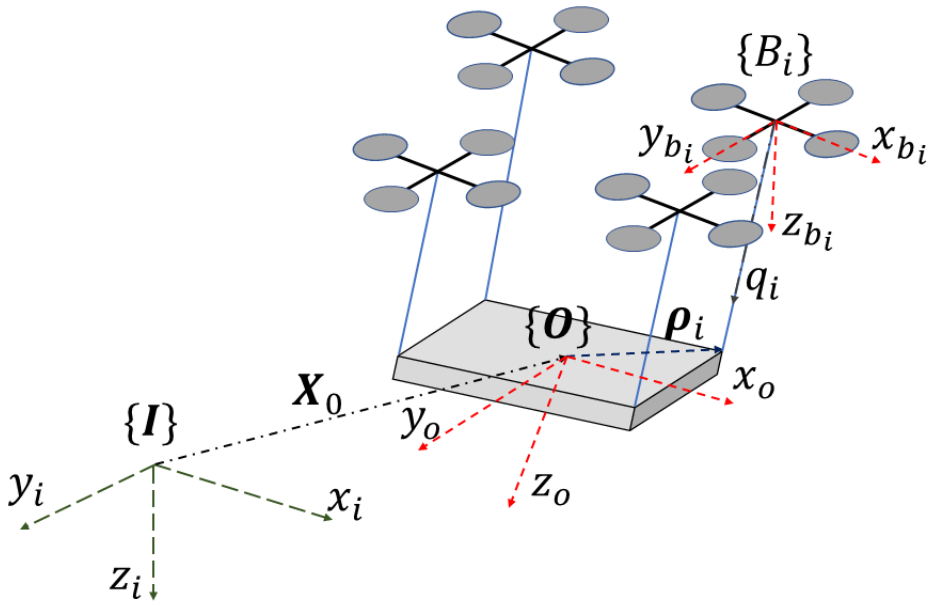

Figure 9.1: Description of coordinate frames associated with the multi-agent system consisting of multiple quadcopters connected to a rigid body payload via cables

denote the location of the center of mass of the payload in the inertial frame; $\mathbf{R}_0 \in SO(3)$ is the direction cosine matrix representing the body frame to inertial frame transformation for the payload and $\mathbf{R}_i \in SO(3)$ is the direction cosine matrix representing the body frame to inertial frame transformation for the i^{th} quadcopter. The mass and the inertia matrix of the payload are denoted by m_0 and $\mathbf{J}_0 \in \mathbb{R}^{3\times3}$ respectively. The mass and the inertia matrix of the i^{th} quadcopter are denoted by m_i and $\mathbf{J}_i \in \mathbb{R}^{3\times3}$ respectively. Let l_i be the length of each cable link and $\mathbf{q}_i \in S^2$ $\left(S^2 = \left\{\mathbf{q}_i \in \mathbb{R}^3 \text{ and } \|\mathbf{q}_i\| = 1\right\}\right)$ be the unit-vector representing the direction of the i^{th} cable measured from the quadcopter towards the payload and $\boldsymbol{\omega}_i$ represent the angular velocity of the i^{th} cable. The body frame angular velocity of the i^{th} quadcopter is represented by $\boldsymbol{\Omega}_i$ and the body frame angular velocity of the payload is denoted by $\boldsymbol{\Omega}_0$. Let $\boldsymbol{\rho}_i \in \mathbb{R}^3$ represent the point on the payload where the cable link from

the i^{th} quadcopter is attached. $\boldsymbol{\rho}_i$ is represented in the body fixed frame $\{\mathbf{O}\}$. The position of the center of mass of the i^{th} quadcopter can be expressed in terms of the position of the payload, $\mathbf{X}_0$, the unit vector $\mathbf{q}_i$, cable length l_i, and the point where the cable is attached to the payload $\boldsymbol{\rho}_i$, as

$$\mathbf{X}_{Qi} = \mathbf{X}_0 + \mathbf{R}_0\boldsymbol{\rho}_i - l_i\mathbf{q_i}$$

To consolidate, the states of the system evolve over the configuration manifold given by

$$\mathbf{Q} = SO(3) \times \mathbb{R}^3 \times \left(S^2 \times SO(3)\right)^n$$

The kinematic equations for the payload, the quadcopters and the cable links are given by

$$\begin{aligned} \dot{\mathbf{q}}_i &= \boldsymbol{\omega}_i \times \mathbf{q}_i \\ \dot{\mathbf{R}}_0 &= \mathbf{R}_0\hat{\boldsymbol{\Omega}}_0 \\ \dot{\mathbf{R}}_i &= \mathbf{R}_i\hat{\boldsymbol{\Omega}}_i \end{aligned} \tag{9.1}$$

The equations of motion for the multiple quadcopters transporting a cable suspended rigid body payload are derived using the Lagrangian mechanics. The kinetic energy of the payload is given by

$$T_0 = \frac{1}{2}m_0\|\dot{\mathbf{X}}_0\|^2 + \frac{1}{2}\boldsymbol{\Omega}_0^T\mathbf{J}_0\boldsymbol{\Omega}_0 \tag{9.2}$$

The total kinetic energy of the n quadcopters is given by

$$T_Q = \frac{1}{2}\sum_{i=1}^{n} m_i\|\dot{\boldsymbol{X}}_0 + \dot{\mathbf{R}}_0\boldsymbol{\rho}_i - l_i\dot{\mathbf{q}}_i\|^2 + \frac{1}{2}\boldsymbol{\Omega}_i^T\mathbf{J}_i\boldsymbol{\Omega}_i \tag{9.3}$$

From eq. (9.1), (9.2) and (9.3), the total kinetic energy of the system is given as

$$\begin{aligned} T =& \frac{1}{2}m_T\|\dot{\mathbf{X}}_0\|^2 + \frac{1}{2}\boldsymbol{\Omega}_0^T\mathbf{J}_0\boldsymbol{\Omega}_0 + \sum_{i=1}^{n}\frac{1}{2}\boldsymbol{\Omega}_i^T\mathbf{J}_i\boldsymbol{\Omega}_i + \dot{\mathbf{X}}_0 \cdot \sum_{i=1}^{n} m_i\left(\mathbf{R}_0\hat{\boldsymbol{\Omega}}_0\boldsymbol{\rho}_i - l_i\dot{\mathbf{q}}_i\right) \\ &+ \sum_{i=1}^{n}\frac{1}{2}m_i\left(\|\mathbf{R}_0\hat{\boldsymbol{\Omega}}_0\boldsymbol{\rho}_i\|^2 + \|l_i\dot{\mathbf{q}}_i\|^2\right) - \sum_{i=1}^{n} m_i\left(\mathbf{R}_0\hat{\boldsymbol{\Omega}}_0\boldsymbol{\rho}_i\right)\cdot(l_i\dot{\mathbf{q}}_i) \end{aligned} \tag{9.4}$$

where, $m_T = m_0 + \sum_{i=1}^{n} m_i$.

The total potential energy of the system is given as

$$V = -m_T g \mathbf{X}_0 \cdot \mathbf{e}_3 - \sum_{i=1}^{n} m_i g \mathbf{e}_3 \cdot (\mathbf{R}_0 \boldsymbol{\rho}_i - l_i \mathbf{q}_i) \tag{9.5}$$

where $\mathbf{e}_3 = \begin{bmatrix} 0 & 0 & 1 \end{bmatrix}^T$.

Using the expression for the total kinetic energy given in eq. (9.4) and total potential energy given in eq. (9.5), the Lagrangian is formulated as

$$\begin{aligned} \mathscr{L} =& \frac{1}{2} m_T \|\dot{\mathbf{X}}_0\|^2 + \frac{1}{2} \Omega_0^T \mathbf{J}_0 \Omega_0 + \sum_{i=1}^{n} \frac{1}{2} \Omega_i^T \mathbf{J}_i \Omega_i + \dot{\mathbf{X}}_0 \cdot \sum_{i=1}^{n} m_i \left(\mathbf{R}_0 \hat{\Omega}_0 \boldsymbol{\rho}_i - l_i \dot{\mathbf{q}}_i \right) \\ &+ \sum_{i=1}^{n} \frac{1}{2} m_i \left(\|\mathbf{R}_0 \hat{\Omega}_0 \boldsymbol{\rho}_i\|^2 + \|l_i \dot{\mathbf{q}}_i\|^2 \right) - \sum_{i=1}^{n} m_i \left(\mathbf{R}_0 \hat{\Omega}_0 \boldsymbol{\rho}_i \right) \cdot (l_i \dot{\mathbf{q}}_i) \\ &+ m_T g \mathbf{X}_0 \cdot \mathbf{e}_3 + \sum_{i=1}^{n} m_i g \mathbf{e}_3 \cdot (\mathbf{R}_0 \boldsymbol{\rho}_i - l_i \mathbf{q}_i) \end{aligned} \tag{9.6}$$

Let $\delta \mathbf{X}_0$ and $\delta \dot{\mathbf{X}}_0$ be the variation in $\mathbf{X}_0$ and $\dot{\mathbf{X}}_0$ respectively. From [55], the variation of a rotation matrix, $\mathbf{R}_j$, the variation in the angular velocity, Ω_j, and the variation of $\mathbf{q}_i$ is given as

$$\begin{aligned} \delta \mathbf{R}_j &= \mathbf{R}_j \hat{\boldsymbol{\eta}}_j \\ \delta \Omega_j &= \dot{\boldsymbol{\eta}}_j + \Omega_j \times \boldsymbol{\eta}_j \\ \delta \mathbf{q}_i &= \boldsymbol{\xi}_i \times \mathbf{q}_i \end{aligned} \tag{9.7}$$

for $\boldsymbol{\eta}_j \in \mathbb{R}^3$ and $\boldsymbol{\xi}_i \in \mathbb{R}^3$. The variation of $\dot{\mathbf{q}}_i$ is given by

$$\delta \dot{\mathbf{q}}_i = \dot{\boldsymbol{\xi}}_i \times \mathbf{q}_i + \boldsymbol{\xi}_i \times \dot{\mathbf{q}}_i \tag{9.8}$$

Now, the derivatives of the Lagrangian $\mathscr{L}$ with respect to $\mathbf{X}_0$, $\dot{\mathbf{X}}_0$, $\mathbf{R}_j$ Ω_j, $\mathbf{q}_i$ and $\dot{\mathbf{q}}_i$ are given by

$$\begin{aligned}
\mathbf{D}_{\mathbf{X}_0}\mathscr{L} &= m_T g\mathbf{e}_3 \\
\mathbf{D}_{\dot{\mathbf{X}}_0}\mathscr{L} &= m_T\dot{\mathbf{X}}_0 + \sum_{i=1}^{n} m_i\left(\mathbf{R}_0\hat{\Omega}_0\boldsymbol{\rho}_i - l_i\dot{\mathbf{q}}_i\right) \\
\mathbf{D}_{\Omega_0}\mathscr{L} &= \bar{\mathbf{J}}_0\Omega_0 + \sum_{i=1}^{n} m_i\hat{\boldsymbol{\rho}}_i\mathbf{R}_0^T\left(\dot{\mathbf{X}}_0 - l_i\dot{\mathbf{q}}_i\right) \\
\mathbf{D}_{\Omega_i}\mathscr{L} &= \mathbf{J}_i\Omega_i \\
\mathbf{D}_{\mathbf{q}_i}\mathscr{L} &= -m_i g l_i\mathbf{e}_3 \\
\mathbf{D}_{\dot{\mathbf{q}}_i}\mathscr{L} &= m_i\left(l_i^2\dot{\mathbf{q}}_i - l_i\dot{\mathbf{X}}_0 - l_i\mathbf{R}_0\hat{\Omega}_0\boldsymbol{\rho}_i\right) \\
\mathbf{D}_{\mathbf{R}_0}\mathscr{L} &= \sum_{i=1}^{n} m_i\hat{\Omega}_0\boldsymbol{\rho}_i\cdot\left(\dot{\mathbf{X}}_0 - l_i\dot{\mathbf{q}}_i\right)
\end{aligned} \tag{9.9}$$

where, $\bar{\mathbf{J}}_0 = \mathbf{J}_0 - \sum_{i=1}^{n} m_i\hat{\boldsymbol{\rho}}_i^2$.

Let $\mathfrak{B} = \int_{t_0}^{t_f}\mathscr{L}dt$ be the action integral. Using the derivatives of the Lagrangian in eq. (9.9) and the variation in $\mathbf{X}_0$ and $\dot{\mathbf{X}}_0$, the rotation matrix, $\mathbf{R}_j$, the angular velocity, Ω_j, and the variation of $\mathbf{q}_i$ and $\dot{\mathbf{q}}_i$ given in eq. (9.7) and (9.8), the variation of the action integral can be written as

$$\begin{aligned}
\delta\mathfrak{B} = \int_{t_0}^{t_f} &\mathbf{D}_{\mathbf{X}_0}\mathscr{L}\cdot\delta\mathbf{X}_0 + \mathbf{D}_{\dot{\mathbf{X}}_0}\mathscr{L}\cdot\delta\dot{\mathbf{X}}_0 + \mathbf{D}_{\Omega_0}\mathscr{L}\cdot\delta\Omega_0 + \mathbf{D}_{\Omega_i}\mathscr{L}\cdot\delta\Omega_i \\
&+ \mathbf{D}_{\mathbf{q}_i}\mathscr{L}\cdot\delta\mathbf{q}_i + \mathbf{D}_{\dot{\mathbf{q}}_i}\mathscr{L}\cdot\delta\dot{\mathbf{q}}_i + \mathbf{D}_{\mathbf{R}_0}\mathscr{L}\cdot\delta\mathbf{R}_0
\end{aligned} \tag{9.10}$$

The virtual work done by the thrust and torques generated by the propellers is given by

$$\mathfrak{W} = \int_{t_0}^{t_f}\sum_{i=1}^{n}\mathbf{R}_i\mathbf{T}_i.\left(\delta\mathbf{X}_0 + \delta\mathbf{R}_0\boldsymbol{\rho}_i - l_i\delta\mathbf{q}_i\right) + \boldsymbol{\tau}_i.\boldsymbol{\eta}_i\,dt \tag{9.11}$$

where, $\mathbf{T}_i$ is the total thrust acting on the i^{th} quadcopter expressed in the body frame (ref. eq. (3.3)) and $\boldsymbol{\tau}_i$ is the torque acting on the i^{th} quadcopter as given in eq. (3.4).

According to the Lagrange-d'Alembert principle, the variation of the action integral is equal to the negative of the virtual work done by the external force and moments. Hence,

$$\delta\mathfrak{B} = -\mathfrak{W} \tag{9.12}$$

From eq. (9.9), (9.10), (9.11) and (9.12), and using integration by parts along with the fact that the variations at the end points vanish [56] results in the following Euler-Lagrange equations

$$\begin{aligned}
\frac{d}{dt}\mathbf{D}_{\dot{\mathbf{X}}_0}\mathscr{L} - \mathbf{D}_{\mathbf{X}_0}\mathscr{L} &= \sum_{i=1}^{n}\mathbf{R}_i\mathbf{T}_i \\
\frac{d}{dt}\mathbf{D}_{\Omega_0}\mathscr{L} + \Omega_0 \times \mathbf{D}_{\Omega_0}\mathscr{L} - \mathbf{d}_{\mathbf{R}_0}\mathscr{L} &= \sum_{i=1}^{n}\hat{\boldsymbol{\rho}}_0\mathbf{R}_0^T\mathbf{R}_i\mathbf{T}_i \\
\hat{\mathbf{q}}_i\frac{d}{dt}\mathbf{D}_{\dot{\mathbf{q}}_i}\mathscr{L} - \hat{\mathbf{q}}_i\mathbf{D}_{\mathbf{q}_i}\mathscr{L} &= -l_i\hat{\mathbf{q}}_i\mathbf{R}_i\mathbf{T}_i \\
\frac{d}{dt}\mathbf{D}_{\Omega_i}\mathscr{L} + \Omega_i \times \mathbf{D}_{\Omega_i}\mathscr{L} &= \boldsymbol{\tau}_i
\end{aligned} \tag{9.13}$$

where, $\mathbf{d}_{\mathbf{R}_0}\mathscr{L} = \sum_{i=1}^{n} m_i\left(\widehat{\hat{\Omega}_0\boldsymbol{\rho}_i}\mathbf{R}_0^T\left(\dot{\mathbf{X}}_0 - l_i\dot{\mathbf{q}}_i\right) + g\hat{\boldsymbol{\rho}}_i\mathbf{R}_0^T\mathbf{e}_3\right)$. Substituting eq. (9.9) in eq. (9.13) and rearranging by the fact that $\ddot{\mathbf{q}}_i = -\hat{\mathbf{q}}_i\dot{\boldsymbol{\omega}}_i - \|\boldsymbol{\omega}\|^2\mathbf{q}_i$ and $\hat{\mathbf{q}}_i\ddot{\mathbf{q}}_i = -\hat{\mathbf{q}}_i^2\dot{\boldsymbol{\omega}}_i = \dot{\boldsymbol{\omega}}_i$ [81], the equations of motion for multiple quadcopters transporting a cable suspended rigid body payload are given by

$$m_T\ddot{\mathbf{X}}_0 + \sum_{i=1}^{n} m_i\left(-\mathbf{R}_0\hat{\boldsymbol{\rho}}_i\dot{\Omega}_0 + l_i\hat{\mathbf{q}}_i\dot{\boldsymbol{\omega}}_i\right) = -\sum_{i=1}^{n} m_i\mathbf{R}_0\hat{\Omega}_0^2\boldsymbol{\rho}_i + m_i l_i\|\boldsymbol{\omega}_i\|^2\mathbf{q}_i + m_T g\mathbf{e}_3 + \sum_{i=1}^{n}\mathbf{R}_i\mathbf{T}_i \tag{9.14}$$

$$\sum_{i=1}^{n} m_i\hat{\boldsymbol{\rho}}_i\mathbf{R}_0^T\ddot{\mathbf{X}}_0 + \bar{\mathbf{J}}_0\dot{\Omega}_0 + \sum_{i=1}^{n} m_i l_i\hat{\boldsymbol{\rho}}_i\mathbf{R}_0^T\hat{\mathbf{q}}_i\dot{\boldsymbol{\omega}}_i = \sum_{i=1}^{n}\hat{\boldsymbol{\rho}}_0\mathbf{R}_0^T\left(\mathbf{R}_i\mathbf{T}_i + m_i g\mathbf{e}_3\right) - m_i l_i\hat{\boldsymbol{\rho}}_i\mathbf{R}_0^T\|\boldsymbol{\omega}_i\|^2\mathbf{q}_i - \hat{\Omega}_0\bar{\mathbf{J}}_0\Omega_0 \tag{9.15}$$

$$-m_i l_i\hat{\mathbf{q}}_i\ddot{\mathbf{X}}_0 + m_i l_i\hat{\mathbf{q}}_i\mathbf{R}_0\hat{\boldsymbol{\rho}}_i\dot{\Omega}_0 + m_i l_i^2\dot{\boldsymbol{\omega}}_i = m_i l_i\hat{\mathbf{q}}_i\mathbf{R}_0\hat{\Omega}_0^2\boldsymbol{\rho}_i - l_i\hat{\mathbf{q}}_i\left(\mathbf{R}_i\mathbf{T}_i + m_i g\mathbf{e}_3\right) \tag{9.16}$$

$$\mathbf{J}_i\dot{\Omega}_i + \Omega_i \times \mathbf{J}_i\Omega_i = \boldsymbol{\tau}_i \tag{9.17}$$

9.2 Controller Design

The strategy to employ multiple quadcopters cooperatively within the extended state observer based active disturbance rejection controller framework is discussed in this section. The control objective is to transport the cable suspended payload connected to the quadcopters via cables along a prescribed path, damp the oscillations of the payload while transportation and maintain the formation of the quadcopter-payload system.

Let $\mathbf{x}_{0d} \in \mathbb{R}^3$ be the desired position of the payload. At equilibrium, the desired attitude of the payload, $\mathbf{R}_{0d} = \mathbf{I}_{3\times 3}$, and the desired unit vector representing the direction of the payload cable from the quadcopter to the payload, $\mathbf{q}_{id} = \mathbf{e}_3 = [0\ 0\ 1]^T$. Hence, the desired position of the quadcopter at equilibrium is given by

$$\mathbf{X}_{Qi\_d} = \mathbf{x}_{0d} + \boldsymbol{\rho}_i - \sum_{a=1}^{n} l_i \mathbf{e}_3 \tag{9.18}$$

Using the desired configuration of the quadcopters, a distributed control strategy is employed to obtain the desired control forces and moments for each quadcopter and accomplish the cooperative control task.

Based on the position feedback for each quadcopter, an extended state observer is used to estimate the disturbances acting on each of the quadcopters due to the aerodynamic profile drag, oscillations of the payload as well as the effect of other agents due to the dynamic coupling in the system. These estimates are used by the disturbance rejection controller described in Chapter 4 to control the position of each of the quadcopter and the payload.

Let $\mathbf{X}_i = \begin{bmatrix} \mathbf{X}_{Qi}^T & \mathbf{V}_{Bi}^T & \boldsymbol{\Theta}_i^T & \boldsymbol{\Omega}_i^T \end{bmatrix}^T$ where, $\mathbf{X}_{Qi} \in \mathbb{R}^3$ is the position of the i^{th} quadcopter, $\mathbf{V}_{Bi} \in \mathbb{R}^3$ is the translational velocity of the i^{th} quadcopter expressed in the body frame, $\boldsymbol{\Theta}_i = [\phi_i\ \theta_i\ \psi_i]^T$ are the Euler angles and $\boldsymbol{\Omega}_i$ is the angular velocity of the i^{th} quadcopter in the body frame. The position of the i^{th} quadcopter along inertial x and y axes can only be controlled by commanding some desired roll and pitch angles θ_{id} and ϕ_{id} for

a given fixed heading angle. The altitude of the quadcopter is controlled using the thrust input. Linearizing the translational kinematics and dynamics of the i^{th} quadcopter given at a certain hover position denoted as $\boldsymbol{X}_{Ti} = \begin{bmatrix} \overline{X}_{Qi}^T & \mathbf{0}_{1\times 3} & \mathbf{0}_{1\times 3} & \mathbf{0}_{1\times 3} \end{bmatrix}$ where, $\overline{X}_{Qi} \in \mathbb{R}^3$ is any constant position and using the roll, pitch and thrust as control inputs results in

$$\begin{aligned} \dot{\mathbf{X}}_{Qi} &= \mathbf{V}_{Bi} \\ \dot{\mathbf{V}}_{Bi} &= \mathbf{B}_i \mathbf{U}_i + \mathbf{f}_i \\ \mathbf{y}_i &= \mathbf{X}_{Qi} \end{aligned} \tag{9.19}$$

where, $\mathbf{U}_i = \begin{bmatrix} \theta_{id} & \phi_{id} & T_i \end{bmatrix}^T$; $\mathbf{B}_i = \begin{bmatrix} -g & 0 & 0 \\ 0 & g & 0 \\ 0 & 0 & \frac{1}{m_i} \end{bmatrix}$; $\mathbf{f}_i$ is the total disturbance acting on the i^{th} quadcopter which is a function of the aerodynamic profile drag, disturbances due to the oscillations of the payload and the effect of other quadcopters in the system due to the dynamic coupling; and $\mathbf{y}_i$ is the position output of the i^{th} quadcopter which is measured and needs to be controlled.

Let $\mathbf{x}_{1i} = \mathbf{X}_{Qi}$, $\mathbf{x}_{2i} = \mathbf{V}_{Bi}$ and treating $\mathbf{x}_{3i} = \mathbf{f}_i$ as an additional state, the state equations for the translational dynamics for the i^{th} quadcopter can be written as,

$$\begin{aligned} \dot{\mathbf{x}}_{1i} &= \mathbf{x}_{2i} \\ \dot{\mathbf{x}}_{2i} &= \mathbf{B}_i \mathbf{U}_i + \mathbf{x}_{3i} \\ \dot{\mathbf{x}}_{3i} &= \mathbf{G}_i(t) \\ \mathbf{y}_i &= \mathbf{x}_{1i} \end{aligned}$$

where, $\dot{\mathbf{x}}_{3i} = \mathbf{G}_i(t)$ is the dynamics of the total disturbance acting on the i^{th} quadcopter which is unknown.

The extended state observer for the i^{th} quadcopter is now constructed as

$$\begin{aligned}
\dot{\hat{\mathbf{x}}}_{1i} &= \hat{\mathbf{x}}_{2i} - \boldsymbol{\beta}_{1i}(\hat{\mathbf{x}}_{1i} - \mathbf{y}_i) \\
\dot{\hat{\mathbf{x}}}_{2i} &= \hat{\mathbf{x}}_{3i} - \mathbf{B}_i\mathbf{U}_i - \boldsymbol{\beta}_{2i}(\hat{\mathbf{x}}_{1i} - \mathbf{y}_i) \\
\dot{\hat{\mathbf{x}}}_{3i} &= -\boldsymbol{\beta}_{3i}(\hat{\mathbf{x}}_{1i} - \mathbf{y}_i)
\end{aligned}$$

where, $\boldsymbol{\beta}_{1i}$, $\boldsymbol{\beta}_{2i}$ and $\boldsymbol{\beta}_{3i}$ are the observer gain matrices; $\hat{\mathbf{x}}_{1i}$, $\hat{\mathbf{x}}_{2i}$ and $\hat{\mathbf{x}}_{3i}$ are the estimates of $\mathbf{x}_{1i}$, $\mathbf{x}_{2i}$ and $\mathbf{f}_i$ respectively.

Using the estimate of the total disturbance $\hat{\mathbf{x}}_{3i}$ for compensation, $\mathbf{U}_i$ is chosen as

$$\mathbf{U}_i = \mathbf{B}_i^{-1}(\mathbf{U}_{0i} - \hat{\mathbf{x}}_{3i})$$

with

$$\boldsymbol{U}_{0i} = -\mathbf{K_{pi}}\left(\mathbf{x}_{1i} - \mathbf{X}_{Qi\_d}\right) - \mathbf{K_{di}}\left(\dot{\mathbf{x}}_1 - \dot{\mathbf{X}}_{Qi\_d}\right) + \ddot{\mathbf{X}}_{Qi\_d}$$

where, $\mathbf{K_{pi}}$ and $\mathbf{K_{di}}$ are the controller gain matrices and $\mathbf{X}_{Qi\_d}$ is the desired value for $\mathbf{x}_{1i}$. This reduces the plant dynamics to

$$\begin{aligned}
\dot{\mathbf{x}}_{1i} &= \mathbf{x}_{2i} \\
\dot{\mathbf{x}}_{2i} &= -\mathbf{K_{pi}}\left(\mathbf{x}_{1i} - \mathbf{x}_{Qi_d}\right) - \mathbf{K_{di}}\left(\dot{\mathbf{x}}_{1i} - \dot{\mathbf{x}}_{Qi_d}\right) + \ddot{\mathbf{x}}_{Qi_d} - \Delta\mathbf{x}_{3i} \\
\mathbf{y} &= \mathbf{x}_1
\end{aligned}$$

where, $\Delta\mathbf{x}_{3i} = \hat{\mathbf{x}}_{3i} - \mathbf{x}_{3i}$. The rate of decay and other transient characteristics of the tracking errors are controlled by tuning the positive gain matrices $\mathbf{K_{pi}}$ and $\mathbf{K_{di}}$. Using the attitude controller developed in section 4.2, the desired moments are calculated. Using the desired thrust and the desired moments, eq. (4.14) is used to compute the individual motor input for each of the quadcopter. The efficacy of this distributed cooperative controller is demonstrated in section 9.3 using the mathematical model formulated in section 9.1.

9.3 Simulation Results

This section presents the implementation of the distributed extended state observer based active disturbance rejection controller for the cooperative control task of stabilization and transportation of a rigid body payload connected to multiple quadcopters via cables. The top view in $x-y$ plane of the desired flight formation for the cooperative control task is shown in figure 9.2. As illustrated in figure 9.2, there are four quadcopters (depicted using the orange circles) carrying a cable suspended rigid body payload (depicted using a green plate). The specifications of the propulsion system, and the mass, inertia and geometric parameters of the quadcopters and the payload used in the simulation are tabulated in table E.1. The observer and controller gains are tabulated in table B.1. The control objective is to maintain the formation of the quadcopter-payload system while tracking the desired trajectory of the payload, and damp the oscillations of the payload. The desired position for each quadcopter is given by eq. (9.18) and the desired unit vector representing the direction of the payload cable from the i^{th} quadcopter to the payload, $\mathbf{q}_{id} = [0\ 0\ 1]^T$. The following cases are used to demonstrate the efficacy of the controller

1. Quadcopters are in hover mode and the payload is perturbed
2. Quadcopter-payload formation is moving with a constant speed along the inertial x axis, is commanded to go in the hover mode

9.3.1 Case 1: Quadcopters are in hover mode and the payload is perturbed

The quadcopters are in a hovering state at the start of the simulation. The payload is perturbed and the initial angle for each cable in the longitudinal plane ($x-z$ plane) is 30° w.r.t the quadcopters. Hence, the initial condition of the unit vector representing the direction of each cable is $\mathbf{q}_i = \begin{bmatrix}\sin\left(\pi/6\right)\ 0\ \cos\left(\pi/6\right)\end{bmatrix}^T$. The control objective is to ensure that as time $t \to \infty$, the quadcopter position, $\mathbf{X}_{Qi} \to \mathbf{X}_{Qi\_d}$, $\mathbf{X}_0 \to \mathbf{x}_{0d}$ and $\mathbf{q}_i \to [0\ 0\ 1]$. The

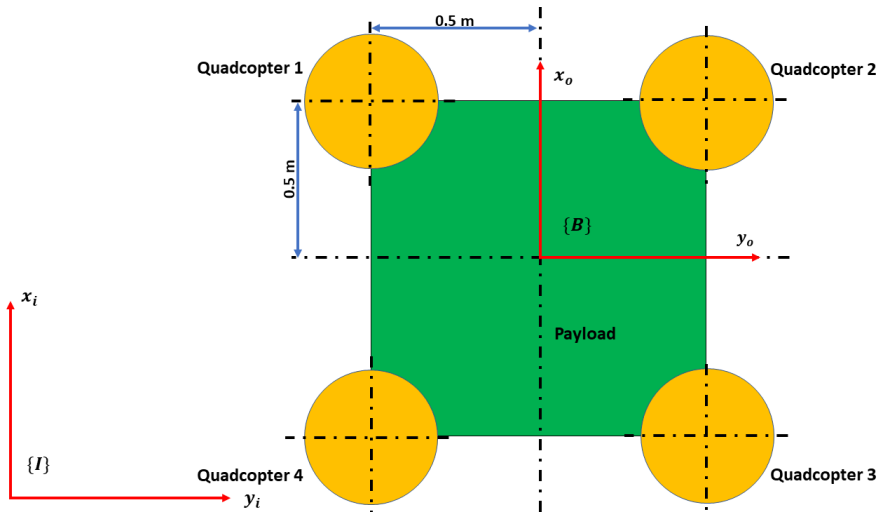

Figure 9.2: Desired Flight Formation (Top View in X-Y Plane)

desired position of the payload is $\mathbf{x}_{0d} = [0,\ 0,\ 0]^T$. From figure 9.2, the initial and desired position of the quadcopters are

$$\begin{aligned}
\mathbf{X}_{Q1_d} = \mathbf{X}_{Q1_initial} &= [0.5, -0.5, -0.75]^T \\
\mathbf{X}_{Q2_d} = \mathbf{X}_{Q2_initial} &= [0.5, 0.5, -0.75]^T \\
\mathbf{X}_{Q3_d} = \mathbf{X}_{Q3_initial} &= [-0.5, 0.5, -0.75]^T \\
\mathbf{X}_{Q4_d} = \mathbf{X}_{Q4_initial} &= [-0.5, -0.5, -0.75]^T
\end{aligned} \tag{9.20}$$

At the start of the simulation, there are disturbances introduced in the system due to the oscillations of the payload as seen in the results shown in figures 9.5, 9.6, 9.7 and 9.8. The controller tries to reject these disturbances while trying to achieve the control objective. From figures F.2, F.5, F.8 and F.11, it can be observed that the attitude controller of each quadcopter in the formation tries to control the pitch angle, thus providing necessary force to control the longitudinal position of the quadcopters (position along the inertial x axis) and damp the oscillations of the payload. Figures F.3, F.6, F.9 and F.12 illustrate the history of the unit vector along each payload cable representing the cable angle. The pitch angle for each quadcopter has an oscillatory behavior as well and it decays to zero as the payload

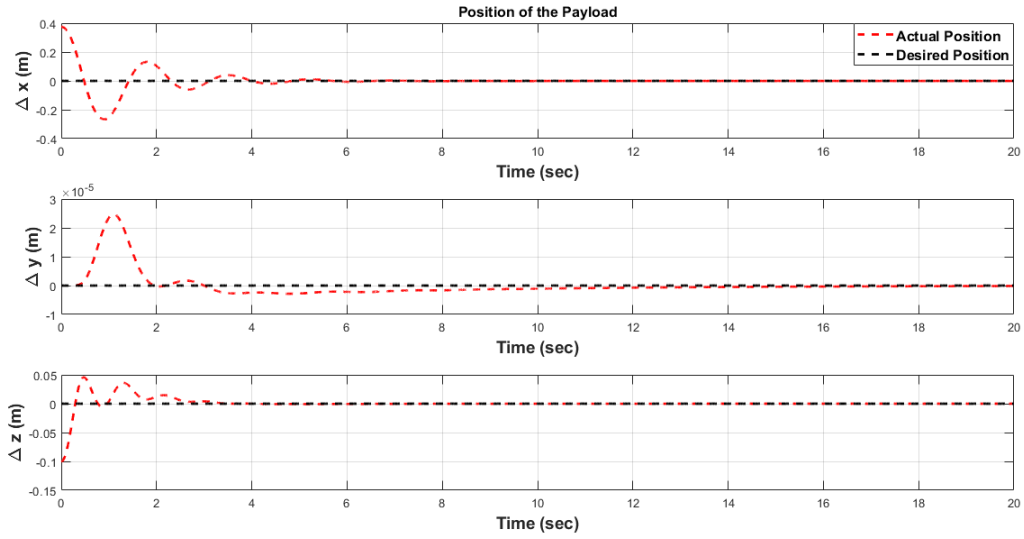

Figure 9.3: Position of the Payload

oscillations (ref. figure 9.3) decay and the quadcopters go back to the initial hover pose (ref. figures F.1, F.4, F.7 and F.10).

It can be seen from figures 9.5, 9.6, 9.7 and 9.8, that the extended state observer for each individual quadcopter tracks the total disturbances TD_x, TD_y, and TD_z acting on the respective quadcopters, in x, y, and z direction respectively. These estimates are used by the active disturbance rejection controller to control the position of each quadcopter and damp the oscillations of the payload. The total disturbance estimates in the z direction (TD_z) converges to a value of 9.81 m/s^2 as the system is stabilized indicates that the only disturbance acting on the system is the acceleration due to gravity as the quadcopter goes back to the hover position.

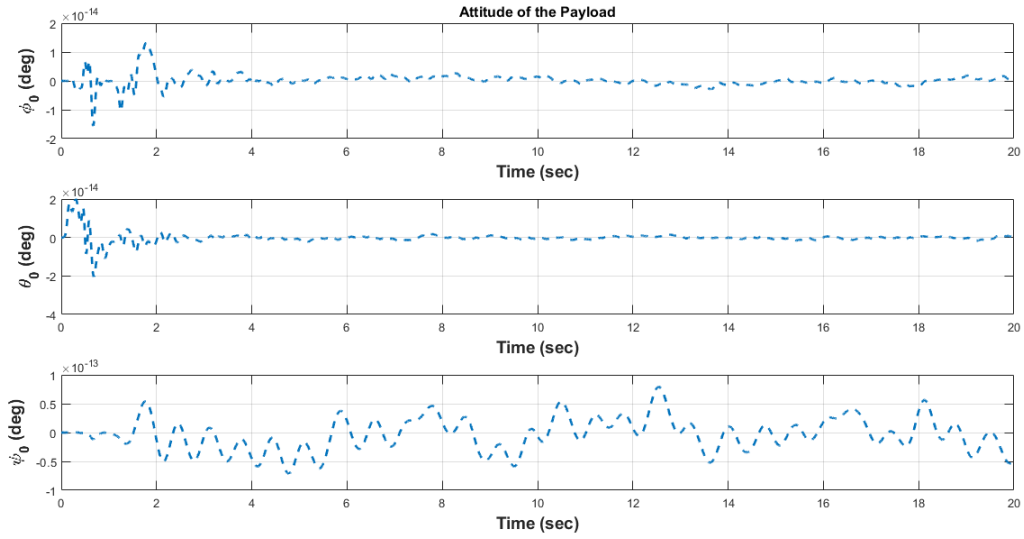

Figure 9.4: Attitude of the Payload

9.3.2 Case 2: Quadcopter-payload formation is moving with a constant speed along the inertial x axis, is commanded to go in the hover mode

At the start of the simulation, the quadcopters are in hover mode and the payload is in a stable configuration. The initial position of the payload, $\mathbf{X}_{0\_initial} = [0,\ 0,\ 0]^T$. From figure 9.2, the initial position of the quadcopters are

$$\begin{aligned}
\mathbf{X}_{Q1_initial} &= [0.5, -0.5, -0.75]^T \\
\mathbf{X}_{Q2_initial} &= [0.5, 0.5, -0.75]^T \\
\mathbf{X}_{Q3_initial} &= [-0.5, 0.5, -0.75]^T \\
\mathbf{X}_{Q4_initial} &= [-0.5, -0.5, -0.75]^T
\end{aligned}$$

The payload is prescribed to follow a straight line trajectory along the inertial x axis with a constant speed of 10.8 kmph $\left(3\ \mathrm{m/s}\right)$ and fixed altitude. This dictates the trajectory of the entire formation. At 50 s, the quadcopter-payload system is commanded to go back to the hover mode with the desired position of the payload as $\mathbf{x}_{0d} = [150,\ 0,\ 0]^T$. From figures 9.9, F.13, F.16, F.19 and F.22 it can be observed that the controller is able to maintain the

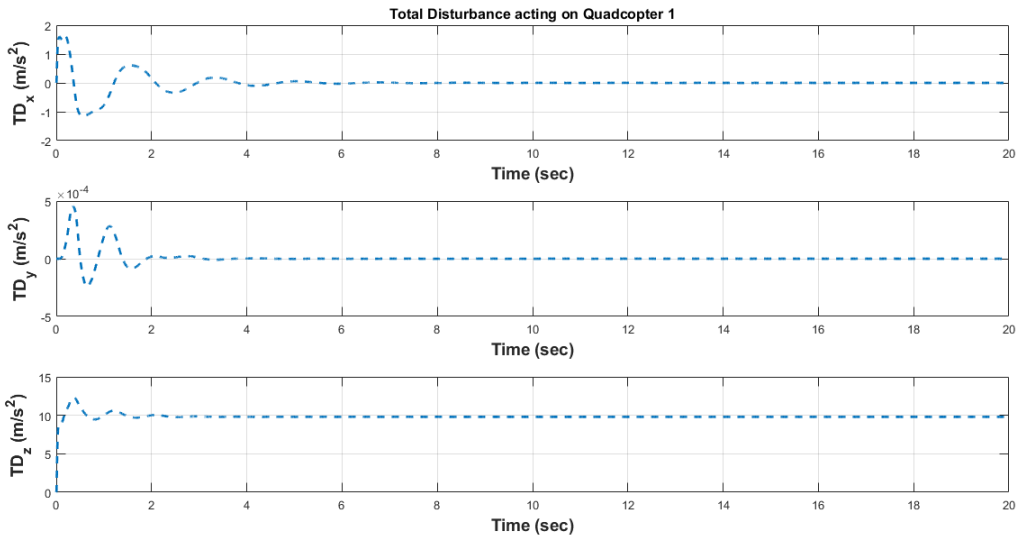

Figure 9.5: Total Disturbance Acting on Quadcopter 1

prescribed trajectory of the quadcopter-payload formation. From figures F.15, F.18, F.21 and F.24, it can be seen that the payload is perturbed due to changes in the quadcopter states at the start of the simulation and the controller stabilizes the payload while the quadcopters are in motion carrying the payload and tracking the prescribed trajectory of the formation in a decentralized manner. The payload is perturbed again when the quadcopters goes back to the hover mode as the formation reaches the desired goal location and the controller is able to stabilize the system.

The quadcopter position and velocity along the inertial x axis is maintained by controlling the pitch angle. From figures F.14, F.17, F.20 and F.23, it is observed that the pitch angle for each quadcopter has a decaying oscillatory behavior as the controller tries to maintain the constant speed straight line trajectory of the formation while attenuating the oscillations of the payload. When the formation is commanded to go back to the hover mode at 50 s, the controller tries to maintain the position and the formation of the quadcopter-payload system and attenuate the oscillations of the payload using the desired pitch angle.

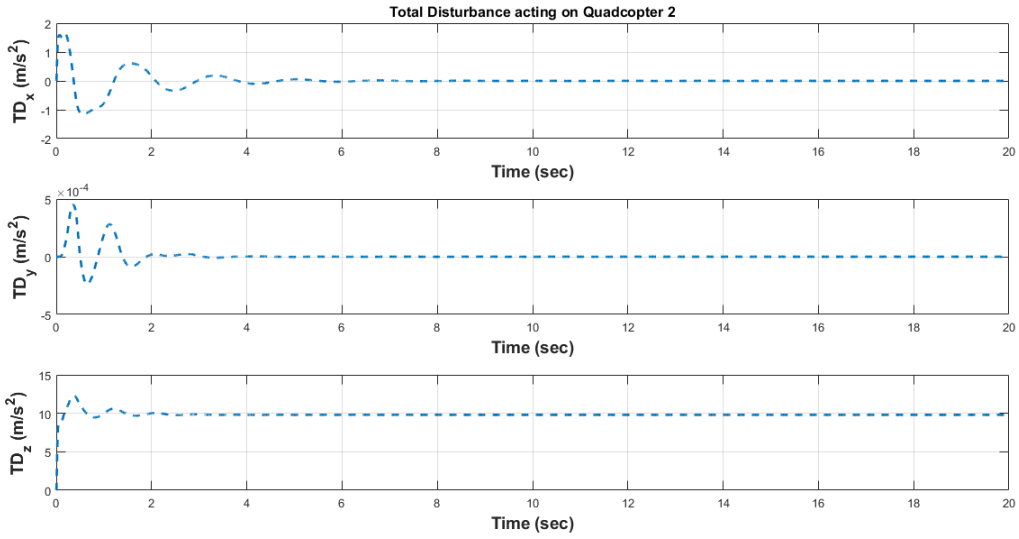

Figure 9.6: Total Disturbance Acting on Quadcopter 2

A decaying oscillatory behavior in the pitch angle of the quadcopter is observed again as the payload oscillations decay and the quadcopters go back to the desired hover pose.

It can be seen from figures 9.12, 9.13, 9.14 and 9.15, that the individual extended state observers are able to track the total disturbances acting on the individual quadcopters. These estimates are used by the active disturbance rejection controller to control the position of the respective quadcopter and damp the oscillations of the payload. Again, the total disturbance estimate along the z direction ($\mathrm{TD_z}$) converges to a value of 9.81 $\mathrm{m/s^2}$, indicating that the disturbance force acting on the system when the quadcopter is either moving along a inertial x axis with constant speed or when the quadcopter goes back in the hover mode and the cable slung payload is in the equilibrium position, is due to the acceleration due to gravity.

Figure 9.11 shows the top view of the trajectory of the formation as the quadcopters transport the payload to the goal location along the prescribed trajectory.

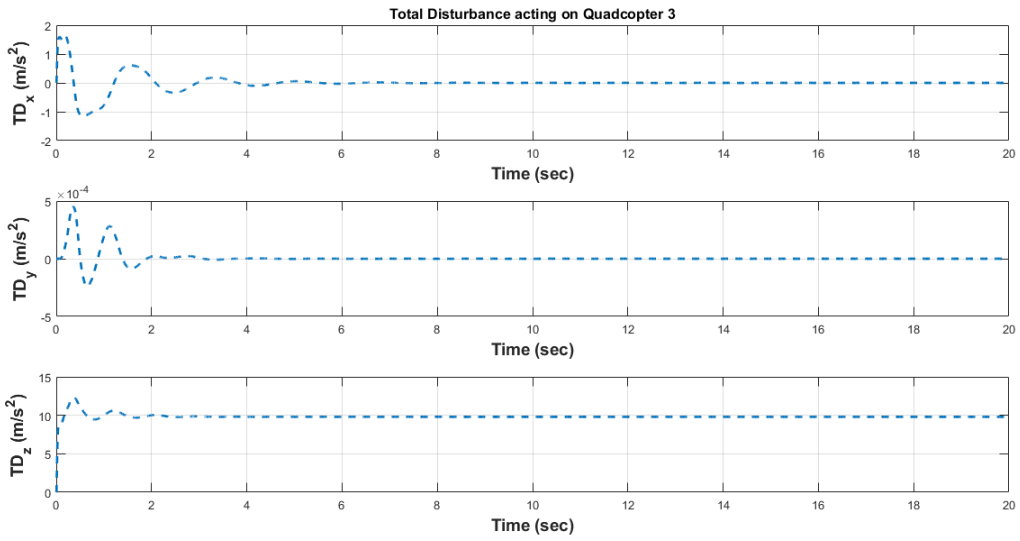

Figure 9.7: Total Disturbance Acting on Quadcopter 3

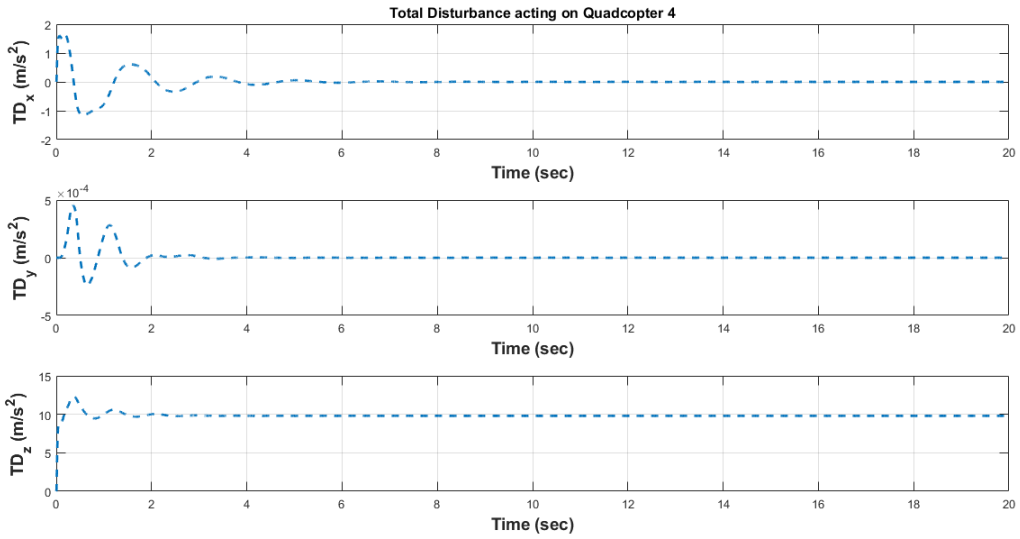

Figure 9.8: Total Disturbance Acting on Quadcopter 4

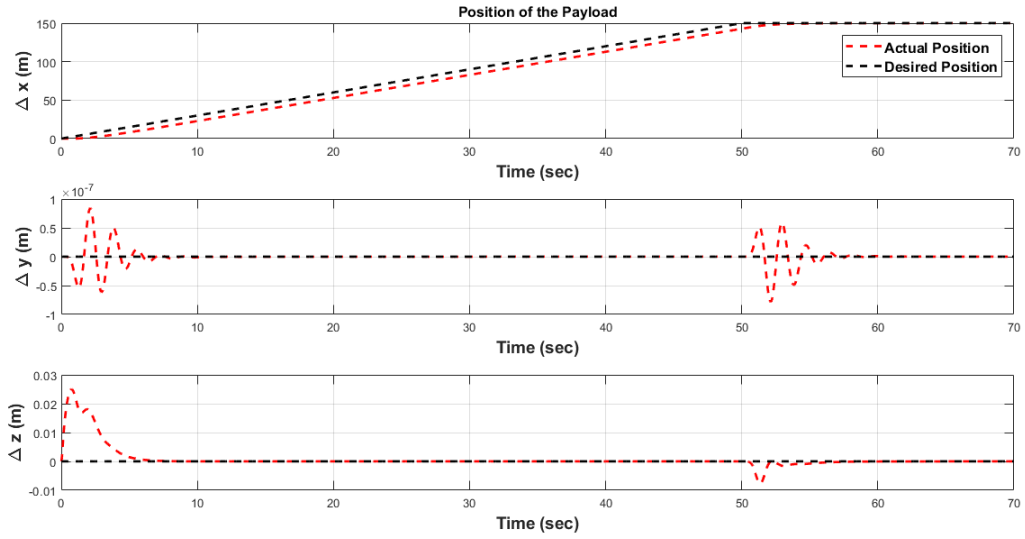

Figure 9.9: Position of the Payload

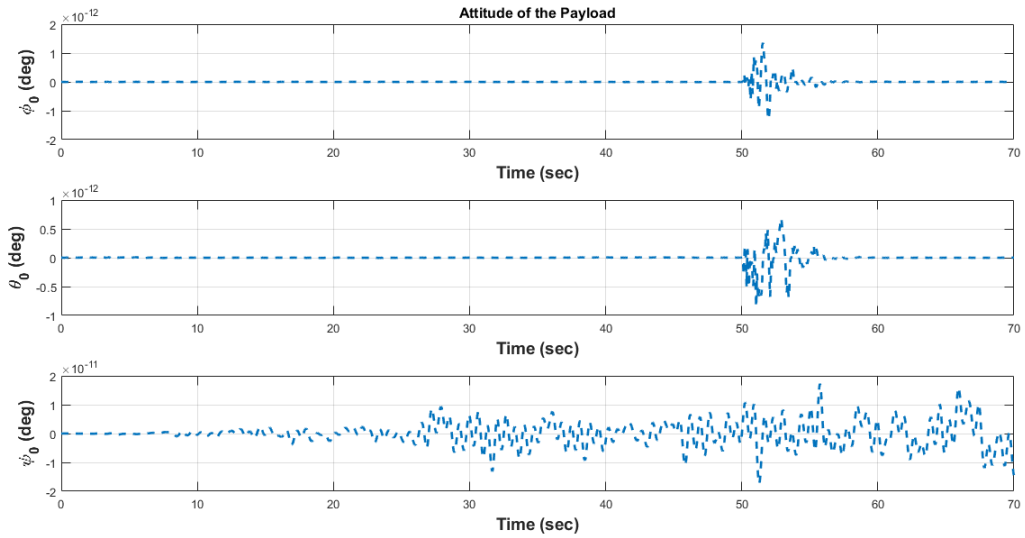

Figure 9.10: Attitude of the Payload

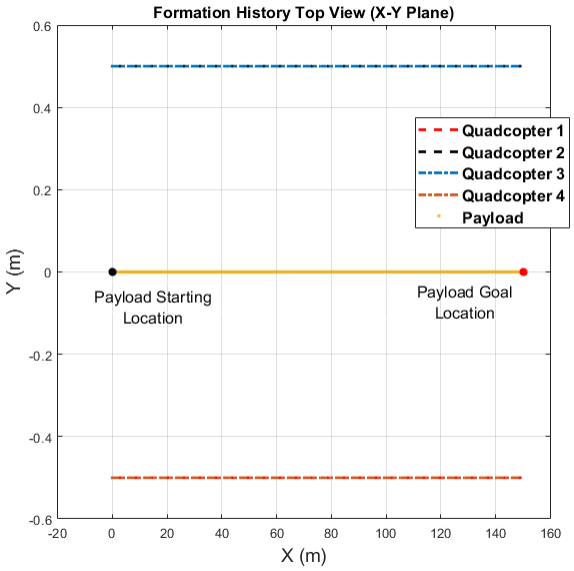

Figure 9.11: Cable suspended Rigid Body Payload Trajectory Tracking using four Quadcopters

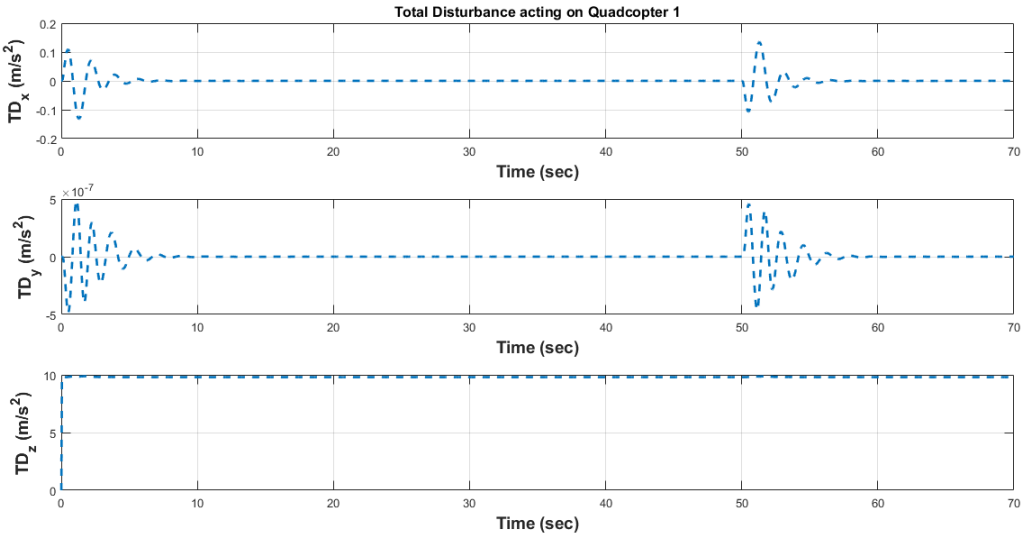

Figure 9.12: Total Disturbance Acting on Quadcopter 1

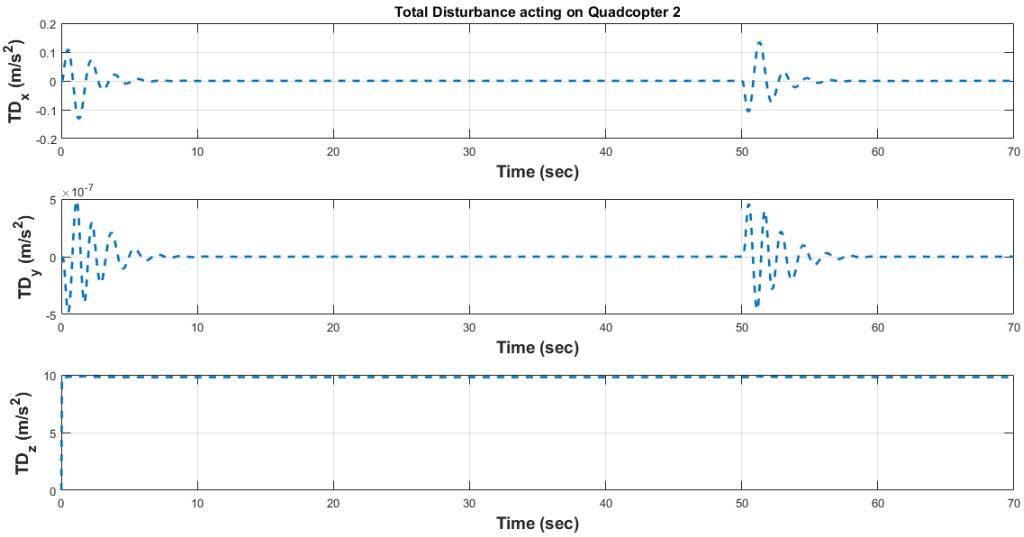

Figure 9.13: Total Disturbance Acting on Quadcopter 2

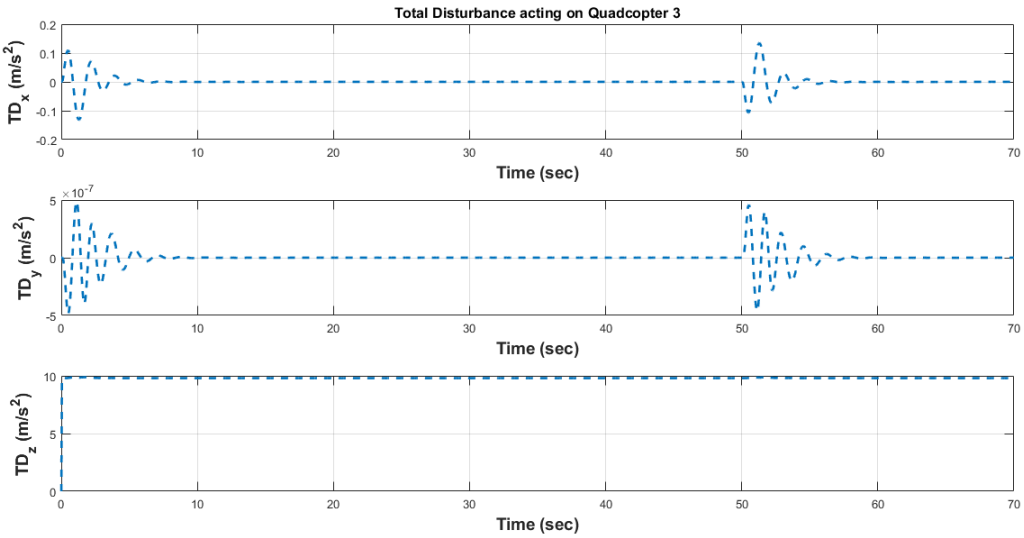

Figure 9.14: Total Disturbance Acting on Quadcopter 3

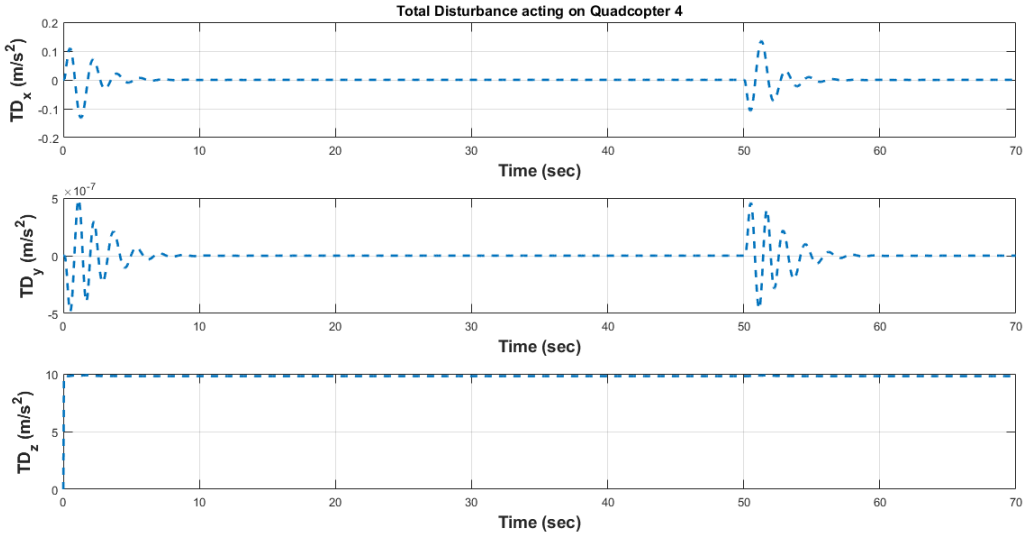

Figure 9.15: Total Disturbance Acting on Quadcopter 4

CHAPTER 10

Summary and Future Work

10.1 Summary and Conclusions

The research presented here emphasized on the comprehensive mathematical modeling of the quadcopter with cable suspended payload which also includes the aerodynamic profile drag model, propulsion system, and the power consumed during the operation. The mathematical model of the quadcopter with cable suspended payload was first derived in two ways using the Newton-Euler approach and the Euler-Lagrange formulation. Since these models assume that the payload cable is massless and always taut, the applicability of these models is restricted when for the cases when the cable is deformed or flexible. Hence an alternate method to model the quadcopter with a payload connected via flexible cable was presented. The flexible cable is approximated as a chain of serially connected linkages and the equations of motion are derived using Lagrangian mechanics. The motion of the payload induces disturbance forces on the quadcopter platform. Hence the requirement for a controller to attenuate the payload oscillations was identified.

In this dissertation, two nonlinear control laws were presented to control the vehicle and stabilize the payload oscillations. The first control law is an extended state observer based active disturbance rejection controller. The concept of total disturbance was first introduced. This total disturbance is treated as an additional state of the system with unknown dynamics. Using the system output (position of the quadcopter), the extended state observer was used to estimate induced disturbances in the system due to the oscillations of the payload. These disturbance estimates were used by the active disturbance rejection controller to control the position of the quadcopter and attenuate the oscillations of the ca-

ble suspended payload. Using Lyapunov theory and the convergence rate analysis of linear systems, it was proved that given a second order system which is locally observable, the extended state observer designed for the system ensures that the estimation errors are uniformly bounded as time $t \to \infty$.

The second control law is an energy based approach called passivity based controller. This controller requires the knowledge of the payload swing angle and its derivatives which are difficult to measure. Assuming that the payload swing angle is measured, a continuous-discrete Kalman filter was used to estimate the angular velocity of the payload cable.

The simulation environment was used to demonstrate the efficacy of the control laws to control the quadcopter and stabilize the oscillations of the payload for a smooth and stable operation. The passivity based controller depends upon the knowledge of the payload swing angle and its derivatives. The payload swing angle is difficult to measure or requires additional on-board sensors. Contrary, the extended state observer based active disturbance rejection controller depends only on the quadcopter states (position information to be precise). This information is used to estimate the disturbances acting on the quadcopter due to the oscillations of the payload. This eliminates the requirement of any additional on-board sensors. This solution can be employed on the quadcopters with cable suspended payloads for indoor as well as outdoor operations provided the position estimates are available all the time.

The extended state observer based active disturbance rejection controller was implemented on a quadcopter platform in the Aerospace Systems Laboratory at The University of Texas at Arlington. A mathematical model for multiple quadcopters carrying a rigid body payload via cables was presented. A distributed extended state observer based active disturbance rejection controller was implemented to address this cooperative control problem using a high-fidelity numerical simulation.

10.2 Future Work

The research focused on the comprehensive mathematical modeling of the quadcopter with cable suspended payload and nonlinear controller design for the control of the vehicle and stabilization of the payload. The simulation and the experimental results demonstrate the effectiveness of the nonlinear controllers in achieving the control objectives. However, there are still areas in this work which can be expanded upon.

Currently, the ground station receives the sensor data and the quadcopter state feedback over the wireless network. The extended state observer and the active disturbance rejection controller run as a ROS node on the ground station in a Simulink model. The control commands generated on the ground station are sent to the on-board computer over the wireless network, which are relayed to the Pixhawk running in the OFFBOARD mode. This adds delays in the control framework. Hence, one of the possible extensions of this work would be moving the controller and the extended state observer from the ground station computer to the on-board computer as a ROS node.

The communication delays is one of the chief challenge in the cyber-physical system architecture used in the experiments. This challenge arises due to the strength of the wireless network being used and the capabilities of the hardware. A characterization of the communication delays can be performed and the controller performance can be compared for various time delays. This study can be used to design safety measures for the instances when the state feedback is unavailable to the controller.

The experiments were performed indoors. Hence, the efficacy of the extended state observer based active disturbance rejection controller can be tested by including experimental results on the experimental testbench in an outdoor environment to capture the effect of the wind on the system under these operating conditions.

Another possible extension of this work would include implementation of the distributed extended state observer based active disturbance rejection controller on the ex-

perimental platform and demonstrate the cooperative control task of multiple quadcopters carrying a rigid body payload using cables. This will allow the distributed cooperative control policy to be validated using the hardware platforms.

APPENDIX A

Specifications of Sub-system Components used in the Quadcopter

Table A.1: Specifications of Sub-system Components of the Quadcopter used in the Simulations and Experimental Setup

Sub-system Details Used in the Simulations and Experiments			
Component	Parameter	Value	Units
DJI 2212/920 kV Motor	kV	920	RPM/V
	K_T	0.0104	Nm/A
	K_e	0.0104	$V/rad/s$
	K_f	2.8915×10^{-5}	$Nm/\left(rad/s\right)$
	R	0.03	Ω
	L	0.33×10^{-3}	H
	$J_p + J_m$	9.866×10^{-5}	Kgm^2
9443 ABS Self-locking Propeller	Diameter, D_p	9.4	in
	Pitch, H_p	4.3	in
	Number of Blades B_p	2	
Turnigy 5000 mAh 3S 25C LiPo	Capacity, C_b	5000	mAh
	Volt, v_{max}	11.1	V
	Configuration	$3S1P$	
	Max. Cont. Discharge	25	C
Mass & Inertia Properties for DJI F450	Total Mass, m_Q	1.2	Kg
	I_{xx}	1.367×10^{-2}	Kgm^2
	I_{yy}	1.367×10^{-2}	Kgm^2
	I_{zz}	2.586×10^{-2}	Kgm^2
	Arm Length, d	0.225	m
Payload mass and Cable Length used for the Simulations			
Payload mass and Cable Length	Mass of the Payload, m_l	0.5	Kg
	Cable Length, l	0.75	m
Payload mass and Cable Length used for the Experiments			
Payload mass and Cable Length	Mass of the Payload, m_l	0.250	Kg
	Cable Length, l	1	m

APPENDIX B

Observer and Controller Gains

Table B.1: Simulation Parameters

Continuous-Discrete Kalman Filter		
Parameter	Covariance	Units
Measurement Error (Zero mean White Noise Process), $v_\phi(t)$	0.01	rad^2
Process Noise (Zero mean White Noise Process), $w_\phi(t)$	0.25	rad^2/s^4
Extended State Observer Gains		
Parameter	Value	
$\boldsymbol{\Omega}$	150	
$\boldsymbol{\beta_1}$	$diag\,[3\Omega,\ 3\Omega,\ 3\Omega]$	
$\boldsymbol{\beta_2}$	$diag\left[3\Omega^2,\ 3\Omega^2,\ 3\Omega^2\right]$	
$\boldsymbol{\beta_3}$	$diag\left[\Omega^3,\ \Omega^3,\ \Omega^3\right]$	
Position Controller Gains		
Parameter	Value	
$\boldsymbol{K}_p$	$\frac{1}{9}diag\,[3.75,\ 3.75,\ 9]$	
$\boldsymbol{K}_d$	$\frac{1}{9}diag\,[15,\ 15,\ 4.5]$	
Attitude Controller Gains		
Parameter	Value	
k_{factor}	1.2	
$k_{p,\phi}$	$1.6301/k_{factor}$	
$k_{p,\theta}$	$1.6301/k_{factor}$	
$k_{p,\psi}$	$1.6301/k_{factor}$	
$k_{p,\dot{\phi}}$	$1.3153/k_{factor}$	
$k_{p,\dot{\theta}}$	$1.3153/k_{factor}$	
$k_{p,\dot{\psi}}$	$1.3153/k_{factor}$	
$k_{i,\phi}$	$0.2603/k_{factor}$	
$k_{i,\theta}$	$0.2603/k_{factor}$	
$k_{i,\psi}$	$0.2603/k_{factor}$	

APPENDIX C

Observer and Controller Gains used for the Experiments

Table C.1: Controller and Observer Gains used in the Experiments

Extended State Observer Gains	
Parameter	Value
Ω	5
$\boldsymbol{\beta_1}$	$diag\,[3\Omega,\ 3\Omega,\ 3\Omega]$
$\boldsymbol{\beta_2}$	$diag\left[3\Omega^2,\ 3\Omega^2,\ 3\Omega^2\right]$
$\boldsymbol{\beta_3}$	$diag\left[\Omega^3,\ \Omega^3,\ \Omega^3\right]$
Position Controller Gains	
Parameter	Value
K_{px}	1.3
K_{py}	1.3
K_{pu}	0.6
K_{pv}	0.6
K_{pz}	0.09
K_{dz}	0.009
K_{iz}	0.003

APPENDIX D

Continuous-Discrete Kalman Filter

Table D.1: Continuous-Discrete Kalman Filter

Model	$\dot{\boldsymbol{x}}(t) = \boldsymbol{F}(t)\boldsymbol{x}(t) + \boldsymbol{B}(t)\boldsymbol{u}(t) + \boldsymbol{G}(t)\boldsymbol{w}(t),\ \boldsymbol{w}(t) \sim N\left(\boldsymbol{0}, Q(t)\right)$ $\tilde{\boldsymbol{y}}_k = \boldsymbol{H}\boldsymbol{x}_k + \boldsymbol{v}_k,\ \boldsymbol{v}_k \sim N(\boldsymbol{0}, R_k)$
Initialize	$\hat{\boldsymbol{x}}(t_0) = \hat{\boldsymbol{x}}_0$ $\boldsymbol{P}_0 = E\left\{\tilde{\boldsymbol{x}}(t_0)\tilde{\boldsymbol{x}}^T(t_0)\right\}$
Gain	$\boldsymbol{K}_k = \boldsymbol{P}_k^- \boldsymbol{H}_k^T \left[\boldsymbol{H}_k \boldsymbol{P}_k^- \boldsymbol{H}_k^T + \boldsymbol{R}_k\right]^{-1}$
Update	$\hat{\boldsymbol{x}}_k^+ = \hat{\boldsymbol{x}}_k^- + \boldsymbol{K}_k\left[\tilde{\boldsymbol{y}}_k - \boldsymbol{H}_k \hat{\boldsymbol{x}}_k^-\right]$ $\boldsymbol{P}_k^+ = [\boldsymbol{I} - \boldsymbol{K}_k \boldsymbol{H}_k]\boldsymbol{P}_k^-$
Propagation	$\dot{\hat{\boldsymbol{x}}}(t) = \boldsymbol{F}(t)\hat{\boldsymbol{x}}(t) + \boldsymbol{B}(t)\boldsymbol{u}(t)$ $\dot{\boldsymbol{P}}(t) = \boldsymbol{F}(t)\boldsymbol{P}(t) + \boldsymbol{P}(t)\boldsymbol{F}^T(t) + \boldsymbol{G}(t)\boldsymbol{Q}(t)\boldsymbol{G}^T(t)$

The continuous-time models and discrete-time measurements taken from a digital signal processor can be modeled as

$$\dot{\boldsymbol{x}}(t) = \boldsymbol{F}(t)\boldsymbol{x}(t) + \boldsymbol{B}(t)\boldsymbol{u}(t) + \boldsymbol{G}(t)\boldsymbol{w}(t) \tag{D.1}$$

$$\tilde{\boldsymbol{y}}_k = \boldsymbol{H}\boldsymbol{x}_k + \boldsymbol{v}_k \tag{D.2}$$

where $\boldsymbol{w}(t)$ is the process noise and $\boldsymbol{v}_k$ is the measurement noise. Both the process and the measurement noise are assumed to be zero mean white noise processes. The mechanism for the filter approach is given in the table D.1.

APPENDIX E

Specifications of Sub-system Components used in the Distributed Cooperative Control Simulations

Table E.1: Specifications of Sub-system Components of the Quadcopter and the Payload used to demonstrate the efficacy of Distributed Extended State Observer Based Active Disturbance Rejection Controller

Sub-system Details Used in the Simulations and Experiments			
Component	Parameter	Value	Units
DJI 2212/920 kV Motor	kV	920	RPM/V
	K_T	0.0104	Nm/A
	K_e	0.0104	$V/rad/s$
	K_f	2.8915×10^{-5}	$Nm/\left(rad/s\right)$
	R	0.03	Ω
	L	0.33×10^{-3}	H
	$J_p + J_m$	9.866×10^{-5}	Kgm^2
9443 ABS Self-locking Propeller	Diameter, D_p	9.4	in
	Pitch, H_p	4.3	in
	Number of Blades B_p	2	
Turnigy 5000 mAh 3S 25C LiPo	Capacity, C_b	5000	mAh
	Volt, v_{max}	11.1	V
	Configuration	$3S1P$	
	Max. Cont. Discharge	25	C
Mass & Inertia Properties for DJI F450	Total Mass, m_i	1.2	Kg
	I_{xx}	1.367×10^{-2}	Kgm^2
	I_{yy}	1.367×10^{-2}	Kgm^2
	I_{zz}	2.586×10^{-2}	Kgm^2
	Arm Length, d	0.225	m
Payload Mass, Inertia and Cable Length			
Payload Mass, Inertia and Cable Length	Mass of the Payload, m_0	2	Kg
	Cable Length, l	0.75	m
	I_{xx}	1.733×10^{-1}	Kgm^2
	I_{yy}	1.733×10^{-1}	Kgm^2
	I_{zz}	1.667×10^{-1}	Kgm^2
	Length	1	m
	Width	1	m
	Height	0.2	m
Location for attaching the Cable to payload			
ρ_i	ρ_1	$[0.5,\ -0.5,\ 0]^T$	m
	ρ_2	$[0.5,\ 0.5,\ 0]^T$	m
	ρ_3	$[-0.5,\ 0.5,\ 0]^T$	m
	ρ_4	$[-0.5,\ -0.5,\ 0]^T$	m

APPENDIX F

Additional Results from the Distributed Cooperative Control Numerical Simulation

F.1 Case 1: Quadcopters are in hover mode and the payload is perturbed

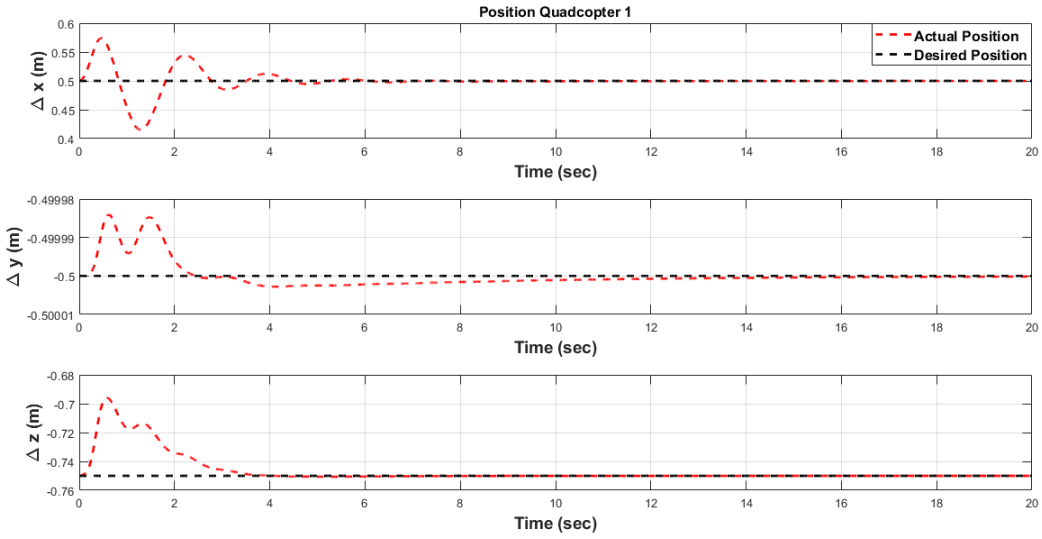

Figure F.1: Position of the Quadcopter 1

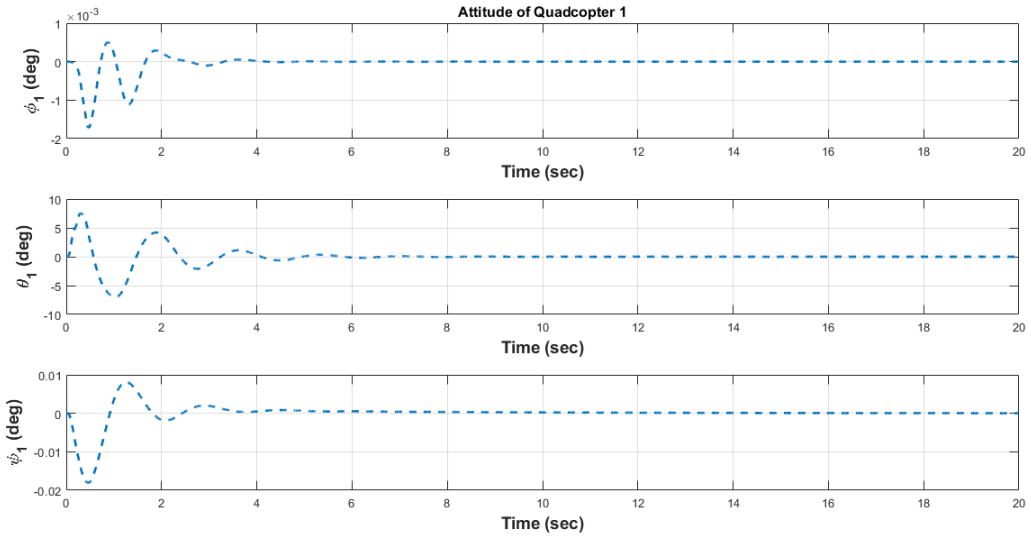

Figure F.2: Attitude of the Quadcopter 1

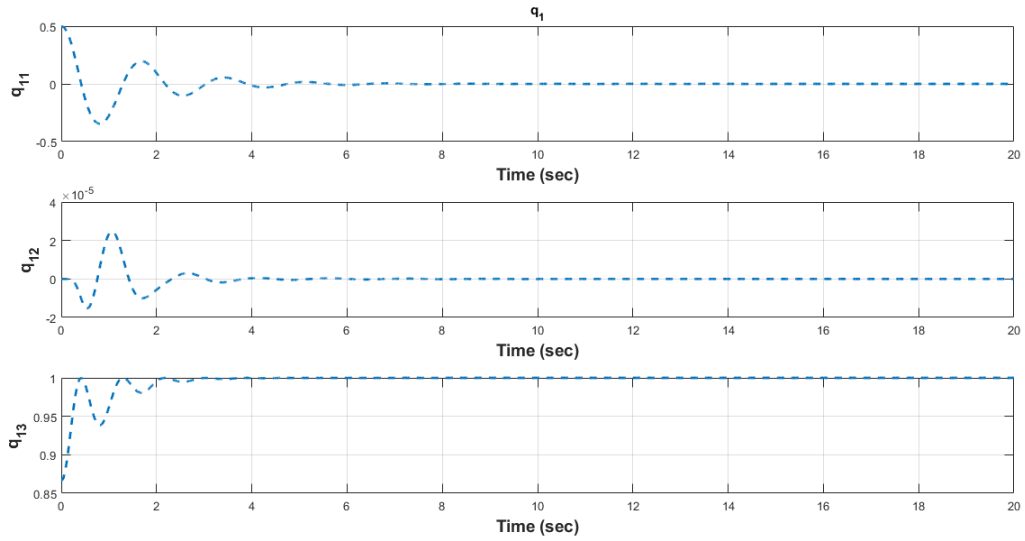

Figure F.3: Unit Vector Representing the Payload Cable Angle for Quadcopter 1

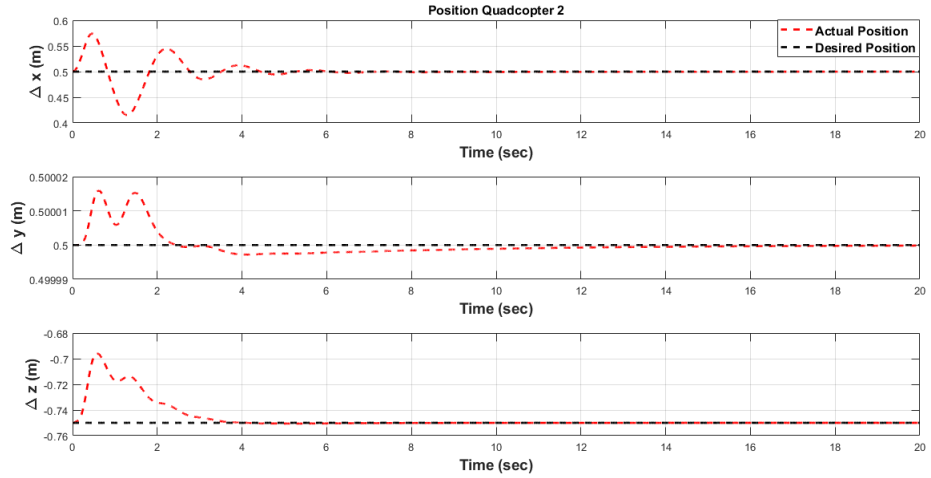

Figure F.4: Position of the Quadcopter 2

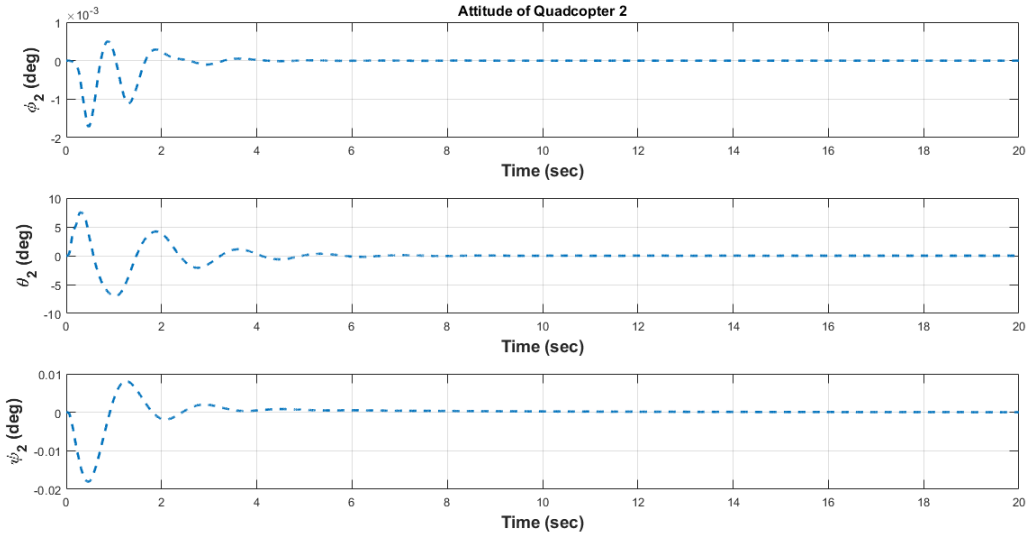

Figure F.5: Attitude of the Quadcopter 2

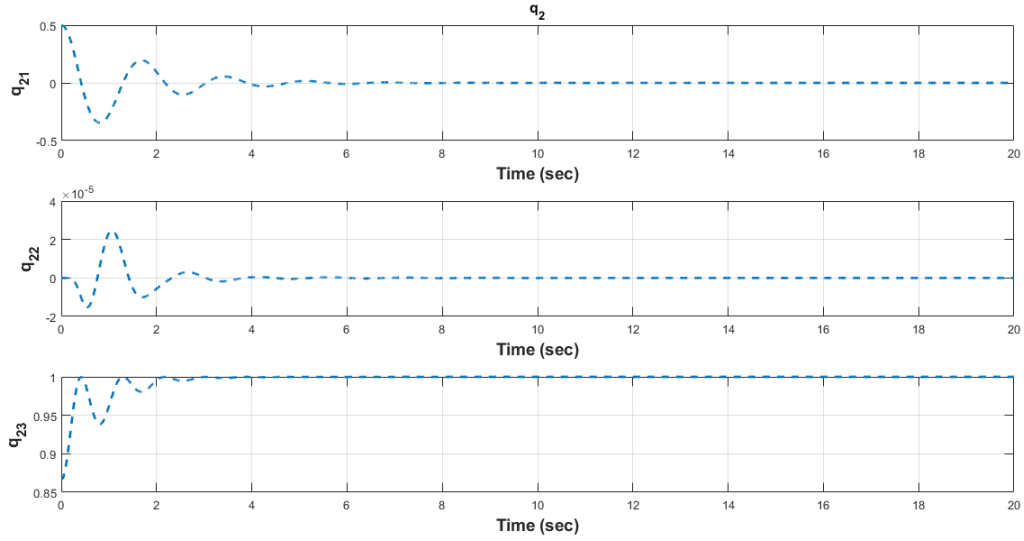

Figure F.6: Unit Vector Representing the Payload Cable Angle for Quadcopter 2

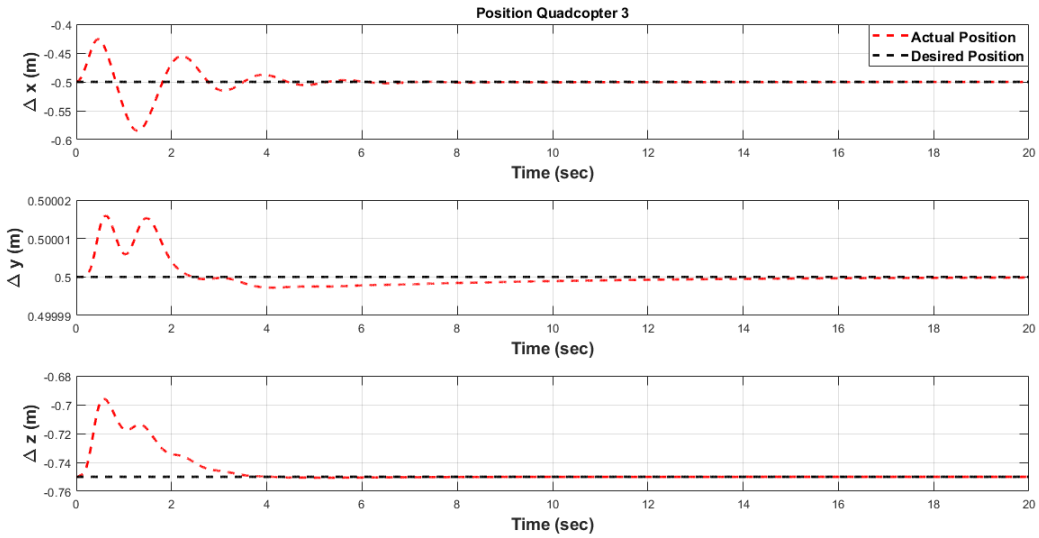

Figure F.7: Position of the Quadcopter 3

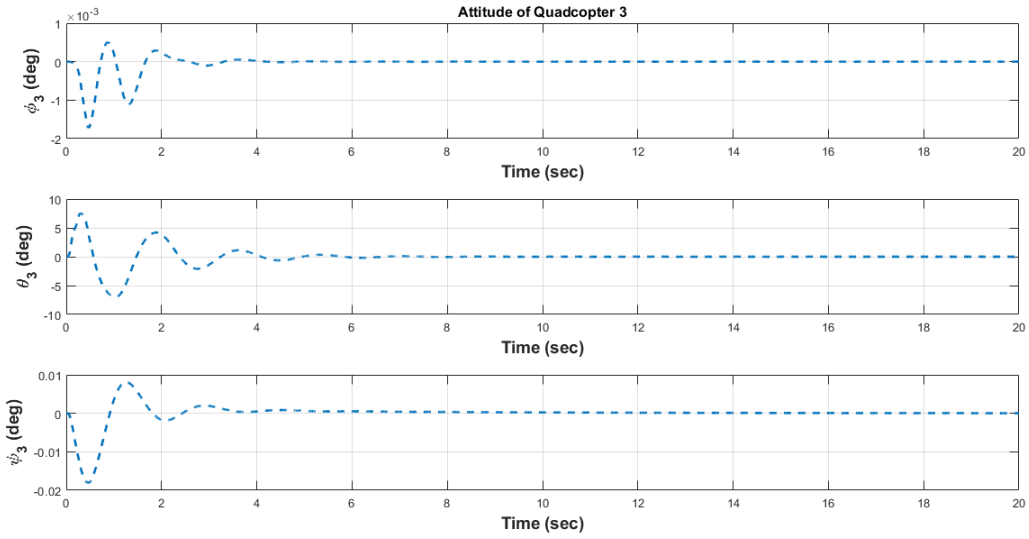

Figure F.8: Attitude of the Quadcopter 3

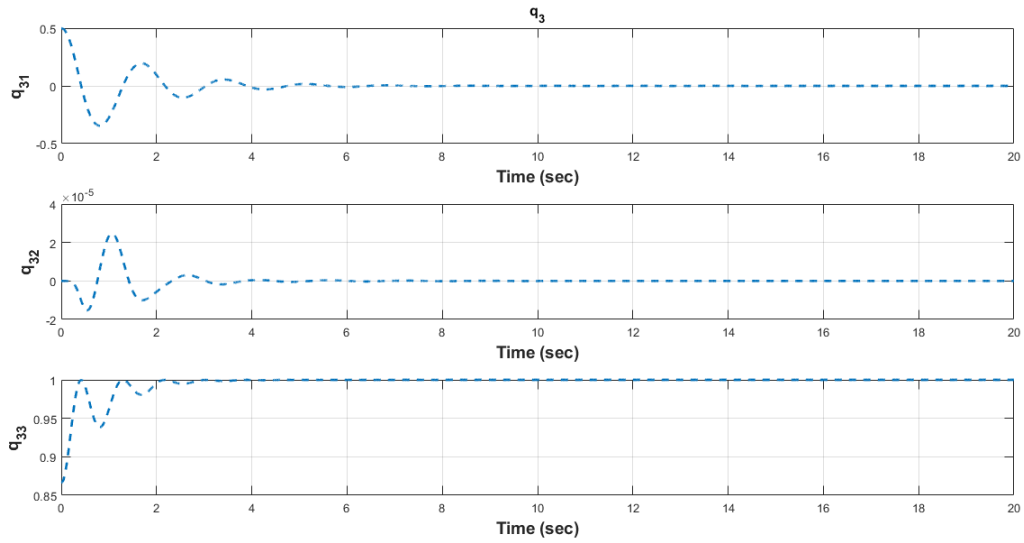

Figure F.9: Unit Vector Representing the Payload Cable Angle for Quadcopter 3

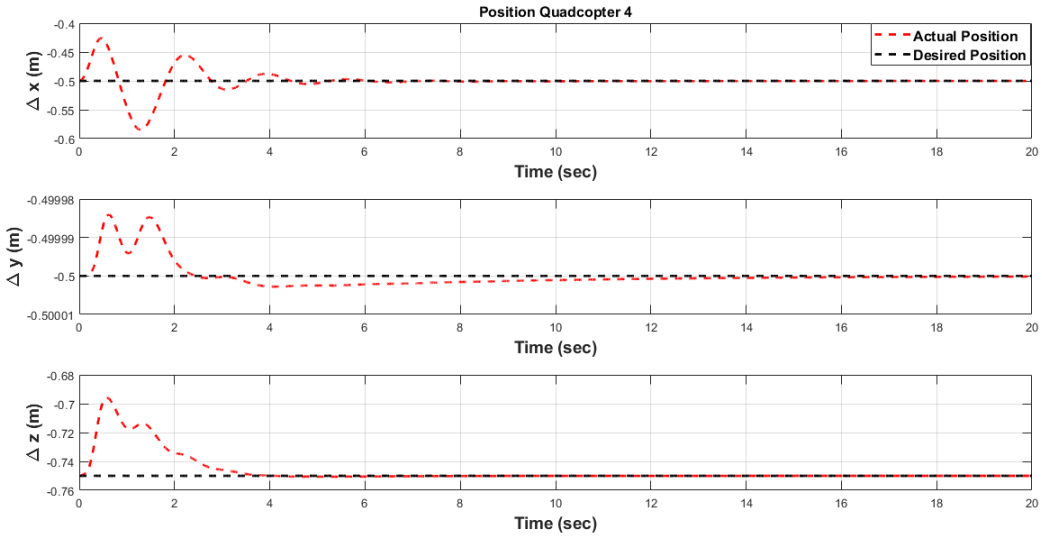

Figure F.10: Position of the Quadcopter 4

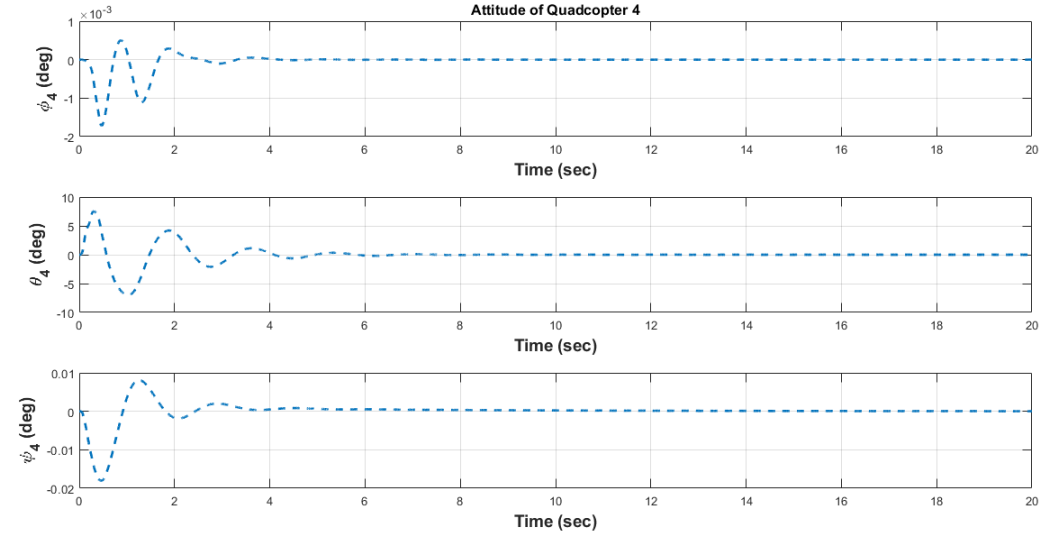

Figure F.11: Attitude of the Quadcopter 4

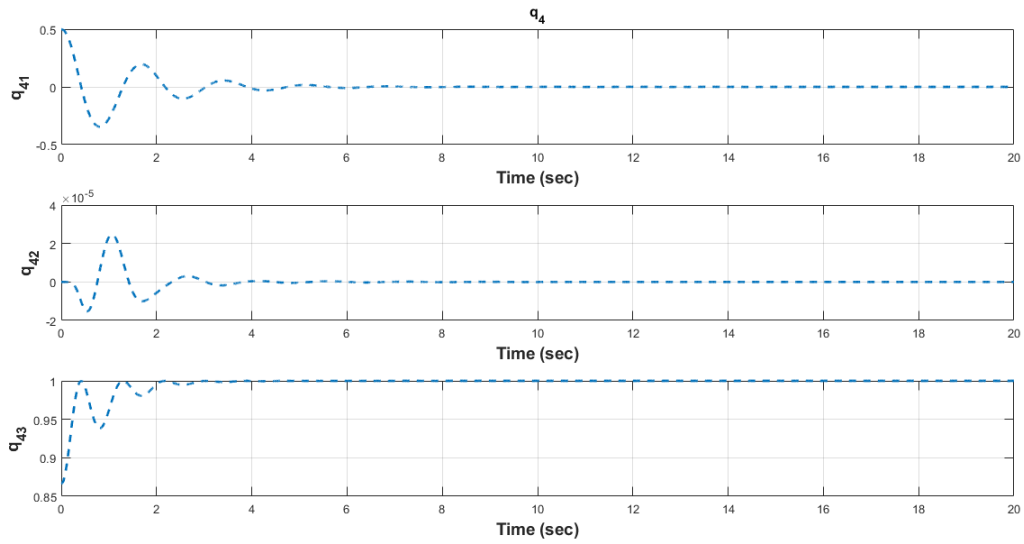

Figure F.12: Unit Vector Representing the Payload Cable Angle for Quadcopter 4

F.2 Case 2: Quadcopters along with the payload moving with a constant speed along inertial x axis (x_i) are commanded to go in the hover mode

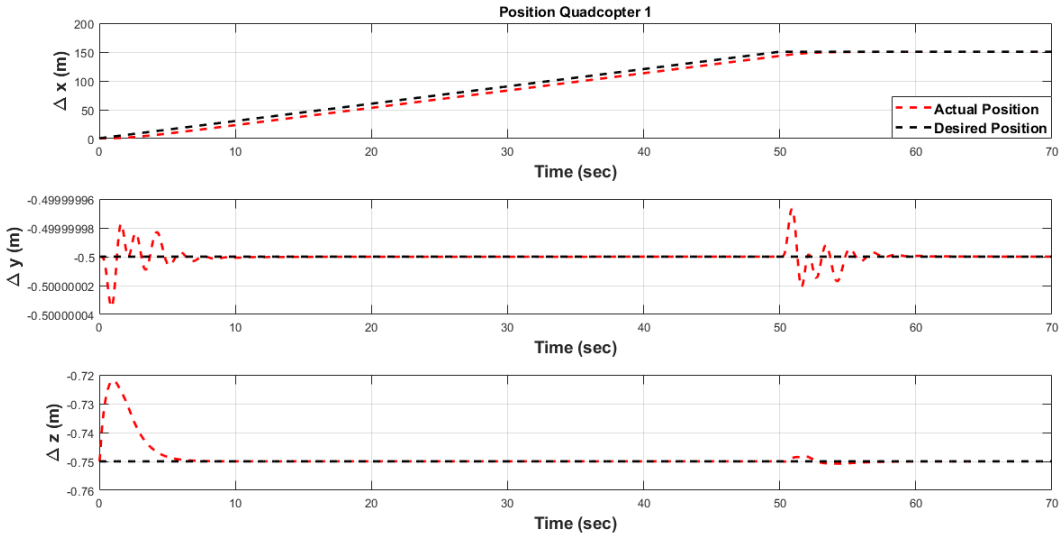

Figure F.13: Position of the Quadcopter 1

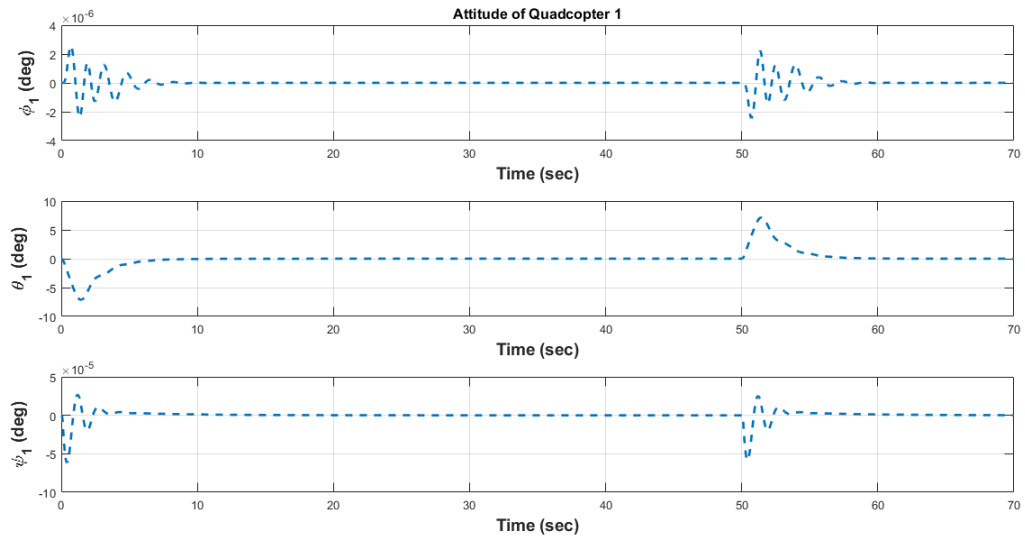

Figure F.14: Attitude of the Quadcopter 1

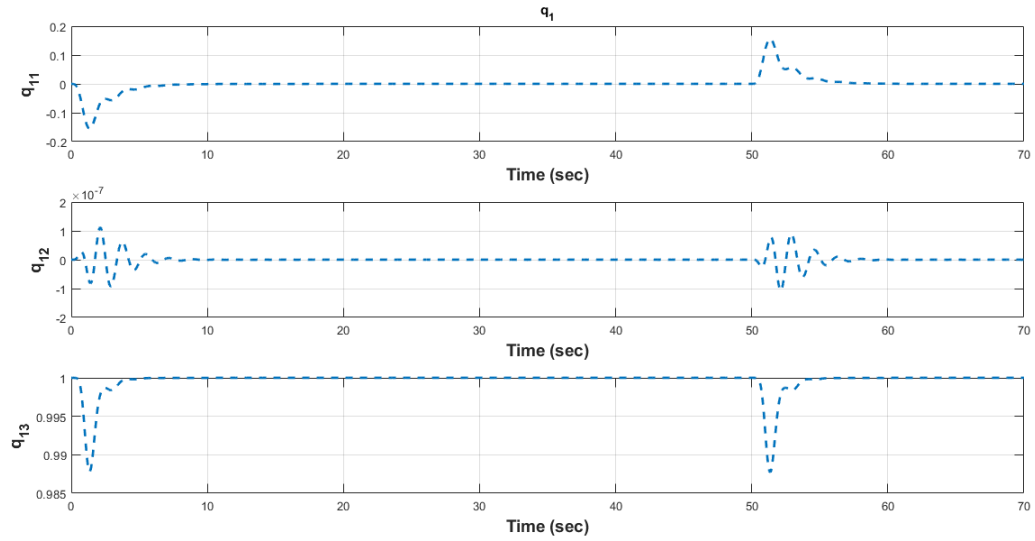

Figure F.15: Unit Vector Representing the Payload Cable Angle for Quadcopter 1

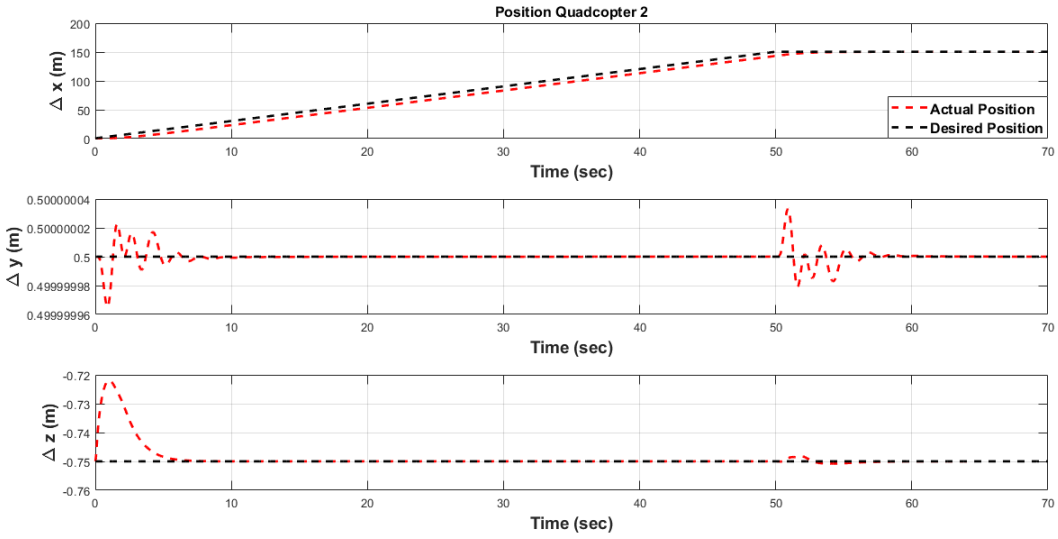

Figure F.16: Position of the Quadcopter 2

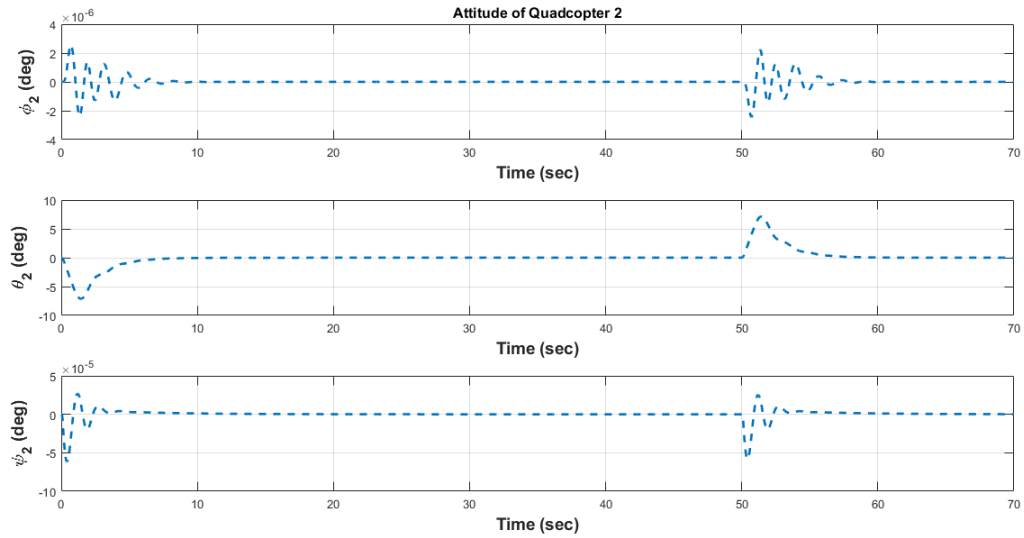

Figure F.17: Attitude of the Quadcopter 2

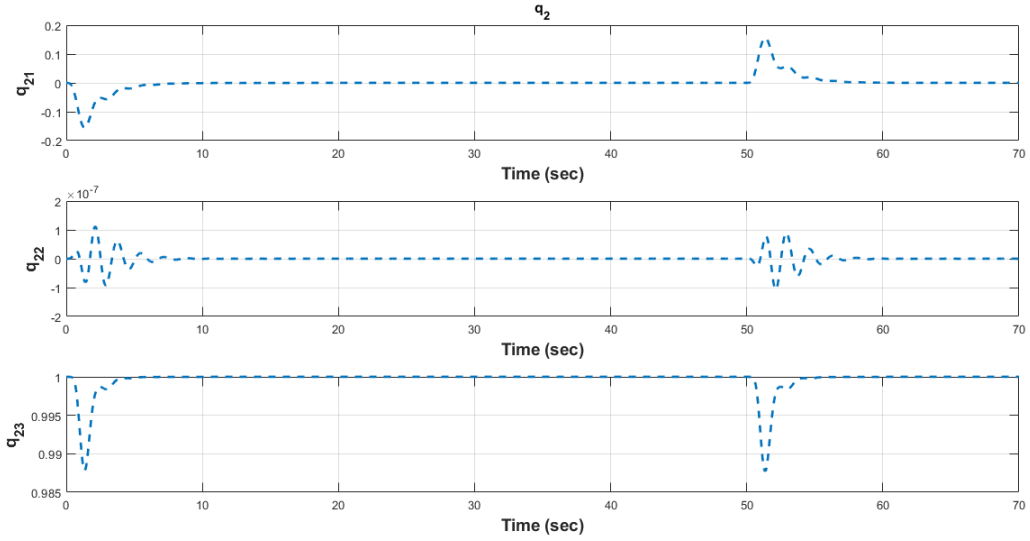

Figure F.18: Unit Vector Representing the Payload Cable Angle for Quadcopter 2

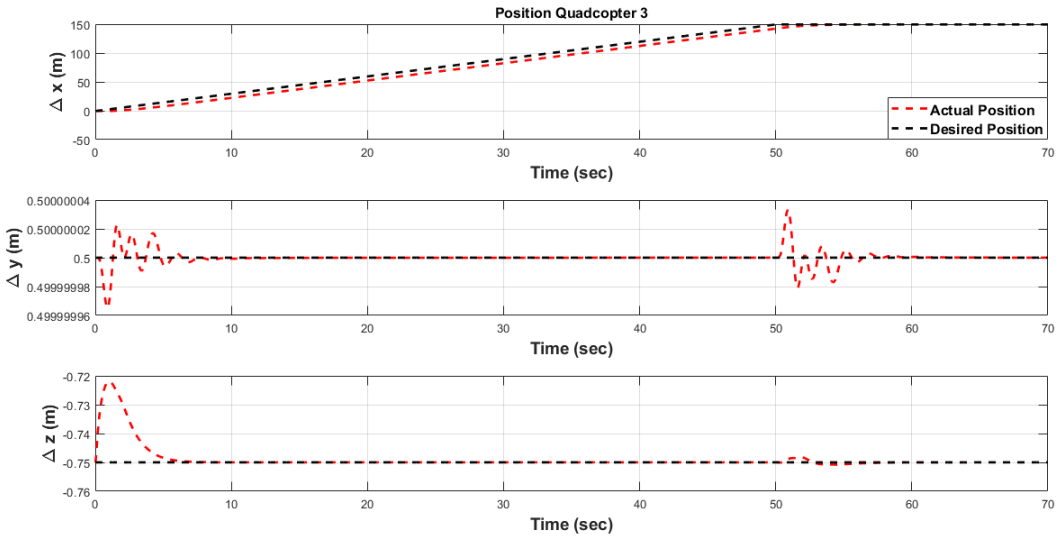

Figure F.19: Position of the Quadcopter 3

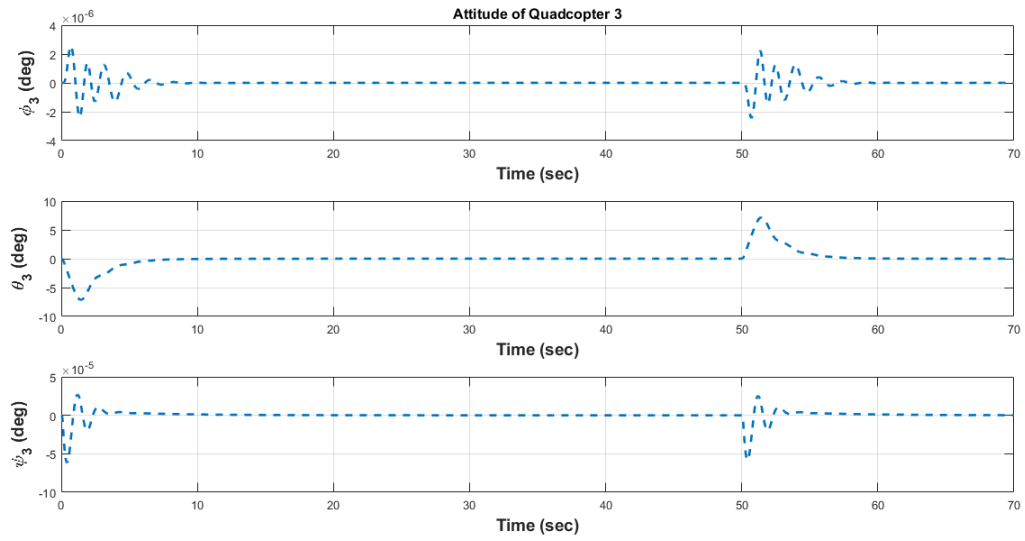

Figure F.20: Attitude of the Quadcopter 3

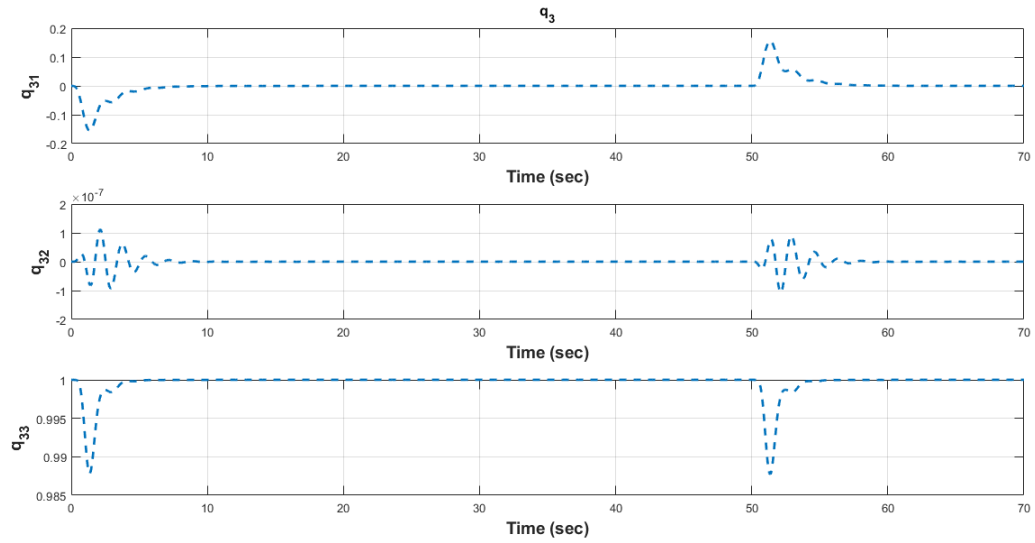

Figure F.21: Unit Vector Representing the Payload Cable Angle for Quadcopter 3

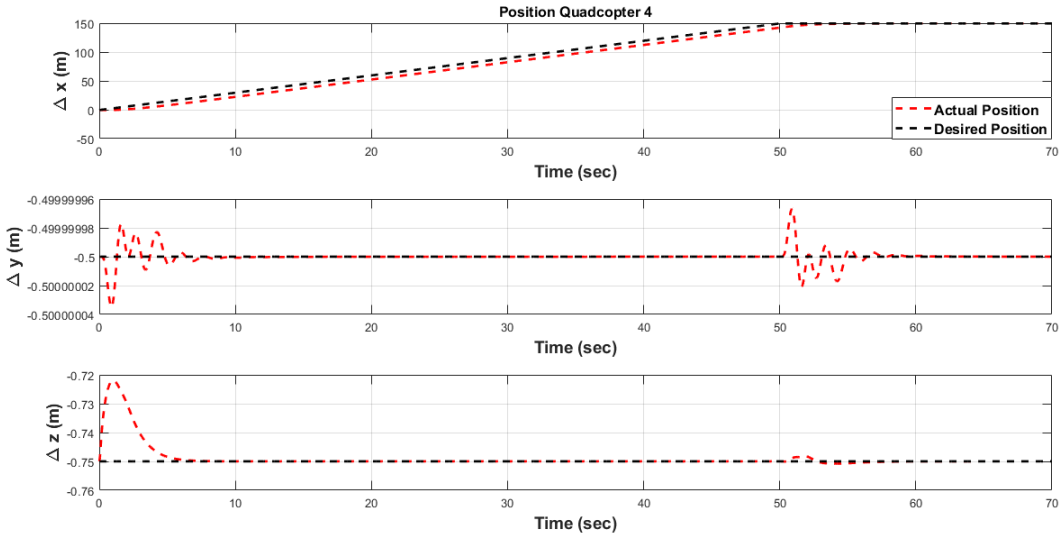

Figure F.22: Position of the Quadcopter 4

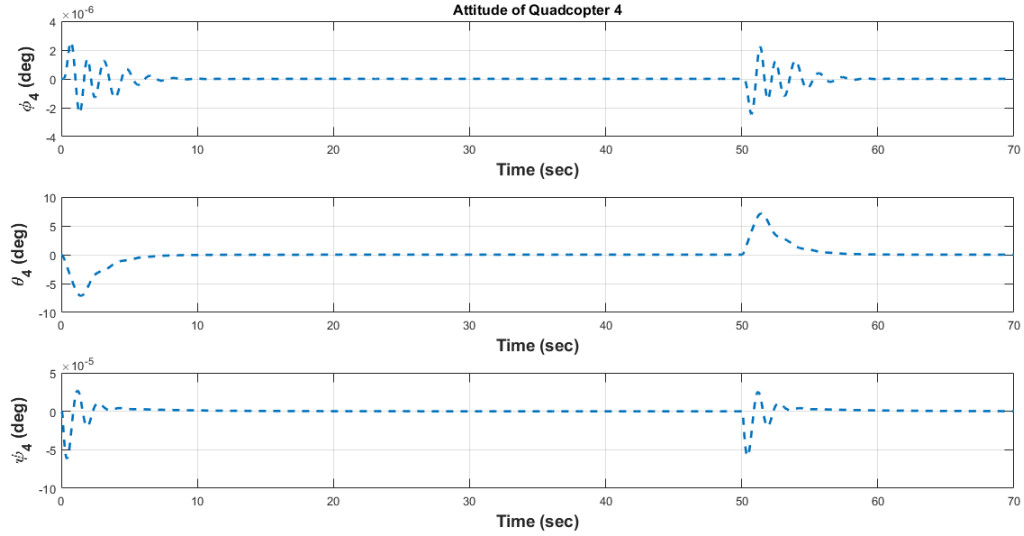

Figure F.23: Attitude of the Quadcopter 4

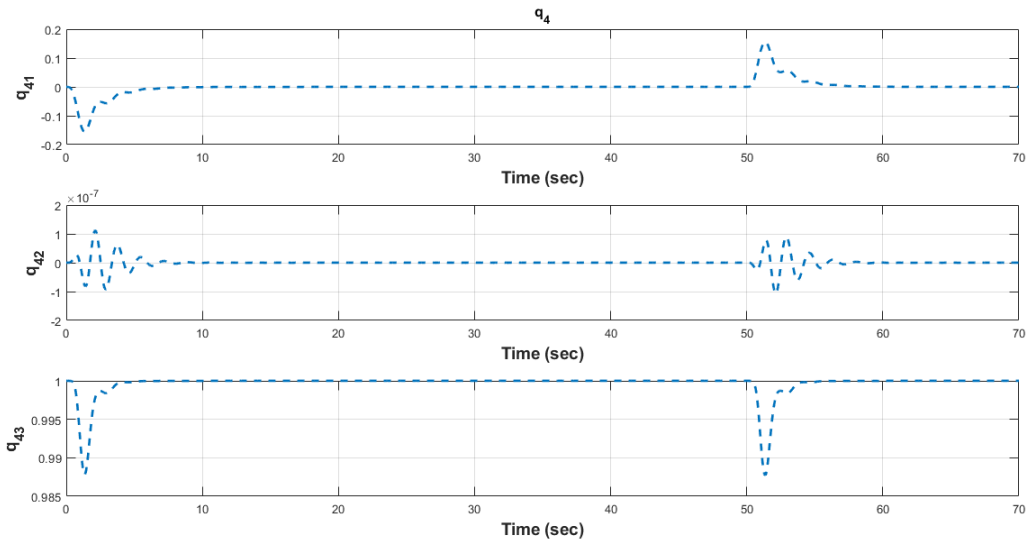

Figure F.24: Unit Vector Representing the Payload Cable Angle for Quadcopter 4

REFERENCES

[1] S. Kim, S. Choi, and H. J. Kim, "Aerial manipulation using a quadrotor with a two dof robotic arm," in *Intelligent Robots and Systems (IROS), 2013 IEEE/RSJ International Conference on*. IEEE, 2013, pp. 4990–4995.

[2] J. Thomas, G. Loianno, J. Polin, K. Sreenath, and V. Kumar, "Toward autonomous avian-inspired grasping for micro aerial vehicles," *Bioinspiration & biomimetics*, vol. 9, no. 2, p. 025010, 2014.

[3] K. Sreenath, N. Michael, and V. Kumar, "Trajectory generation and control of a quadrotor with a cable-suspended load-a differentially-flat hybrid system," in *Robotics and Automation (ICRA), 2013 IEEE International Conference on*. IEEE, 2013, pp. 4888–4895.

[4] A. R. Godbole, K. Subbarao, A. Dogan, and B. Huff, "Range and endurance characterization of a quadcopter subject to steady wind," in *2018 International Conference on Unmanned Aircraft Systems (ICUAS)*. IEEE, 2018, pp. 1279–1287.

[5] A. Godbole, K. Subbarao, A. Dogan, and B. Huff, "Semi-analytical range and endurance computation of battery-powered multi-copter unmanned aerial systems under steady wind conditions," *Proceedings of the Institution of Mechanical Engineers, Part G: Journal of Aerospace Engineering*, April, 2019. [Online]. Available: https://doi.org/10.1177/0954410019842714

[6] I. Palunko, R. Fierro, and P. Cruz, "Trajectory generation for swing-free maneuvers of a quadrotor with suspended payload: A dynamic programming approach," in *Robotics and Automation (ICRA), 2012 IEEE International Conference on*. IEEE, 2012, pp. 2691–2697.

[7] D. Fusato, G. Guglieri, and R. Celi, "Flight dynamics of an articulated rotor helicopter with an external slung load," *Journal of the American Helicopter Society*, vol. 46, no. 1, pp. 3–13, 2001.

[8] T. Oktay and C. Sultan, "Modeling and control of a helicopter slung-load system," *Aerospace Science and Technology*, vol. 29, no. 1, pp. 206–222, 2013.

[9] R. P. K. Jain, "Transportation of cable suspended load using unmanned aerial vehicles: A real-time model predictive control approach," 2015.

[10] M. Kanazawa, S. Nakaura, and M. Sampei, "Inverse optimal control problem for bilinear systems: Application to the inverted pendulum with horizontal and vertical movement," in *Decision and Control, 2009 held jointly with the 2009 28th Chinese Control Conference. CDC/CCC 2009. Proceedings of the 48th IEEE Conference on*. IEEE, 2009, pp. 2260–2267.

[11] D. Zameroski, G. Starr, J. Wood, and R. Lumia, "Rapid swing-free transport of nonlinear payloads using dynamic programming," *Journal of Dynamic Systems, Measurement, and Control*, vol. 130, no. 4, p. 041001, 2008.

[12] J. Schultz and T. Murphey, "Trajectory generation for underactuated control of a suspended mass," in *2012 IEEE International Conference on Robotics and Automation*. IEEE, 2012, pp. 123–129.

[13] I. García-Fernández, M. Pla-Castells, and R. J. Martínez-Durá, "Elevation cable modeling for interactive simulation of cranes," in *Proceedings of the 2008 ACM SIGGRAPH/Eurographics Symposium on Computer Animation*. Eurographics Association, 2008, pp. 173–181.

[14] K.-i. Anjyo, Y. Usami, and T. Kurihara, "A simple method for extracting the natural beauty of hair," *ACM SIGGRAPH Computer Graphics*, vol. 26, no. 2, pp. 111–120, 1992.

[15] E. Hergenröther and P. Dähne, "Real-time virtual cables based on kinematic simulation," 2000.

[16] S. Hadap and N. Magnenat-Thalmann, "Modeling dynamic hair as a continuum," in *Computer Graphics Forum*, vol. 20, no. 3. Wiley Online Library, 2001, pp. 329–338.

[17] T. Lee, M. Leok, and N. H. McClamroch, "Dynamics and control of a chain pendulum on a cart," in *2012 IEEE 51st IEEE Conference on Decision and Control (CDC)*. IEEE, 2012, pp. 2502–2508.

[18] F. A. Goodarzi, D. Lee, and T. Lee, "Geometric stabilization of a quadrotor uav with a payload connected by flexible cable," in *2014 American Control Conference*. IEEE, 2014, pp. 4925–4930.

[19] N. Yanai, M. Yamamoto, and A. Mohri, "Feedback control for wire-suspended mechanism with exact linearization," in *IEEE/RSJ International Conference on Intelligent Robots and Systems*, vol. 3, Sept 2002, pp. 2213–2218 vol.3.

[20] J. Yu, F. L. Lewis, and T. Huang, "Nonlinear feedback control of a gantry crane," in *Proceedings of 1995 American Control Conference - ACC'95*, vol. 6, June 1995, pp. 4310–4315 vol.6.

[21] J. Schultz and T. Murphey, "Trajectory generation for underactuated control of a suspended mass," in *2012 IEEE International Conference on Robotics and Automation*, May 2012, pp. 123–129.

[22] G. Starr, J. Wood, and R. Lumia, "Rapid transport of suspended payloads," in *Proceedings of the 2005 IEEE International Conference on Robotics and Automation*, April 2005, pp. 1394–1399.

[23] S. Sadr, S. A. A. Moosavian, and P. Zarafshan, "Dynamics modeling and control of a quadrotor with swing load," *Journal of Robotics*, vol. 2014, 2014.

[24] K. Sreenath, T. Lee, and V. Kumar, "Geometric control and differential flatness of a quadrotor uav with a cable-suspended load," in *52nd IEEE Conference on Decision and Control*, Dec 2013, pp. 2269–2274.

[25] R. Ortega, A. van der Schaft, B. Maschke, and G. Escobar, "Interconnection and damping assignment passivity-based control of port-controlled hamiltonian systems," *Automatica*, vol. 38, no. 4, pp. 585 – 596, 2002. [Online]. Available: http://www.sciencedirect.com/science/article/pii/S0005109801002783

[26] M. Guerrero, D. Mercado, R. Lozano, and C. García, "Ida-pbc methodology for a quadrotor uav transporting a cable-suspended payload," in *Unmanned Aircraft Systems (ICUAS), 2015 International Conference on*. IEEE, 2015, pp. 470–476.

[27] B. Yüksel, C. Secchi, H. H. Bülthoff, and A. Franchi, "Reshaping the physical properties of a quadrotor through ida-pbc and its application to aerial physical interaction," in *2014 IEEE International Conference on Robotics and Automation (ICRA)*, May 2014, pp. 6258–6265.

[28] R. Ortega, M. W. Spong, F. Gomez-Estern, and G. Blankenstein, "Stabilization of a class of underactuated mechanical systems via interconnection and damping assignment," *IEEE Transactions on Automatic Control*, vol. 47, no. 8, pp. 1218–1233, Aug 2002.

[29] S. Tang, V. Wüest, and V. Kumar, "Aggressive flight with suspended payloads using vision-based control," *IEEE Robotics and Automation Letters*, vol. 3, no. 2, pp. 1152–1159, 2018.

[30] M. Bisgaard, A. la Cour-Harbo, and J. D. Bendtsen, "Adaptive control system for autonomous helicopter slung load operations," *Control Engineering Practice*, vol. 18, no. 7, pp. 800–811, 2010.

[31] S. J. Lee and H. J. Kim, "Autonomous swing-angle estimation for stable slung-load flight of multi-rotor uavs," in *2017 IEEE International Conference on Robotics and Automation (ICRA)*. IEEE, 2017, pp. 4576–4581.

[32] F. A. Goodarzi, D. Lee, and T. Lee, "Geometric control of a quadrotor uav transporting a payload connected via flexible cable," *International Journal of Control, Automation and Systems*, vol. 13, no. 6, pp. 1486–1498, 2015.

[33] M. E. Guerrero-Sanchez, H. Abaunza, P. Castillo, R. Lozano, C. Garcia-Beltran, and A. Rodriguez-Palacios, "Passivity-based control for a micro air vehicle using unit quaternions," *Applied Sciences*, vol. 7, no. 1, p. 13, 2016.

[34] M. Weijers, "Minimum swing control of a uav with a cable suspended load," Master's thesis, University of Twente, 2015.

[35] A. R. Godbole and K. Subbarao, "Mathematical modeling and control of an unmanned aerial system with a cable suspended payload," in *2018 IEEE 14th International Conference on Control and Automation (ICCA)*. IEEE, 2018, pp. 570–575.

[36] Godbole, Ameya R and Subbarao, Kamesh, "Nonlinear control of unmanned aerial vehicles with cable suspended payloads," *Aerospace Science and Technology*, vol. 93, p. 105299, 2019, doi: https://doi.org/10.1016/j.ast.2019.07.032. [Online]. Available: http://www.sciencedirect.com/science/article/pii/S1270963818325185

[37] H. Wang, Y. Huang, and C. Xu, "Adrc methodology for a quadrotor uav transporting hanged payload," in *2016 IEEE International Conference on Information and Automation (ICIA)*, Aug 2016, pp. 1641–1646.

[38] J. Han, "From pid to active disturbance rejection control," *IEEE Transactions on Industrial Electronics*, vol. 56, no. 3, pp. 900–906, March 2009.

[39] C. Meissen, K. Klausen, M. Arcak, T. I. Fossen, and A. Packard, "Passivity-based formation control for uavs with a suspended load," *IFAC-PapersOnLine*, vol. 50, no. 1, pp. 13 150–13 155, 2017.

[40] T. Lee, K. Sreenath, and V. Kumar, "Geometric control of cooperating multiple quadrotor uavs with a suspended payload," in *52nd IEEE conference on decision and control*. IEEE, 2013, pp. 5510–5515.

[41] F. A. Goodarzi and T. Lee, "Stabilization of a rigid body payload with multiple cooperative quadrotors," *Journal of Dynamic Systems, Measurement, and Control*, vol. 138, no. 12, p. 121001, 2016.

[42] H. Rastgoftar and E. M. Atkins, "Cooperative aerial lift and manipulation (calm)," *Aerospace Science and Technology*, vol. 82, pp. 105–118, 2018.

[43] T. Lee, "Geometric control of quadrotor uavs transporting a cable-suspended rigid body," *IEEE Transactions on Control Systems Technology*, vol. 26, no. 1, pp. 255–264, 2017.

[44] S. H. Nair, R. N. Banavar, and D. S. Maithripala, "Control synthesis for an underactuated cable suspended system using dynamic decoupling," *arXiv preprint arXiv:1707.00661*, 2017.

[45] T. Lee, "Geometric control of multiple quadrotor uavs transporting a cable-suspended rigid body," *53rd IEEE Conference on Decision and Control*, pp. 6155–6160, 2014.

[46] G. Antonelli, F. Arrichiello, and S. Chiaverini, "The null-space-based behavioral control for autonomous robotic systems," *Intelligent Service Robotics*, vol. 1, no. 1, pp. 27–39, 2008.

[47] J. Gimenez, D. C. Gandolfo, L. R. Salinas, C. Rosales, and R. Carelli, "Multi-objective control for cooperative payload transport with rotorcraft uavs," *ISA transactions*, vol. 80, pp. 491–502, 2018.

[48] H. Sira-Ramírez, Z. Gao, and E. Canuto, "An active disturbance rejection control approach for decentralized tracking in interconnected systems," in *2014 European Control Conference (ECC)*. IEEE, 2014, pp. 588–593.

[49] A. Godbole, M. VNV, P. Quillen, and K. Subbarao, "Optimal trajectory design and control of a planetary exploration rover," in *AIAA SPACE*, vol. 2017, 2017.

[50] H. K. Khalil, "Noninear systems," *Prentice-Hall, New Jersey*, vol. 2, no. 5, pp. 5–1, 1996.

[51] J.-J. E. Slotine, W. Li *et al.*, *Applied nonlinear control*. Prentice hall Englewood Cliffs, NJ, 1991, vol. 199, no. 1.

[52] P. Ru and K. Subbarao, "Nonlinear model predictive control for unmanned aerial vehicles," *Aerospace*, vol. 4, no. 2, p. 31, 2017.

[53] F. M. White, "Fluid mechanics, wcb," *Ed McGraw-Hill Boston*, 1999.

[54] A. R. Godbole and K. Subbarao, "Nonlinear control of unmanned aerial vehicles with cable suspended payloads," *Aerospace Science and Technology*, 2019.

[55] T. Lee, "Computational geometric mechanics and control of rigid bodies." Ph.D. dissertation, 2008.

[56] D. E. Kirk, *Optimal control theory: an introduction*. Courier Corporation, 2012.

[57] S. A. Erturk, "Performance analysis, dynamic simulation and control of mass-actuated airplane," Ph.D. dissertation, 2016.

[58] A. Kiruthika, A. A. Rajan, and P. Rajalakshmi, "Mathematical modelling and speed control of a sensored brushless dc motor using intelligent controller," in *2013 IEEE International Conference ON Emerging Trends in Computing, Communication and Nanotechnology (ICECCN)*, March 2013, pp. 211–216.

[59] D. Shi, X. Dai, X. Zhang, and Q. Quan, "A practical performance evaluation method for electric multicopters," *IEEE/ASME Transactions on Mechatronics*, 2017.

[60] (2018, February) Battery discharge/charge using keithley series 2400 sourcemeter instruments. [Online]. Available: https://www.tek.com/

[61] R. Ortega, A. J. V. D. Schaft, I. Mareels, and B. Maschke, "Putting energy back in control," *IEEE Control Systems Magazine*, vol. 21, no. 2, pp. 18–33, April 2001.

[62] M. M. Nicotra, E. Garone, R. Naldi, and L. Marconi, "Nested saturation control of an uav carrying a suspended load," in *American Control Conference (ACC), 2014*. IEEE, 2014, pp. 3585–3590.

[63] E. deVries and K. Subbarao, "Backstepping based nested multi-loop control laws for a quadrotor," in *11th International Conference on Control, Automation, Robotics and Vision, ICARCV 2010*, December 07-10 2010.

[64] J. L. Crassidis and J. L. Junkins, *Optimal estimation of dynamic systems*. CRC press, 2011.

[65] (2018, December) Pixhawk. [Online]. Available: http://pixhawk.org/

[66] (2018, December) Ros. [Online]. Available: http://www.ros.org/

[67] (2019, July) Pixhawk4 mini. [Online]. Available: http://www.holybro.com/product/pixhawk4-mini/

[68] (2019, July) What is px4? [Online]. Available: https://px4.io/

[69] (2019, July) Qgroundcontrol user guide. [Online]. Available: https://docs.qgroundcontrol.com/en/

[70] (2019, July) Mavlink developer guide. [Online]. Available: https://mavlink.io/en/

[71] (2019, July) What is motion capture? [Online]. Available: https://www.vicon.com/what-is-motion-capture

[72] L. Joseph, *Mastering ROS for robotics programming*. Packt Publishing Ltd, 2015.

[73] (2019, July) Robot operating system (ros) support from robotics system toolbox. [Online]. Available: https://www.mathworks.com/hardware-support/robot-operating-system.html

[74] (2019, July) Mavros – mavlink extendable communication node for ros with proxy for ground control station. [Online]. Available: http://wiki.ros.org/mavros

[75] (2019, July) Ros/network setup. [Online]. Available: http://wiki.ros.org/ROS/NetworkSetup

[76] (2019, July) Configure ros network addresses. [Online]. Available: https://www.mathworks.com/help/robotics/ug/configure-ros-network-addresses.html

[77] (2019, July) vicon_bridge. [Online]. Available: http://wiki.ros.org/vicon_bridge

[78] (2019, July) Offboard mode. [Online]. Available: https://docs.px4.io/v1.9.0/en/flight_modes/offboard.html

[79] (2019, July) Using vision or motion capture systems for position estimation. [Online]. Available: http://dev.px4.io/v1.9.0/en/ros/external_position_estimation.html

[80] A. Martinez Martinez, "Onboard payload mass estimation and electric propulsion modeling for multicopters with application in unmanned aerial vehicles," 2019.

[81] T. Lee, M. Leok, and N. H. McClamroch, "Lagrangian mechanics and variational integrators on two-spheres," *International Journal for Numerical Methods in Engineering*, vol. 79, no. 9, pp. 1147–1174, 2009.

BIOGRAPHICAL STATEMENT

Ameya R. Godbole was born in Kalyan, India, in 1992. He received his Bachelor of Engineering degree in Mechanical Engineering from K.J.Somaiya College of Engineering, Mumbai University, India, in 2013. He earned his Master of Science degree in Mechanical Engineering from the University of Texas at Arlington in Spring 2015 and enrolled in the Doctoral program at the same institution.

Ameya worked as a Research Student in the Aerospace Systems Lab (ASL) with Dr. Kamesh Subbarao during his Masters and Doctoral program at the University of Texas at Arlington. Ameya was a part of the ASL team which won the first place in graduate division at the NASA and NIA organized RASC-AL forum in 2014. He worked as a Physical Modeling Quality Engineering Intern at the MathWorks Inc. during his doctoral studies from January 2017 to August 2017 and was awarded the summer 2019 Dissertation Fellowship from the University of Texas at Arlington.

After earning his Ph.D., Ameya will be joining The MathWorks Inc. as a Senior Quality Engineer with the Simscape Fluids and Simscape Driveline Team. His areas of interest include Robotics, Modeling and Simulation of Dynamic Systems, Control Systems Design, State and Parameter Estimation, Unmanned Vehicle Systems and System Identification.